UNIVERSITY OF SOUTHAMPTON

The Higgs Sector of Non-Minimal Supersymmetric Models

by

Shoaib Munir

A thesis submitted for the degree of

Doctor of Philosophy

School of Physics and Astronomy

May 2007

To my mother;

and to my brothers and sister.

UNIVERSITY OF SOUTHAMPTON

ABSTRACT

FACULTY OF SCIENCE

SCHOOL OF PHYSICS AND ASTRONOMY

Doctor of Philosophy

THE HIGGS SECTOR OF NON-MINIMAL SUPERSYMMETRIC MODELS

Shoaib Munir

The Minimal Supersymmetric Standard Model (MSSM), despite being a theoretically successful and highly predictive model, suffers from some technical setbacks and leaves ample room for further modification. We analyzed two extended versions of the minimal model; an MSSM with explicit CP–violation in the Higgs sector, and a model with an extra singlet scalar Higgs field in addition to the two MSSM doublets, referred to as the Next-to-Minimal Supersymmetric Standard Model (NMSSM). We looked for Higgs signatures in both these non-minimal models, focussing mainly on the di-photon decay mode of the Higgs boson, and found significant deviations from the MSSM scenario in each case.

Contents

List of Figures

List of Tables

Preface

The work described in this thesis was carried out in collaboration with Dr. S. Moretti and Dr. P. Poulose. The following list details our original work and gives the references for the material:

- Chapter 3:

  1. S. Moretti, S. Munir, P. Poulose, Phys. Lett. B **649** (2007) 206 [arXiv:hep-ph/0702242].

- Chapter 4:

  1. S. Moretti, S. Munir, Eur. Phys. J. C **47** (2006) 791 [arXiv:hep-ph/0603085].
  2. S. Moretti, S. Munir, CP Studies and Non-Standard Higgs Physics, CERN Yellow Reports 2006, 210 [arXiv:hep-ph/0608079].
  3. S. Moretti, S. Munir, P. Poulose, Phys. Lett. B **644** (2007) 241 [arXiv:hep-ph/0608233].

No claims to originality is made for the content of chapters 1 and 2 which were compiled using a variety of other sources.

Acknowledgements

The first and foremost gratitude belongs to the Almighty, the belief in whom has instilled in me the strength and the will to explore the unseen.

I feel thoroughly indebted to my dedicated supervisor, Dr. Stefano Moretti, for his expert academic guidance, assistance and backing, as well as for his humble concern and advice in my personal crises, of which there has been no dearth throughout the duration of my course. I am also thankful to my research collaborator Dr. Poulose Poulose for his abundantly helping hand in the completion of this research.

I am very grateful to my school for offering me a yearly bursary, without which continuing my course would have been impossible, and to its administrative staff for their hearty co-operation in crucial matters. Words of thanks must also go to HEC, Pakistan, for granting me a much needed stipend towards the end of my course.

I owe a lot to my fellow research students; the Jonathans, Tom, Martin, James, Andrew, Michael and all others for putting up with me, for engaging in long and fruitful discussions and explanations, and for providing a great educational and social environment, memories of which will indeed go a long way with me.

I must also acknowledge my friend Umar Masood, who has been a constant source of encouragement in my life. Finally, my getting this far wouldn't have been probable without the love and support of my family, may God bless them.

Chapter 1

Introduction

1.1 Preliminaries

1.1.1 Motivation

The Standard Model (SM) of particle physics successfully classifies particles that exist in nature and explicates their behaviour. It has endured many tests and precision measurements throughout the later part of the 20th century. The discovery of W and Z bosons [1, 2] and, more recently, the top quark [3] have served as important milestones in the quest for validating the model as an ultimate description of nature. However, with the passage of time it is showing certain loose ends and keeps ceasing to answer questions pertinent to certain crucial phenomena. For example, the original form of the SM thoery does not allow neutrinos to be massive while we now have plenty of evidence that these particles indeed carry mass. Moreover, the model does not provide sufficient explanation for the observed relic dark matter density and baryon asymmetry in the universe.

To account for the masses of particles, which are originally forbidden in the model by the electroweak (EW) symmetry, a so–called Higgs mechanism has to be incorporated

into the SM. This mechanism conjectures the ad–hoc presence of a scalar Higgs field in nature which interacts with all other particles, save photons, and imparts masses to them by *spontaneous* electroweak symmetry breaking (EWSB). Thus the Higgs mechanism makes up a vital cornerstone of the SM. In turn, the mechanism necessitates the existence of one neutral scalar Higgs particle in the model.

The Higgs particle is perhaps the most elusive particle predicted by the SM. It remains undiscovered four decades on since its postulation despite a hugely successful LEP era and continued searches at the Tevatron. The Large Hadron Collider (LHC), expected to begin operation in late 2007, bears a lot of promise in this regard as it is set to venture into realms of high energy previously unexplored. However, before another round of diligent hunting for the Higgs boson begins, we need to dig into the reason why the collider searches so far have failed to reveal it, if it indeed exists in nature.

The SM, while hugely banking upon the Higgs mechanism for its own survival, fails to provide any estimates on the mass of the Higgs particle. On the one hand, the model requires the Higgs mass to be close to that of the Z boson for its phenomenological justification while, on the other hand, the perturbative nature of the underlying theory threatens to generate a Higgs mass too heavy to adeptly explain EWSB. Until this ambiguity in the Higgs sector of the model is removed, an aura of speculation will always surround the existence of a Higgs boson and its detectability at future colliders.

As a result of the above mentioned theoretical shortcomings, one is compelled to think that the SM is not the sole representative of nature, and that there must lie physics beyond it. The model, at best, could only be a low–energy effective limit of a much more comprehensive theory with a far richer structure to explain particle dynamics at very high energies. There are alternatives to the Higgs mechanism itself, advocating dynamical generation of particle masses, which could result in the evasion

of the Higgs mass problem altogether from the theory. But owing to the technical appeal and theoretical conformity of the Higgs mechanism, coupled with other basic flaws of the SM, it seems a more appropriate choice to extend the model in a way that the issues faced by it are emphatically addressed. Such efforts are also greatly upheld by the inability of the SM to assimilate one of the four fundamental forces of nature – gravitational force.

Supersymmetry (SUSY) was proposed some time ago as a symmetry of nature along with the ones of the SM. The mere inclusion of this symmetry into the SM drastically changes the whole picture. In a supersymmetric model, the Higgs field and the nature of its mass term need not be mere improvisations, thus resulting in an answer to the Higgs mass problem in a natural way.

The minimal (by particle content and gauge groups) extension of SM based on SUSY, known as the Minimal Supersymmetric Standard Model (MSSM), predicts a total of five Higgs particles in nature, two charged and three neutral. Importantly, however, it fixes to a great deal the absolute waywardness in the mass of its lightest (SM–like) Higgs boson, as the arbitrary parameter λ on which it depends in the SM is now defined in terms of the $U(1)_Y$ and $SU(2)_L$ gauge couplings g_1 and g_2. This provides the experimentalists with a much narrower window to search for the Higgs particle within. The direct implication is that the LHC has got a tremendous opportunity to come up with a concrete verdict; either testify the existence of a Higgs boson by discovering it, or discard the idea altogether.

However, the MSSM, although not only exquisitely answers questions relevant to the Higgs particle but also throws adequate light on other unresolved matters, appears to be pretty much a work in progress for various reasons. The bounds it sets on the mass of the lightest Higgs, although crucial, are already in close range of current collider

experiments, resulting in the exclusion of a fair portion of its parameter space. In addition, even if a single Higgs is observed at the Tevatron or LHC, over a large MSSM parameter region no definite statement can be made from its mass or the currently attainable level of precision in the measurement of its couplings, as to whether it belongs to the SM or the MSSM. Finally, from a theoretical perspective, it suffers from the notorious μ–problem, making it all the more disputable.

Unless the experiments validate the MSSM in its current form, there lie a number of ways in which it could be modified. One such possibility emerges through the exploitation of certain new sources of CP–violation, apart from the CKM one which originates from the inter–generational mixings in the quark sector of the SM. Moreover, the Higgs sector of the minimal model could itself be further expanded in an attempt to address the μ–problem.

One such (minimal) extension is the Next–to–Minimal Supersymmetric Standard Model (NMSSM) which predicts seven Higgs particles. This model, besides raising the upper bound on the lightest MSSM Higgs mass by several GeVs, promises a distinctive Higgs sector from that of the SM and the MSSM. Our aim with the present work is to investigate such extensions of the MSSM and look for hints of new physics that more efficiently and convincingly expounds nature and at the same time deviates from the findings of both the SM and the MSSM.

1.1.2 Thesis structure

The thesis is organised as follows. In the remainder of this chapter we offer a brief introduction of the SM followed by that of the Higgs mechanism. The generation of masses for the SM particles is explained. We then overview the Higgs sector of the SM and the problems that have hindered its discovery in experiments so far. We also dicuss

the production and decay channels of the SM Higgs and finally outline the prospects of finding it in future experiments towards the end of the chapter.

The second chapter aims at building up a theoretical background to our work and so starts off by shedding some light on the need to look beyond the SM. We focus on two major problems of the SM, the *hierarchy* and *naturalness* problems, and discuss the most adequate solution to them, supplied by SUSY. The structure of the minimal model incorporating SUSY, the MSSM, is then thoroughly inspected. We briefly outline the consequences of SUSY breaking, which is inevitable in the MSSM due to the non–observation of an exact SUSY in nature. The final two sections of the chapter are dedicated to the Higgs sector of the model. Emphasis is laid on the mass spectrum of the Higgses and the bounds induced by the model on it. We then analyse the phenomenology of the MSSM neutral Higgs sector focussing on its production and decay modes favoured at the LHC. In the end, we sum up the results from the earlier and current searches as well as potential signatures at future colliders.

In the third chapter we scrutinise a very crucial aspect of the MSSM left unaddressed in the basic model. We examine how non–SM CP–violation can be explicitly invoked in the MSSM Higgs sector, thus helping to generate the right amount of CP–asymmetry as suggested by the baryogenesis in the universe. We then look for ways of estimating the CP–violating effects after highlighting the numerical procedures that we adopted for this purpose. By a comparative analysis with a CP–conserving MSSM, we emphasize that evidence for CP–violation in the Higgs sector could emerge at the LHC through precise measurements of the Higgs branching ratio into two photons. We also investigate the various factors contributing to CP–violation in the Higgs to $\gamma\gamma$ decay mode.

In the fourth chapter we delve into the NMSSM. We present a theoretical justification of the model, noticing that it only extends the Higgs and Higgsino sectors of the

MSSM, while the rest of the particle spectrum remains essentially the same. We then investigate the Higgs sector of the NMSSM and reestablish that the model promises the discovery of at least one Higgs particle at the LHC if the complementarity of the various production modes is thoroughly exploited. With a detailed numerical study we then attempt to search for regions in the parameter space of the NMSSM which exhibit distinctive signatures in the NMSSM from those in the MSSM. A thorough signal–to–background analysis of the di–photon decay mode of the Higgs boson alone evokes an enormous possibility of affirming the non–minimal nature of the underlying model. Such scenarios are presented at the end of the chapter.

Finally, in the last chapter, we sum up our conclusions and findings from the research we indulged in and highlight the relevant projects that could follow.

1.2 The Standard Model

1.2.1 Structure of the Model

The Glashow–Weinberg–Salam EW theory [4] which describes the electromagnetic and weak interactions between quarks and leptons, is a Yang–Mills theory [5] based on the symmetry group $SU(2)_L \times U(1)_Y$. Combined with the $SU(3)_C$ based QCD gauge theory [6] which describes the strong interactions between quarks, it provides a unified framework, the SM, for these three forces of nature. The model, in its original form, entails two kinds of fields:

i) The spin–1/2 fermionic or *matter* fields, which include the three generations of left–handed and right–handed chiral quarks and leptons, $f_{L,R} = \frac{1}{2}(1 \mp \gamma_5) f$. The left–handed

fermions are in weak isodoublets,

$$
\begin{aligned}
& & L_1 = \begin{pmatrix} \nu_e \\ e^- \end{pmatrix}_L , \quad & Q_1 = \begin{pmatrix} u \\ d \end{pmatrix}_L , \\
I_f^{3L} = \pm\frac{1}{2} \quad : \quad & L_2 = \begin{pmatrix} \nu_\mu \\ \mu^- \end{pmatrix}_L , \quad & Q_2 = \begin{pmatrix} c \\ s \end{pmatrix}_L , \\
& L_3 = \begin{pmatrix} \nu_\tau \\ \tau^- \end{pmatrix}_L , \quad & Q_3 = \begin{pmatrix} t \\ b \end{pmatrix}_L .
\end{aligned}
\tag{1.1}
$$

The right–handed fermions are in weak isosinglets (neutrinos are taken to be massless here and so appear only with their left–handed components),

$$
\begin{aligned}
& e_{R_1} = e_R^-, \quad u_{R_1} = u_R, \quad d_{R_1} = d_R, \\
I_f^{3R} = 0 \quad : \quad & e_{R_2} = \mu_R^-, \quad u_{R_2} = c_R, \quad d_{R_2} = s_R, \\
& e_{R_3} = \tau_R^-, \quad u_{R_3} = t_R, \quad d_{R_3} = b_R.
\end{aligned}
\tag{1.2}
$$

The fermion hypercharge, defined in terms of the third component of the weak isospin I_f^3 and the electric charge Q_f in units of the proton charge $+e$, is given by (i=1,2,3)

$$
Y_f = 2Q_f - 2I_f^3 \;\; \rightarrow \;\; Y_{L_i} = -1, \; Y_{e_{R_i}} = -2, \; Y_{Q_i} = \frac{1}{3}, \; Y_{u_{R_i}} = \frac{4}{3}, \; Y_{d_{R_i}} = -\frac{2}{3}. \tag{1.3}
$$

ii) The gauge fields corresponding to the spin–1 bosons, that mediate the interactions between the fermions. In the EW sector, we have the field B_μ which corresponds to the generator Y of the $\mathrm{U}(1)_Y$ group and the three fields $W_\mu^{1,2,3}$ which correspond to the generators T^a [with a=1,2,3] of the $\mathrm{SU}(2)_L$ group; these generators are in fact equivalent to half of the non–commuting 2×2 Pauli matrices

$$
T^a = \frac{1}{2}\tau^a ; \quad \tau_1 = \begin{pmatrix} 0 & 1 \\ 1 & 0 \end{pmatrix} , \; \tau_2 = \begin{pmatrix} 0 & -i \\ i & 0 \end{pmatrix} , \; \tau_3 = \begin{pmatrix} 1 & 0 \\ 0 & -1 \end{pmatrix} , \tag{1.4}
$$

with the commutation relations between these generators given by

$$[T^a, T^b] = i\epsilon^{abc} T_c \quad \text{and} \quad [Y, Y] = 0, \tag{1.5}$$

where ϵ^{abc} is the antisymmetric tensor. In the strong interaction sector, there is an octet of gluon fields $G_\mu^{1,\cdots,8}$ which correspond to the eight generators of the $SU(3)_C$ group (since the number of generators of an SU(N) gauge group $= N^2 - 1$, giving eight generators for N = 3, which are equivalent to half of the eight 3×3 anti–commuting Gell–Mann matrices), which obey the relations

$$[T^a, T^b] = i f^{abc} T_c \quad \text{with} \quad \mathrm{Tr}[T^a T^b] = \frac{1}{2}\delta_{ab}, \tag{1.6}$$

where f^{abc} is for the structure constants of the $SU(3)_C$ group. The field strengths are given by

$$\begin{aligned} G^a_{\mu\nu} &= \partial_\mu G^a_\nu - \partial_\nu G^a_\mu + g_3\, f^{abc} G^b_\mu G^c_\nu, \\ W^a_{\mu\nu} &= \partial_\mu W^a_\nu - \partial_\nu W^a_\mu + g_2\, \epsilon^{abc} W^b_\mu W^c_\nu, \\ B_{\mu\nu} &= \partial_\mu B_\nu - \partial_\nu B_\mu, \end{aligned} \tag{1.7}$$

with g_3, g_2 and g_1 being the coupling constants of $SU(3)_C$, $SU(2)_L$ and $U(1)_Y$, respectively.

Because of the non–abelian nature of the SU(2) and SU(3) groups, there are self–interactions between their gauge fields, $V_\mu \equiv W_\mu$ or G_μ, leading to

$$\text{triple gauge boson couplings} \;:\; i g_i\, \mathrm{Tr}(\partial_\nu V_\mu - \partial_\mu V_\nu)[V_\mu, V_\nu], \tag{1.8}$$

$$\text{quartic gauge boson couplings} \;:\; \frac{1}{2} g_i^2\, \mathrm{Tr}[V_\mu, V_\nu]^2. \tag{1.9}$$

Fields	$SU(3)_C$	$SU(2)_L$	$U(1)_Y$
Q_i	3	2	$\frac{1}{6}$
u_{R_i}	3	1	$\frac{2}{3}$
d_{R_i}	3	1	$-\frac{1}{3}$
L_i	1	2	$-\frac{1}{2}$
e_{R_i}	1	1	-1
G^a_μ	8	1	0
W^a_μ	1	3	0
B_μ	1	1	0

Table 1.1: Transformation properties of the fermion and gauge fields under the SM gauge group.

The matter fields ψ are minimally coupled to the gauge fields through the covariant derivative D_μ which, in the case of quarks (to accommodate $SU(3)_C$), is defined as

$$D_\mu\psi = \left(\partial_\mu - ig_s T_a G^a_\mu - ig_2 T_a W^a_\mu - ig_1 \frac{Y_q}{2} B_\mu\right)\psi \tag{1.10}$$

and which leads to unique couplings between the fermion fields and gauge fields V_μ of the form $-g_i\overline{\psi}V_\mu\gamma^\mu\psi$.

The SM Lagrangian, without mass terms for fermions and gauge bosons is then given by

$$\begin{aligned}\mathcal{L}_{\rm SM} &= -\frac{1}{4}G^a_{\mu\nu}G^{\mu\nu}_a - \frac{1}{4}W^a_{\mu\nu}W^{\mu\nu}_a - \frac{1}{4}B_{\mu\nu}B^{\mu\nu} + \bar{L}_i\, iD_\mu\gamma^\mu\, L_i + \bar{e}_{Ri}\, iD_\mu\gamma^\mu\, e_{R_i} \\ &\quad + \bar{Q}_i\, iD_\mu\gamma^\mu\, Q_i + \bar{u}_{Ri}\, iD_\mu\gamma^\mu\, u_{R_i} + \bar{d}_{Ri}\, iD_\mu\gamma^\mu\, d_{R_i}.\end{aligned} \tag{1.11}$$

This Lagrangian is invariant under local $SU(3)_C \times SU(2)_L \times U(1)_Y$ gauge transformations for fermion and gauge fields. The transformation properties of the these fields under the SM gauge group are listed in tab. 1.1.

1.2.2 Origin of Particle Masses

In the SM discussed so far, the gauge fields and the fermions fields have been kept massless. In the case of strong interactions, the gluons are indeed massless particles while mass terms of the form $-m_q\overline{\psi}\psi$ can be generated for the coloured quarks (and for the leptons) in an SU(3) gauge invariant way since both the left– and right–handed quarks are triplets of the $SU(3)_C$ gauge group (while the leptons are singlets). In the case of the EW sector, however, if we add mass terms, $\frac{1}{2}m_V^2 W_\mu W^\mu$, for the gauge bosons (since experimentally, they have been proved to be massive), this will violate local $SU(2)_L\times$ $U(1)_Y$ gauge invariance. This statement can be visualised by taking the example of QED where the photon is massless because of the $U(1)_Q$ local symmetry

$$\frac{1}{2}m_A^2 A_\mu A^\mu \rightarrow \frac{1}{2}m_A^2(A_\mu - \frac{1}{e}\partial_\mu\alpha)(A^\mu - \frac{1}{e}\partial^\mu\alpha) \neq \frac{1}{2}m_A^2 A_\mu A^\mu. \tag{1.12}$$

In addition, if we include explicitly a mass term $-m_f\overline{\psi}_f\psi_f$ for each SM fermion f in the Lagrangian, we would have, for the electron for instance,

$$-m_e\bar{e}e = -m_e\bar{e}\left(\frac{1}{2}(1-\gamma_5) + \frac{1}{2}(1+\gamma_5)\right)e = -m_e(\bar{e}_R e_L + \bar{e}_L e_R), \tag{1.13}$$

which is manifestly non–invariant under the isospin symmetry transformations discussed above, since e_L is a member of an $SU(2)_L$ doublet while e_R is a member of a singlet. Thus, the incorporation by brute force of mass terms for gauge bosons and for fermions leads to a manifest breakdown of the local $SU(2)_L\times$ $U(1)_Y$ gauge symmetry. Thus, for the theory to be thoroughly valid, there should be a way to generate the gauge boson and the fermion masses without violating $SU(2)_L\times$ $U(1)_Y$ gauge invariance.

1.3 Electroweak Symmetry Breaking

1.3.1 Higgs Mechanism: An Abelian Example

Consider an abelian gauge theory in which a complex scalar field ϕ is coupled to itself and to an electromagnetic field:

$$\mathcal{L} = -\frac{1}{4}(F_{\mu\nu})^2 + |D_\mu \phi|^2 - V(\phi), \tag{1.14}$$

where $F_{\mu\nu}$ is the usual electromagnetic field strength tensor and D_μ is the covariant derivative given as $D_\mu = \partial_\mu + ieA_\mu$. This Lagrangian is invariant under the local U(1) transformation

$$\phi(x) \rightarrow e^{i\alpha(x)}\phi(x), \qquad A_\mu(x) \rightarrow A_\mu(x) - \frac{1}{e}\partial_\mu \alpha(x), \tag{1.15}$$

where $\alpha(x)$ is the generator of the $\mathrm{U}(1)_Q$ transformation, and thus no $(\text{mass})^2$ term is allowed for the A_μ field. If we choose the scalar potential to be of the form

$$V(\phi) = -\mu^2 \phi^* \phi + \frac{\lambda}{2}(\phi^* \phi)^2, \tag{1.16}$$

with $\mu^2 > 0$, the field ϕ will acquire a *vacuum expectation value* (VEV), conventionally written as v, and the $\mathrm{U}(1)_Q$ symmetry will be spontaneously broken, as shown in fig. 1.1. The minimum of the potential, instead of occurring at the minimum–energy classical configuration $\langle\phi\rangle \equiv \phi_0 = 0$, now occurs at

$$\langle\phi\rangle \equiv v = \left(\frac{\mu^2}{\lambda}\right)^{1/2}, \tag{1.17}$$

or at any other value related by the U(1) symmetry, eq. (1.15).

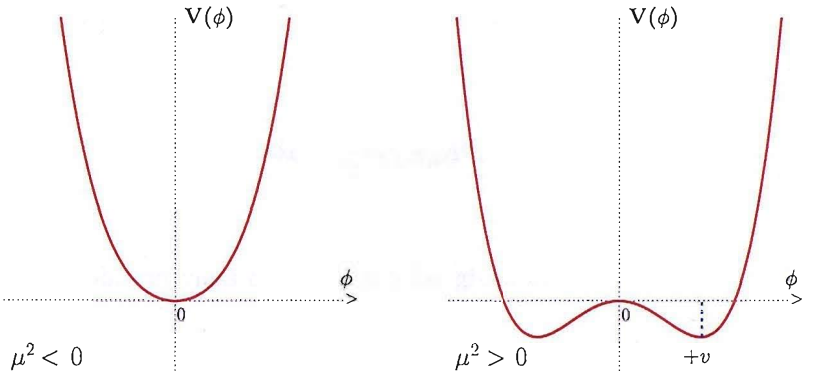

Figure 1.1: The potential V of the scalar field ϕ in the cases when $\mu^2 < 0$ (left) and when $\mu^2 > 0$ (right).

The Lagrangian is now expanded about the vacuum state v. The decomposition of the scalar field is carried out around this vacuum as

$$\phi(x) = v + \frac{1}{\sqrt{2}}(\phi_1(x) + i\phi_2(x)), \tag{1.18}$$

and the potential is rewritten in terms of the new fields ϕ_1 and ϕ_2 as

$$V(\phi) = -\frac{1}{2\lambda}\mu^4 + \frac{1}{2} \cdot 2\mu^2\phi_1^*\phi_1 + \mathcal{O}(\phi_i^3). \tag{1.19}$$

Clearly, we have a massive field ϕ_1 with mass $m_{\phi_1} = \sqrt{2}\mu = \sqrt{2\lambda}v$, while no mass term appears for the field ϕ_2. Such a massless field is referred to as a *Goldstone* boson, and follows from the Goldstone theorem [7] which states that for every spontaneously broken continuous symmetry, the theory must contain a massless particle.

The covariant terms in the Lagrangian are also written in terms of the new fields ϕ_1 and ϕ_2 as

$$|D_\mu\phi|^2 = \frac{1}{2}(\partial_\mu\phi_1)^2 + \frac{1}{2}(\partial_\mu\phi_2)^2 + ev \cdot A_\mu\partial^\mu\phi_2 + \frac{1}{2}e^2v^2A_\mu A^\mu + \cdots, \tag{1.20}$$

up to terms cubic and quartic in the fields A_μ, ϕ_1 and ϕ_2. Evidently, the last term in

eq. (1.20) has the form

$$\delta\mathcal{L} = \frac{1}{2}m_A^2 A_\mu A^\mu, \tag{1.21}$$

and hence is the photon mass term, with mass given as

$$m_A^2 = e^2 v^2. \tag{1.22}$$

Thus, as a result of non–vanishing VEV of the field ϕ, the photon has acquired a mass. This process of spontaneous breaking of symmetry to yield masses for the vector bosons is referred to as the Higgs mechanism [8]. The Goldstone boson emerging as a result of this mechanism plays an important role in the theory by supplying a vertex of the form $iev(-ik^\mu) = m_A k^\mu$ (k^μ being its four–momentum) and hence exactly the right pole to make the vacuum polarisation amplitude properly transverse. However, it does not appear as an independent physical particle, and so can be safely removed from the theory. The easiest way to do it is to use the local U(1) symmetry of the theory to move to the *unitary* gauge, in which the field ϕ_2 appears to have been 'abosrbed' by the gauge boson to make up its longitudinal polarisation state [9].

1.3.2 Higgs Mechanism in the SM

In the slightly more complicated non–abelian case of the SM, we need to generate masses for the three gauge bosons $W^\pm$ and Z but the photon should remain massless and QED must stay an exact symmetry. Therefore, we need at least 3 degrees of freedom for the scalar fields. The simplest choice is a complex scalar field ϕ in the

spinor representation of SU(2):

$$\Phi = \begin{pmatrix} \phi^+ \\ \phi^0 \end{pmatrix}, \quad Y_\phi = +1. \tag{1.23}$$

The SM Lagrangian discussed in sect. 1.2.1, without the strong interaction part, may be written as

$$\mathcal{L}_{\rm SM} = -\frac{1}{4} W^a_{\mu\nu} W_a^{\mu\nu} - \frac{1}{4} B_{\mu\nu} B^{\mu\nu} + \overline{L}\, i D_\mu \gamma^\mu\, L + \overline{e}_R\, i D_\mu \gamma^\mu\, e_R \; + \cdots, \tag{1.24}$$

where the covariant derivative D_μ is given in eq. (1.10). We add the $\mathrm{SU(2)}_L \times \mathrm{U(1)}_Y$ invariant terms for the above scalar field given as

$$\mathcal{L}_S = (D^\mu \Phi)^\dagger (D_\mu \Phi) - V(\Phi), \quad \text{with } V(\Phi) = -\mu^2 \Phi^\dagger \Phi + \lambda (\Phi^\dagger \Phi)^2, \tag{1.25}$$

to the Lagrangian in eq. (1.24). For $\mu^2 > 0$, the neutral component of the doublet field Φ will develop a VEV

$$\langle\, \Phi \,\rangle = \begin{pmatrix} 0 \\ \frac{v}{\sqrt{2}} \end{pmatrix}, \quad \text{with } \; v = \left(\frac{\mu^2}{\lambda}\right)^{1/2}. \tag{1.26}$$

We now repeat the same exercise as we did in the abelian case in the previous section. The field Φ is written in terms of four fields $\theta_{1,2,3}(x)$ and $H(x)$ as

$$\Phi(x) = \begin{pmatrix} \theta_2 + i\theta_1 \\ \frac{1}{\sqrt{2}}(v + H) - i\theta_3 \end{pmatrix} = e^{i\theta_a(x)\tau^a(x)/v} \begin{pmatrix} 0 \\ \frac{1}{\sqrt{2}}(v + H(x)\,) \end{pmatrix}. \tag{1.27}$$

Notice that the VEV should not be taken in the charged direction to preserve $\mathrm{U(1)}_Q$. In order to prevent the Goldstone boson from appearing, we perform an SU(2) $\times$ U(1)

transformation on the scalar field to move to the unitary gauge, so that

$$\Phi(x) \rightarrow e^{-i\theta_a(x)\tau^a(x)}\,\Phi(x) = \frac{1}{\sqrt{2}}\begin{pmatrix} 0 \\ v + H(x) \end{pmatrix}. \tag{1.28}$$

The term $|D_\mu\Phi|^2$ of the Lagrangian $\mathcal{L}_S$ is then expanded as:

$$\begin{aligned} |D_\mu\Phi)|^2 &= \left|\left(\partial_\mu - ig_2\frac{\tau_a}{2}W_\mu^a - ig_1\frac{1}{2}B_\mu\right)\Phi\right|^2 \\ &= \frac{1}{2}\left|\begin{pmatrix} \partial_\mu - \frac{i}{2}(g_2W_\mu^3 + g_1B_\mu) & -\frac{ig_2}{2}(W_\mu^1 - iW_\mu^2) \\ -\frac{ig_2}{2}(W_\mu^1 + iW_\mu^2) & \partial_\mu + \frac{i}{2}(g_2W_\mu^3 - g_1B_\mu) \end{pmatrix}\begin{pmatrix} 0 \\ v + H \end{pmatrix}\right|^2 \\ &= \frac{1}{2}(\partial_\mu H)^2 + \frac{1}{8}g_2^2(v+H)^2|W_\mu^1 + iW_\mu^2|^2 + \frac{1}{8}(v+H)^2|g_2W_\mu^3 - g_1B_\mu|^2. \end{aligned} \tag{1.29}$$

Here we define new fields $W_\mu^\pm$ and Z_μ (A_μ being the field orthogonal to Z_μ) as:

$$W^\pm = \frac{1}{\sqrt{2}}(W_\mu^1 \mp iW_\mu^2)\ ,\ Z_\mu = \frac{g_2W_\mu^3 - g_1B_\mu}{\sqrt{g_2^2 + g_1^2}}\ ,\ A_\mu = \frac{g_2W_\mu^3 + g_1B_\mu}{\sqrt{g_2^2 + g_1^2}}, \tag{1.30}$$

and from the Lagrangian, eq. (1.29), pick up the terms which are bilinear in these fields $W^\pm, Z, A$:

$$m_W^2W_\mu^+W^{-\mu} + \frac{1}{2}m_Z^2Z_\mu Z^\mu + \frac{1}{2}m_A^2A_\mu A^\mu \tag{1.31}$$

We see that the W and Z bosons have acquired masses

$$m_W = \frac{1}{2}vg_2\ ,\ m_Z = \frac{1}{2}v\sqrt{g_2^2 + g_1^2}\ , \tag{1.32}$$

while our choice of VEV has left the photon massless, $m_A = 0$. Thus, by spontaneously breaking the symmetry $\mathrm{SU}(2)_L\times\ \mathrm{U}(1)_Y$ to $\mathrm{U}(1)_Q$, three Goldstone bosons have been

absorbed by the $W^{\pm}$ and Z bosons to form their longitudinal components and to get their masses. Since the $U(1)_Q$ symmetry is still unbroken, the photon, which is its generator, remains massless as it should be.

The fermion masses are also generated using the same scalar field Φ, with hypercharge $Y{=}{+}1$, and the isodoublet $\tilde{\Phi} = i\tau_2\Phi^*$, which has hypercharge $Y{=}{-}1$. For any fermion generation, we introduce the $SU(2)_L \times U(1)_Y$ invariant Yukawa Lagrangian

$$\mathcal{L}_F = -\lambda_e \bar{L}\,\Phi\, e_R - \lambda_d \bar{Q}\,\Phi\, d_R - \lambda_u \bar{Q}\,\tilde{\Phi}\, u_R \;+\; h.c., \tag{1.33}$$

and repeat the same exercise as above. For instance, in the case of the electron one obtains

$$\begin{aligned} \mathcal{L}_F &= -\frac{1}{\sqrt{2}}\lambda_e\,(\bar{\nu}_e, \bar{e}_L) \begin{pmatrix} 0 \\ v+H \end{pmatrix} e_R \;+\cdots \\ &= -\frac{1}{\sqrt{2}}\,\lambda_e\,(v+H)\,\bar{e}_L e_R \;+\cdots . \end{aligned} \tag{1.34}$$

The constant term in front of $\bar{f}_L f_R$ (and h.c.) is identified with the electron mass

$$m_e = \frac{\lambda_e\, v}{\sqrt{2}}. \tag{1.35}$$

It's straight forward to see that we can obtain similar mass terms for the up–type and down–type quarks, given as

$$m_u = \frac{\lambda_u\, v}{\sqrt{2}}, \quad m_d = \frac{\lambda_d\, v}{\sqrt{2}}. \tag{1.36}$$

Thus, with the same isodoublet Φ of scalar fields, we have generated the masses of both the weak vector bosons $W^{\pm}, Z$ and the fermions, while preserving the $SU(2)_L \times$

$U(1)_Y$ gauge symmetry, which is now spontaneously broken or 'hidden'. The electromagnetic $U(1)_Q$ symmetry as well as the $SU(3)_C$ symmetry stay unbroken. The SM generally referred to in the literature is, in fact, the $SU(3)_C \times SU(2)_L \times U(1)_Y$ gauge invariance combined with the Higgs mechanism.

1.3.3 The Higgs particle in the SM

The kinetic term for the Higgs field, $\frac{1}{2}(\partial_\mu H)^2$, comes from the part in the Lagrangian involving the covariant derivative $|D_\mu \Phi|^2$, while the mass and self–interaction terms come from the scalar potential $-V(\Phi) = \mu^2 \Phi^\dagger \Phi + \lambda(\Phi^\dagger \Phi)^2$ as

$$V = -\frac{\mu^2}{2}(0, v+H)\begin{pmatrix} 0 \\ v+H \end{pmatrix} + \frac{\lambda}{4}\left|(0, v+H)\begin{pmatrix} 0 \\ v+H \end{pmatrix}\right|^2. \quad (1.37)$$

Using the relation $v^2 = \mu^2/\lambda$, one obtains

$$V = -\frac{1}{2}\lambda v^2 (v+H)^2 + \frac{1}{4}\lambda (v+H)^4. \quad (1.38)$$

The Lagrangian containing the Higgs field H is then given by

$$\begin{aligned} \mathcal{L}_H &= \frac{1}{2}(\partial_\mu H)(\partial^\mu H) - V \\ &= \frac{1}{2}(\partial^\mu H)^2 - \lambda v^2 H^2 - \lambda v H^3 - \frac{\lambda}{4} H^4. \end{aligned} \quad (1.39)$$

From this Lagrangian, one can see that the Higgs boson mass simply reads

$$M_H^2 = \lambda v^2 = 2\mu^2, \quad (1.40)$$

and the Feynman rules for the Higgs self–interaction vertices are given by

$$g_{H^3} = (3!)i\lambda v = 3i\,\frac{M_H^2}{v}\ ,\ g_{H^4} = (4!)i\frac{\lambda}{4} = 3i\frac{M_H^2}{v^2}. \tag{1.41}$$

From the Lagrangian describing the gauge boson and fermion masses given in eq. (1.29), one also obtains the Higgs boson couplings to gauge bosons and fermions of the form:

$$g_{Hff} = i\frac{m_f}{v}\ \ ,\ g_{HVV} = -2i\frac{m_V^2}{v}\ \ ,\ g_{HHVV} = -2i\frac{m_V^2}{v^2}. \tag{1.42}$$

Finally, the propagator of the Higgs boson is simply given, in momentum space, by

$$\Delta_{HH}(q^2) = \frac{i}{q^2 - M_H^2 + i\epsilon}. \tag{1.43}$$

1.3.4 Theoretical Bounds on the Higgs Mass

As seen in eq. (1.40), the Higgs mass is given as $M_H^2 = \lambda v^2 = 2\mu^2$. The VEV v is fixed in terms of the W boson mass m_W or the Fermi constant G_μ determined from the muon decay,

$$m_W = \frac{1}{2}g_2 v = \left(\frac{\sqrt{2}g_2^2}{8G_\mu}\right)^{1/2} \Rightarrow v = \frac{1}{(\sqrt{2}G_\mu)^{1/2}} \simeq 246\ \text{GeV}, \tag{1.44}$$

but there is no way one can determine the coupling λ without information on the Higgs mass spectrum itself. Thus λ remains a free parameter of the SM leaving the Higgs mass entirely inestimable.

However, the underlying theory of the model sets some important constraints [10] on this Higgs mass which help tune down the complete arbitrariness in it. These

constraints include:

- **Vacuum Stability**: The requirement that $V(v) < V(0)$, that is v is the true minimum of the potential, which in turn requires λ to be positive at all scales Λ up to which the SM is valid, gives a lower bound on the Higgs mass [11]

$$M_H^2 > \frac{v^2}{8\pi^2}[-12g_t^4 + \frac{3}{16}(2g_2^4 + (g_2^2 + g_1^2)^2)] \ln(\frac{\Lambda}{v^2}), \tag{1.45}$$

where $g_t \equiv -m_t/v$. Thus the radiative corrections from the top quark and gauge couplings play a very crucial role in setting a limit on the Higgs mass, particularly for small λ (light Higgs boson). If the SM is only valid up to 1 TeV, using the two loop renormalised effective potential, a much simpler expression for the lower bound is obtained as

$$M_H(\text{GeV}) > 71 + .74(m_t - 174). \tag{1.46}$$

If, instead, the SM is required to be valid up to scales of order 10^{16} GeV, the above limit becomes

$$M_H(\text{GeV}) > 130.5 + 2.1(m_t - 174), \tag{1.47}$$

giving, roughly, $M_H \gtrsim 130$ GeV.

- **Unitarity Constraints**: For longitudinal W bosons, the scattering amplitude via Higgs boson at high center–of–mass energy, $s(M_H^2) > m_W^2, m_Z^2$, would be

$$\mathcal{A}(W_L^+ W_L^- \to W_L^+ W_L^-) = -\sqrt{2} G_F M_H^2 \left[\frac{s}{s - M_H^2} + \frac{t}{t - M_H^2}\right], \tag{1.48}$$

which clearly violates unitarity as $M_H \to \infty$, but it may do so even for a finite value of M_H. The contribution to $J = 0$ partial wave for $s \gg M_H^2$ is

$$a_0 = -\frac{G_F M_H^2}{4\pi\sqrt{2}}. \tag{1.49}$$

Partial wave unitarity requires that $|a_J|^2 \leq |\mathcal{I}(a_J)|$, which implies that

$$(\mathcal{R}(a_J))^2 \leq |\mathcal{I}(a_J)|(1 - |\mathcal{I}(a_J)|) \quad \Rightarrow \quad |\mathcal{R}(a_J)| \leq \frac{1}{2}, \tag{1.50}$$

since $0 < |\mathcal{I}(a_J)| < 1$.

From these conditions on J_0, one gets an upper bound of, roughly

$$M_H < 750 \text{ GeV}. \tag{1.51}$$

- **Triviality**: The running of λ from a large scale Λ down to v is given by

$$\lambda(v) = \lambda(\Lambda)\left[1 - \frac{3\lambda(v)}{4\pi^2}\ln\left(\frac{\Lambda^2}{v^2}\right)\right]. \tag{1.52}$$

This relation, along with the requirement that the SM remains perturbative up to a scale $\lambda(\Lambda) < \infty$, can be translated into an upper bound on M_H as

$$M_H^2 \lesssim \frac{8\pi^2 v^2}{3\ln(\Lambda^2/v^2)} \simeq 700 \text{ GeV}. \tag{1.53}$$

Fig. 1.2 shows the variation in the lower bound on the Higgs mass with the scale Λ [12].

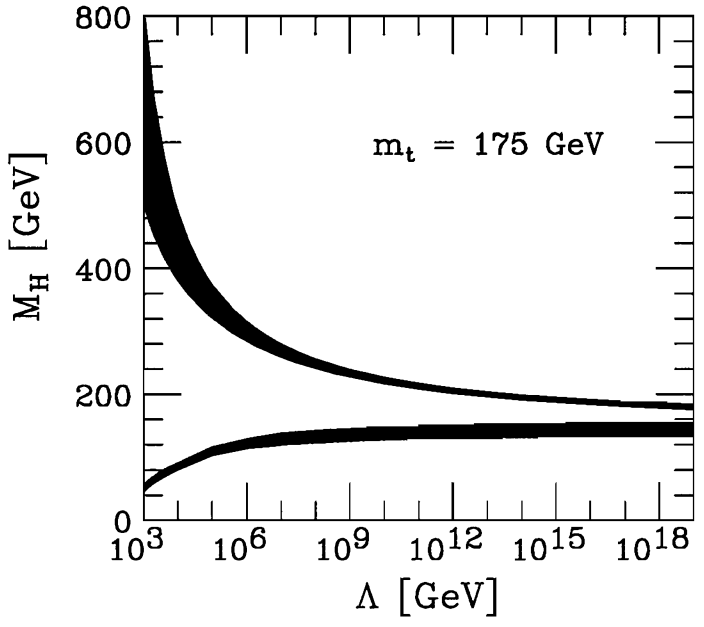

Figure 1.2: Higgs mass upper bound as a function of the scale Λ [12].

1.4 Phenomenology of the SM Higgs

1.4.1 Higgs Decay Modes

Higgs decay modes into SM particles include:

- lepton and quark pair decays,
- decay into gluons – mediated by heavy quark loops,
- decay into photon pairs – mediated by W boson and heavy fermion loops,
- decay to photon and Z boson – mediated by W and heavy fermion loops,
- decays into gauge bosons.

The corresponding branching ratios (BR), with different approximations for each decay mode [13], are shown in fig. 1.3, as a function of the Higgs mass.

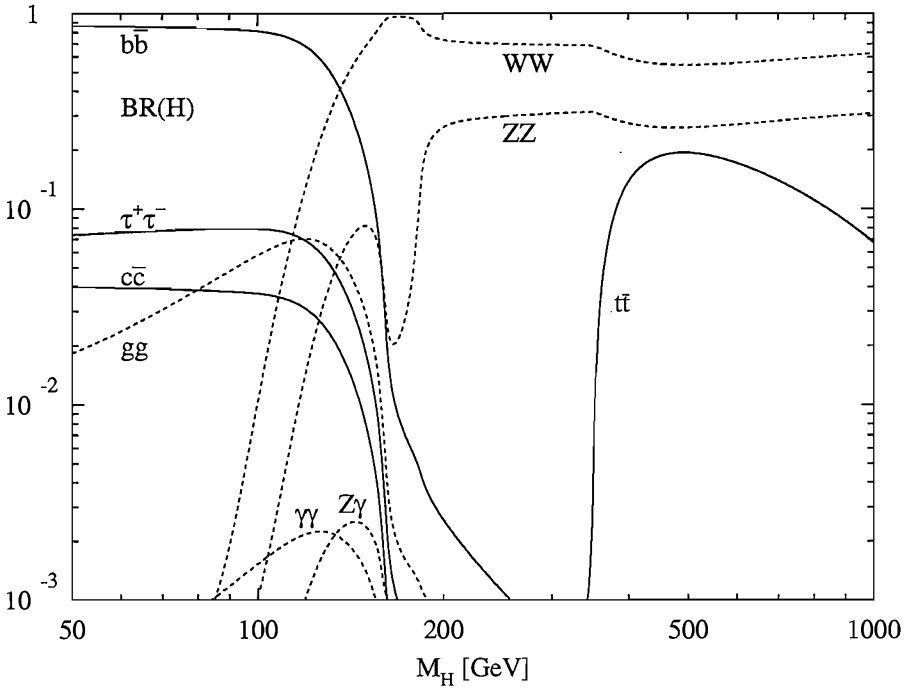

Figure 1.3: BRs of the Higgs boson into various SM particles [13].

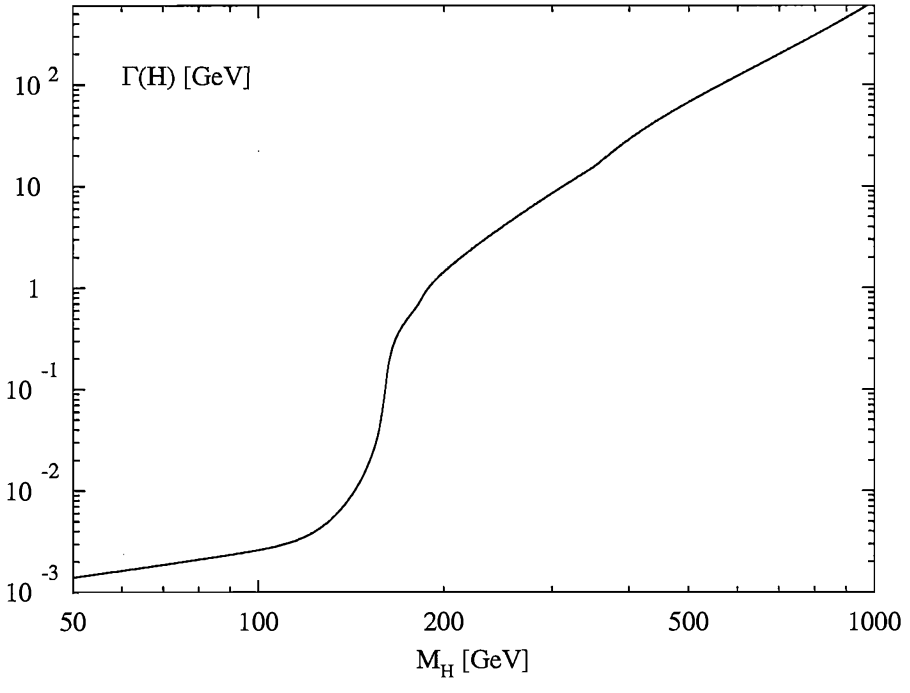

Figure 1.4: Total decay width of the SM Higgs as a function of its mass [13].

Clearly, for Higgs masses below ~ 140 GeV, where the total width amounts to less than 10 MeV as seen in fig. 1.4, the dominant decay mode is the $b\bar{b}$ channel with a BR up to $\sim 85\%$. The remaining 10–20% is supplied by the $\tau^+\tau^-, c\bar{c}$ and gg decay modes, the BRs of which amount to 6.6%, 4.6% and 6% respectively, for $M_H = 120$ GeV (the $b\bar{b}$ BR is about 78% for this Higgs mass). The $\gamma\gamma$ ($Z\gamma$) BR turns out to be sizeable only for Higgs masses 80 (120) GeV $\lesssim M_H \lesssim$ 150 (160) GeV, where they exceed the 10^{-3} level.

Starting from $M_H \sim 140$ GeV the WW decay takes over the dominant role joined by the ZZ decay mode. Around the WW threshold of 150 GeV $\lesssim M_H \lesssim$ 180 GeV, where the W pair of the dominant WW channel becomes on–shell, the ZZ BR drops down to a level of $\sim 2\%$ and reaches again a BR $\sim 30\%$ above the ZZ threshold. Above the $t\bar{t}$ threshold $M_H = 2m_t$, the $t\bar{t}$ decay mode opens up quickly, but never exceeds a BR of $\sim 20\%$. This is caused by the fact that the leading WW and ZZ decay widths grow with the third power of the Higgs mass due to the longitudinal W, Z components, which are dominating for large Higgs masses, whereas the $t\bar{t}$ decay width increases only with the first power [13]. Consequently the total Higgs width grows rapidly at large Higgs masses and reaches a level of ~ 600 GeV at $M_H = 1$ TeV, rendering the Higgs width of the same order as its mass. At $M_H = 1$ TeV the WW (ZZ) BR approximately reaches its asymptotic value of 2/3 (1/3).

1.4.2 Production Channels

A neutral Higgs boson can be produced at hadron colliders, such as the Tevatron and the LHC, through

- gluon–fusion via heavy–quark loops: $pp \to gg \to H$,

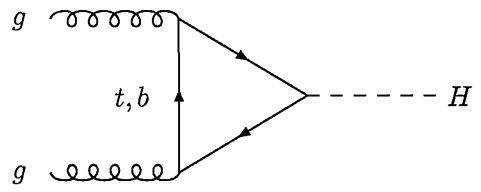

Figure 1.5: The $gg \to H$ production mode at lowest order.

- Higgs–strahlung: $q\bar{q} \to V^* \to VH$ $(V = W^{\pm}, Z)$,

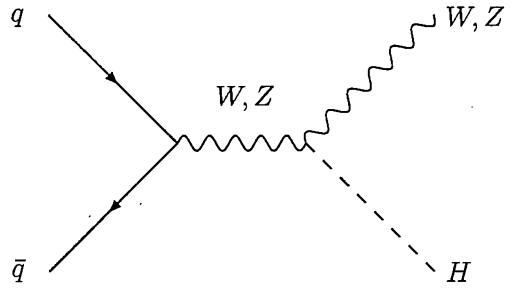

Figure 1.6: Diagram contributing to $q\bar{q} \to V^* \to VH$ at lowest order.

- vector–boson fusion (VBF): $qq \to qqV^*V^* \to qqH$,

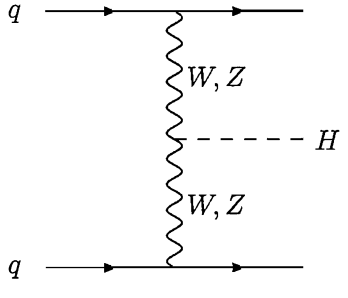

Figure 1.7: Diagram contributing to $qq \to qqV^*V^* \to qqH$ at lowest order.

- associated production with top quarks: $gg/q\bar{q} \to t\bar{t}H$.

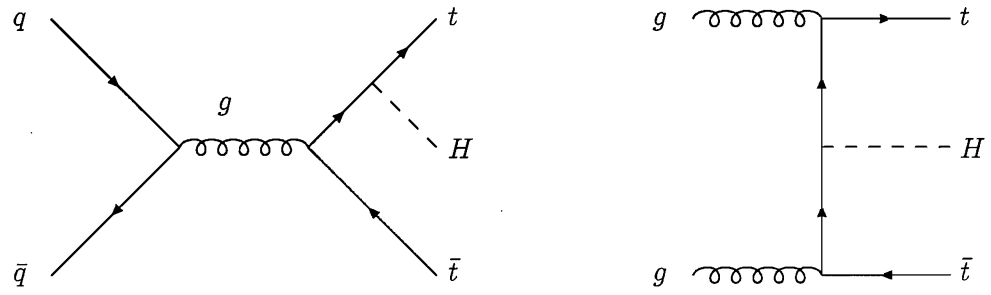

Figure 1.8: Typical diagrams contributing to $q\bar{q}/gg \rightarrow t\bar{t}H$ at lowest order.

These are the so–called 'direct' Higgs production modes [14]. Higher order corrections have been evaluated up to two–loop or next–to–next–to–leading order (NNLO) for the gluon–fusion process [15] and could increase the leading order (LO) production cross–section by about 60–90%. For the Higgs–strahlung and VBF processes, the QCD corrections have been calculated up to next–to–leading order (NLO) and could amount to about 25–40% and 8–10% increase in the cross–section for the two cases, respectively [16, 17]. The NLO QCD corrections to $Ht\bar{t}$ have also been recently estimated. These are found to be negative for the Tevatron and can reduce the LO cross–section by about 1–20%, while at the LHC they can enhance the cross-section by 20–40% [18, 19].

The present level of these perturbative corrections leads to a significantly improved and reliable determination of the signal processes involved in the Higgs boson search at collider experiments. The production cross–section of the SM Higgs through the above channels at the $\sqrt{s_{q\bar{q}}} \sim 2$ TeV Tevatron, which will continue its present run until 2009, and the $\sqrt{s_{qq}} \sim 14$ TeV LHC, which is expected to begin operation in late 2007, is given in fig. 1.9.

Evidently, the gluon–fusion mode provides the dominant production cross–section throughout the accessible Higgs mass range at the Tevatron, as well as for the entire

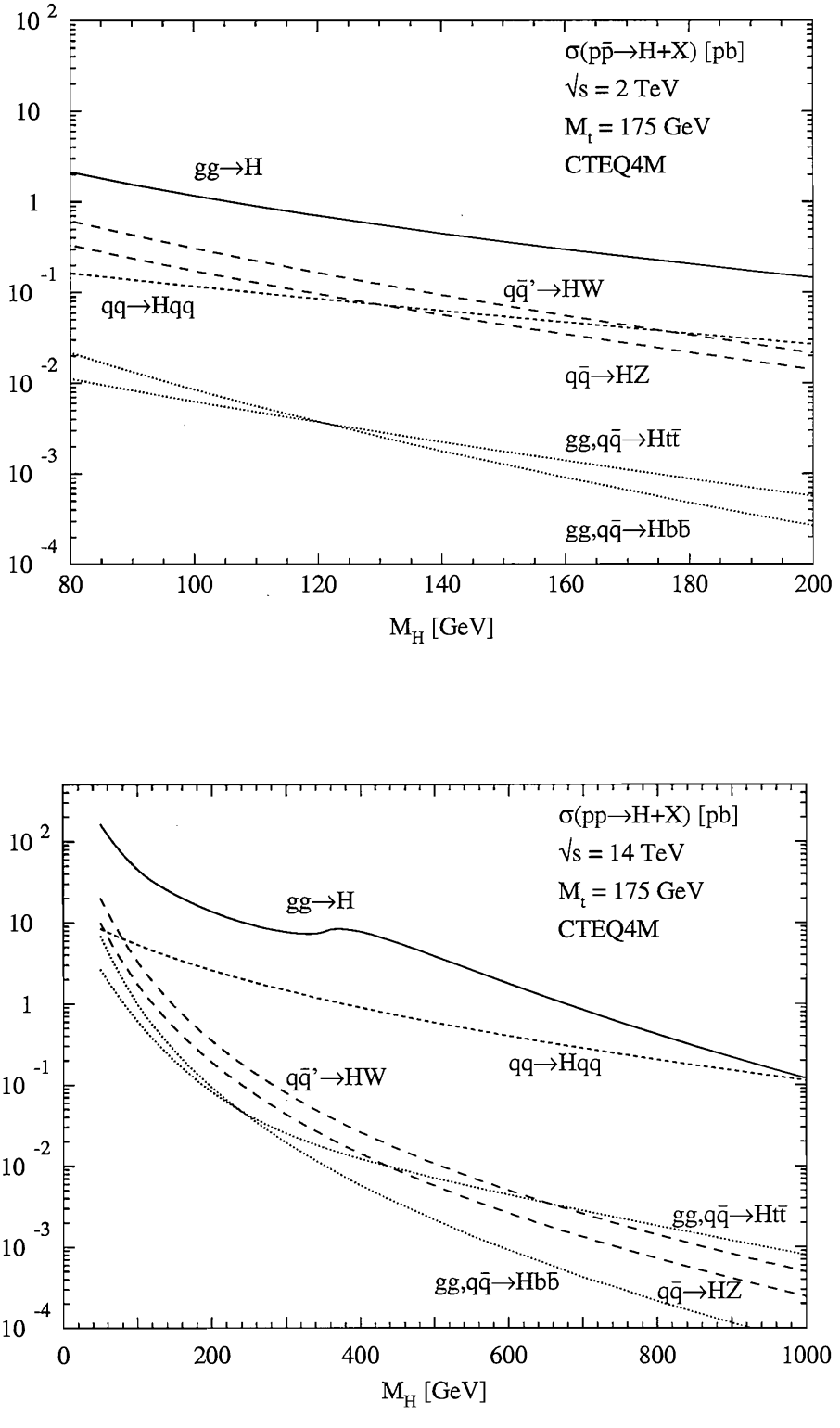

Figure 1.9: Higgs prodcution cross–section through various production channels at the Tevatron (above) [20] and the LHC (below) [13] as a function of its mass.

Higgs mass region up to $M_H \sim 1$ TeV at the LHC. In the intermediate mass range the gluon–fusion cross section is at least one order of magnitude larger than all other Higgs production mechanisms. In the case of LHC, only for Higgs masses $M_H \gtrsim 800$ GeV, the VBF ($qq \to Hqq$) mechanism becomes competitive and deviates from the gluon–fusion cross section by less than a factor 2 for $M_H \gtrsim 800$ GeV. At the Tevatron, however, the VBF channel is dominated by Higgs–strahlung processes off W and Z bosons for $M_H \lesssim 180$ GeV, at which point the former becomes comparable to the latter two modes. For the LHC, at the lower end of the Higgs mass range $M_H \lesssim 100$ GeV, the associated production channels of $H + V, H + t\bar{t}$ yield sizeable cross–section of about one order of magnitude below the gluon–fusion process.

1.4.3 Experimental Searches

The direct searches in the LEP2 experiments at CERN via the process $e^+e^- \to Z^* \to ZH$ yielded a lower bound of ~ 114.4 GeV on the Higgs mass at 95% confidence level (C.L.) [21]. As for the currently operating Tevatron, sensitivity to production of low–mass Higgs bosons beyond the LEP limits has already started to be reached [20]. For a SM Higgs bosons decaying to $b\bar{b}$, the production in association with W or Z bosons is the most promising channel. In the mass range between ~150 and ~180 GeV, Higgs bosons produced via gluon–fusion might be observable in their decays to WW. Given the current projections for the integrated Tevatron luminosity of about 8 fb^{-1} by 2009, a 5σ discovery of a SM Higgs boson will be very difficult to achieve. Nevertheless combining results from all search channels should provide sensitivity for exclusion of Higgs boson production at the 95% C.L. up to masses of 180 GeV/c^2 [20], as illustrated by fig. 1.10.

At the LHC, for a Higgs mass below ~140 GeV, because of the overwhelming QCD

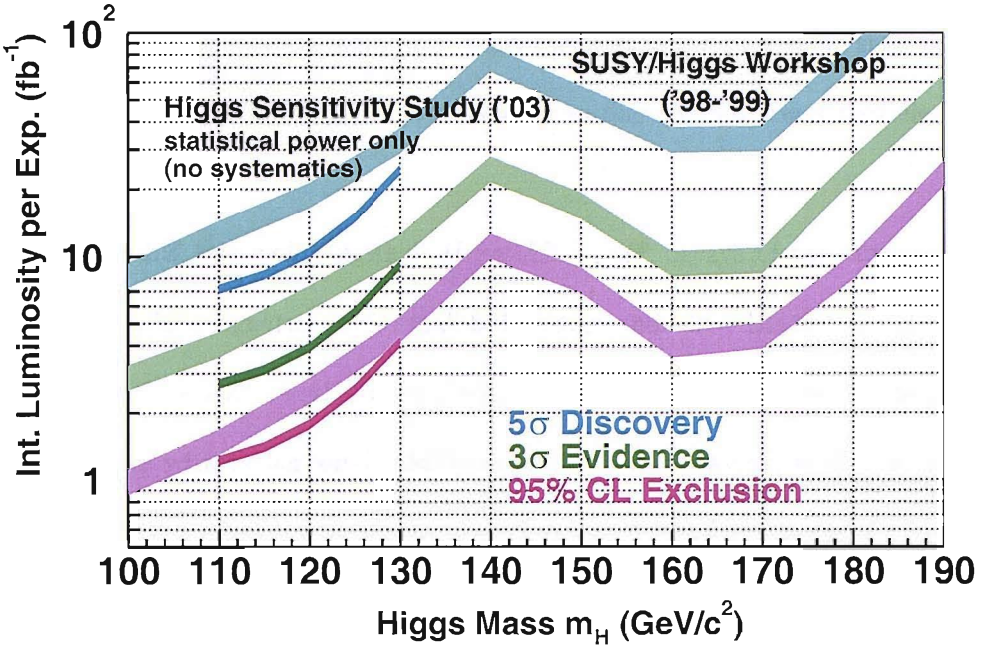

Figure 1.10: The integrated luminosity required per experiment for a 95% C.L. exclusion, a 3σ evidence and a 5σ discovery of a SM Higgs boson at the Tevatron as a function of its mass [20]. Thin lines show recent estimates with no systematic uncertainties included [22]. Thick lines are based on the results of an earlier study [23] and their thickness indicates the impact of systematic uncertainties.

background, the $b\bar{b}$ signal will be extremely difficult to extract [24]. The associated production of the Higgs boson with a $t\bar{t}$ pair or a W boson may increase the significance of the $H \to b\bar{b}$ decay due to the additional isolated leptons from t and W decays, but the rates will be considerably smaller than single Higgs production via gluon–fusion [25, 26]. The same holds for the $H \to \tau^+\tau^-$ decay mode because of the huge backgrounds from $t\bar{t}$ and Drell–Yan $\tau^+\tau^-$ pair production [27]. The BR into off–shell Z pairs is too small to allow for a detection of four–lepton final states [28].

The only promising channel for the detection of the Higgs boson with masses $M_H \lesssim$ 140 GeV is provided by the rare $H \to \gamma\gamma$ decay mode [29] with a BR of $\mathcal{O}(10^{-3})$. In order to reject the large backgrounds from the $\gamma\gamma$ continuum production and the two–photon decay mode of the neutral pions, $\pi^0 \to \gamma\gamma$, the detection of the rare photonic

decay mode requires excellent energy and geometric resolution of the photon detectors (i.e., electromagnetic calorimeters) [29]. Thus the LHC studies conclude that the rare photonic decay mode will be the best possibility to find the SM Higgs particle in the lower mass range.

Above the ZZ threshold, on–shell $H \rightarrow ZZ \rightarrow 4l^{\pm}$ decays of the Higgs particle provide a very clean signature with small SM backgrounds [28]. Below the ZZ threshold, off–shell $H \rightarrow ZZ^{*} \rightarrow 4l^{\pm}$ decays, where one of the Z bosons is on–shell, yield clean signatures with rather small SM backgrounds [28]. However, in the mass range 155 GeV $\lesssim M_H \lesssim$ 180 GeV, where the ZZ BR drops down to values of about 2%, the number of events at the LHC allows for a discovery of the Higgs boson only if the maximal luminosity will be reached [29]. For such a value of the Higgs mass, the channel $H \rightarrow WW^{*} \rightarrow 2l^{\pm} +$ *missing energy*, provides the best chances.

For large Higgs masses the total Higgs decay width exceeds 100 GeV and reaches a value of about 600 GeV for $M_H = 1$ TeV, as seen in sect. 1.4.1. Thus the Higgs resonance peaks in the 4–lepton final states become broad and, owing to the decreasing number of events with growing Higgs mass, the signal $H \rightarrow ZZ \rightarrow 4l^{\pm}$ will no longer be visible. In order to extend the Higgs search to masses beyond 1 TeV, the decay modes $H \rightarrow ZZ, WW \rightarrow l^{+}l^{-}\nu\bar{\nu}$ will be the only possible signatures. Fig. 1.11 shows the expected signal significance at the ATLAS detector in the LHC experiment as a function of the SM Higgs mass after using the full experimental data samples. It is apparent that after reaching the full integrated luminosity, the SM Higgs signal may be extracted in the whole relevant mass region [29].

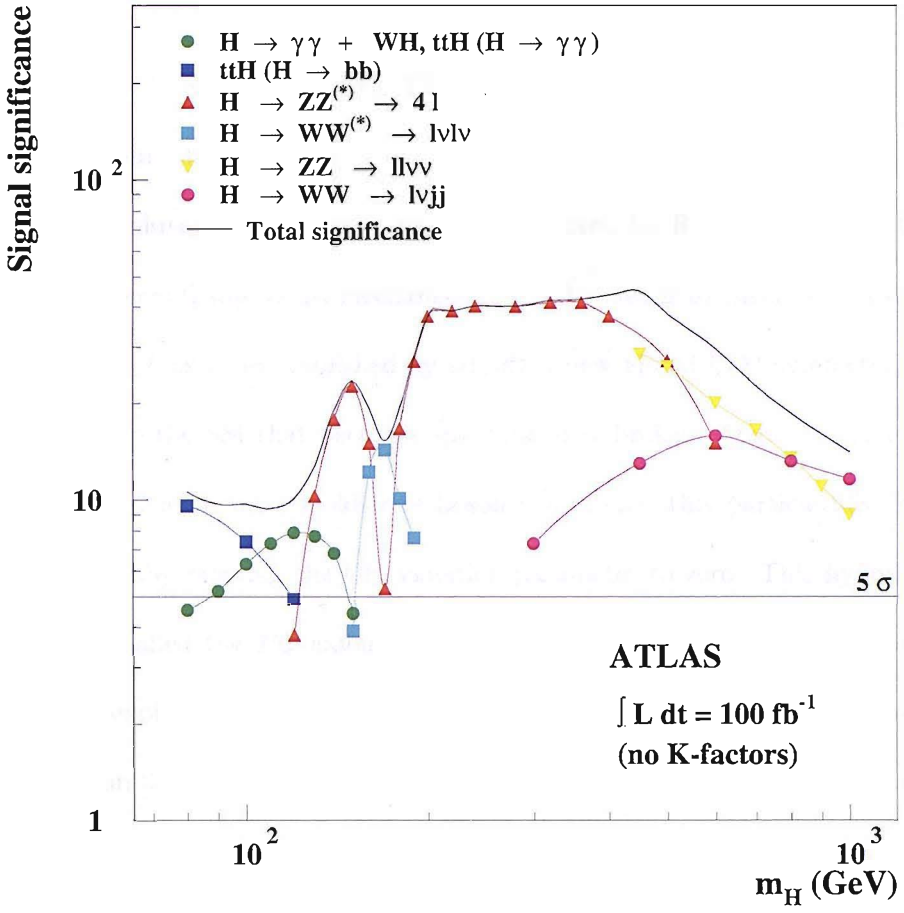

Figure 1.11: ATLAS sensitivity for the discovery of a SM Higgs boson for an integrated luminosity of 30 fb^{-1} over the full mass region. The signal significance is plotted for individual search channels as well as for the combination of channels [30].

1.5 Peccei-Quinn Mechanism

The QCD sector of the SM possesses a non-trivial vacuum structure that violates CP. Together with the CP–violating effects generated by the weak interactions [31], an effective strong CP–violating term, Θ, appears as an SM input parameter which is not predicted by the theory. However, large CP–violating interactions originating from QCD would result in a large electric dipole moment (EDM) for the neutron [32]. Experimental constraints on the currently unobserved neutron's EDM imply that CP violation arising from QCD must be extremely tiny and hence Θ must itself be extremely small or absent. Since a priori Θ could have any value between 0 and 2, the SM is faced

by another naturalness problem, that is, why should Θ be so close to 0? In other words, why should QCD be CP–preserving?. This question constitutes what is known as the strong CP problem [33].

An elegant solution to this problem was postulated by R. Peccei and H. Quinn, known as the Peccei-Quinn (PQ) mechanism [34]. The idea is to effectively promote Θ to a scalar field. This is accomplished by adding a new global U(1) symmetry, called PQ symmetry, to the SM that becomes spontaneously broken. Once this new global symmetry breaks, a massless Goldstone boson results and this particle fills the role of Θ, thus naturally relaxing the CP–violation parameter to zero. This hypothesised new particle is called the PQ-axion. The non-trivial QCD vacuum effects spoil the PQ symmetry explicitly and provide a small mass for the axion. Hence it is a pseudo–Goldstone boson [35].

1.6 Why The SM Does Not Suffice

At the end of this chapter we briefly revisit the reasons why the era of the SM seems to be approaching an end, giving way to new physics of which it would serve as only a low energy effective theory. The major shortcomings of the SM include:

1. The hierarchy and naturalness problems. The former basks in the unaccountability of the SM for physical phenomena that might exist between the EW and the Planck scales, while the latter arises as a result of the complete arbitrariness in the Higgs mass. Both these problems will be addressed in a greater detail in the next chapter.

2. No acceptable dark matter candidate. It is now an established fact that the universe constitutes only about 4% of the baryonic matter and the rest is made

up of dark matter and dark energy [36]. The only suitable dark matter candidate that the SM provides is the neutrino but there is no way this particle can be produced in the SM in quantities sufficient to account for the observed dark matter abundance. The neutrino also fails to comply with the relativistic and cosmological constraints on the dark matter [37, 38].

3. No true unification of gauge couplings at the GUT scale. This is a crucial factor deterring the SM from qualifying as a unified theory of nature.

4. Does not say anything about the fourth fundamental force of nature, the gravitational force.

5. Does not incorporate masses for the neutrinos despite the fact that their being massive has now been verified [39, 40].

6. Fails to explain the quantum numbers as well as the fermion mass patterns.

7. It has a fairly large number of unfixed parameters: 19 (+9 coming from a massive neutrino sector).

8. Does not generate CP–violation enough to justify the dominance of matter over anti–matter in the universe.

Chapter 2

Supersymmetry and The Minimal Supersymmetric Standard Model

2.1 Solving the SM Problems

2.1.1 Hierarchy and Naturalness

The Higgs potential in the SM, as seen in sect. 1.3.3, is given as

$$V = -\frac{1}{2}M_H^2|H|^2 + \frac{1}{4}\lambda|H|^4\,, \tag{2.1}$$

with the VEV for H, v, occurring at the minimum of the potential. Since we know experimentally that (at tree–level) v is approximately 174 GeV, from measurements of the properties of the weak interactions, it must be that M_H^2 is very roughly of order $-(100\text{ GeV})^2$. The problem is that M_H^2 receives enormous quantum corrections from the virtual effects of every particle that couples, directly or indirectly, to the Higgs

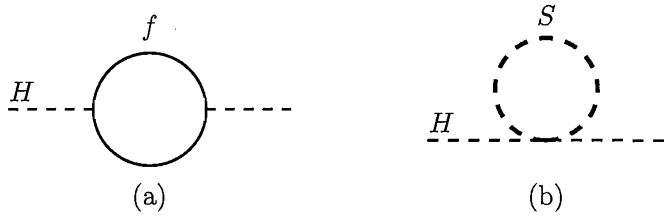

Figure 2.1: One–loop quantum corrections to the Higgs squared mass parameter M_H^2 due to (a) a Dirac fermion f and (b) a scalar S.

field.

For example, fig. 2.1a shows a correction to M_H^2 from a loop containing a Dirac fermion f with mass M_f. If the Higgs field couples to f with a term $-\lambda_f H\bar{f}f$ in the Lagrangian, then the Feynman diagram in fig. 2.1a yields a correction [41]

$$\Delta M_H^2 = \frac{\lambda_f^2}{8\pi^2}\left[-\Lambda_{\rm UV}^2 + 6m_f^2\ln(\frac{\Lambda_{\rm UV}}{m_f}) - 2m_f^2\right] + \mathcal{O}(1/\Lambda_{\rm UV}^2). \tag{2.2}$$

Here $\Lambda_{\rm UV}$ is an ultraviolet momentum cut–off used to regulate the loop integral; the energy scale at which new physics enters to alter the high–energy behaviour of the theory. The problem is that if $\Lambda_{\rm UV}$ is of order M_P (Planck mass), say, then this quantum correction to M_H^2 is some 30 orders of magnitude larger than the required value of $M_H^2 \sim -(100\text{ GeV})^2$. Thus, for the SM boson to stay relatively light, at least $M_H \lesssim 1$ TeV for unitarity and perturbativity reasons, we need to add a counterterm to the mass squared and adjust it with a precision of $\mathcal{O}(10^{-30})$, which seems highly unnatural. This is what is called the *naturalness* or *fine–tuning* problem [42].

A related question, the *hierarchy* problem, arises due to the existence of a large gap between the Higgs mass and the Planck scale, i.e., why $\Lambda_{\rm UV} >> m_Z$? Incidentally, these problems are only directly relevant for corrections to the Higgs scalar boson squared mass, because quantum corrections to fermion and gauge boson masses do not have the direct quadratic sensitivity to $\Lambda_{\rm UV}$ found in eq. (2.2). However, the quarks and leptons and the EW gauge bosons Z, $W^\pm$ of the SM all obtain masses from v, as seen in sect.

1.3.2, so that the entire mass spectrum of the SM is directly or indirectly sensitive to the cut–off $\Lambda_{\rm UV}$.

Furthermore, eq. (2.2) shows that there are contributions proportional to m_f^2 itself. Any arbitrarily heavy particles that might exist in nature will have similar virtual effects on the Higgs mass, besides the latter's dependence on the cut–off scale. For example, suppose there exists a number N_S of heavy complex scalar particle S with mass m_S and quadrilinear coupling to the Higgs boson given by λ_S, that couple to the Higgs with a Lagrangian term $-\lambda_S|H|^2|S|^2$. Then the Feynman diagram in fig. 2.1b gives a correction [41]

$$\Delta M_H^2 = \frac{\lambda_S}{16\pi^2}\left[-\Lambda_{\rm UV}^2 + 2m_S^2\ln(\frac{\Lambda_{\rm UV}}{m_S})\right] + \mathcal{O}(1/\Lambda_{\rm UV}). \tag{2.3}$$

Additionally, if m_S is very large, its effects in the SM also make it difficult to understand why M_H^2 is so small.

2.1.2 Supersymmetry: Our Rescue

The systematic cancellation of the dangerous contributions to ΔM_H^2 can only be brought about if we make the assumption that the Higgs coupling of the scalar particles are related to the Higgs–fermion couplings. In eqs. (2.2) and (2.3), if we set $\lambda_f^2 = 2m_f^2/v^2 = -\lambda_S$, the quadratic divergences due to $\Lambda_{\rm UV}$ disappear [43]. The logarithmic divergences, though still present, contribute very little for physically justifiable scalar masses, even for values $\Lambda_{\rm UV} \sim M_P$ of the cut–off. These logarithmic divergences disappear also if, in addition, we assume that the fermion and the two scalars have the same mass, $m_S = m_f$. In fact, in the latter case the total correction to the Higgs boson mass squared vanishes altogether.

The above cancellation strongly suggests that there ought to exist a new symmetry that relates fermions and bosons, because of the relative minus sign between fermion loop and boson loop contributions to ΔM_H^2, since λ_S must naturally be positive for the scalar potential to be bounded from below. If each of the quarks and leptons of the SM is accompanied by complex scalars with $-\lambda_S = \lambda_f^2$, then the $\Lambda_{\rm UV}^2$ contributions of figs. 2.1a and 2.1b will neatly cancel. This new symmetry is the one termed SUSY.

A SUSY transformation turns a bosonic state into a fermionic state and vice versa. The operator Q that generates such transformations must be an anticommuting spinor, so that

$$Q|\text{Boson}\rangle = |\text{Fermion}\rangle, \qquad Q|\text{Fermion}\rangle = |\text{Boson}\rangle. \tag{2.4}$$

Spinors are intrinsically complex objects, so $Q^\dagger$ (the hermitian conjugate of Q) is also a SUSY generator.

The single–particle states of a supersymmetric theory fall into irreducible representations of the SUSY algebra, called *supermultiplets*. Each supermultiplet contains both fermion and boson states, which are commonly known as *superpartners* of each other. Since the squared–mass operator $-P^2$ commutes with the operators Q and $Q^\dagger$, it follows that particles inhabiting the same supermultiplet must have equal masses. The SUSY generators Q and $Q^\dagger$ also commute with the generators of gauge transformations. Therefore, particles in the same supermultiplet must also be in the same representation of the gauge group, and so must have the same electric charges, weak isospin and colour degrees of freedom. Moreover, each supermultiplet contains an equal number of fermion and boson degrees of freedom, $n_B = n_F$??.

2.2 The Minimal Supersymmetric Standard Model

2.2.1 Minimal Particle Content

The invocation of SUSY in the SM, with minimally extended particle content, results in the Minimal Supersymmetric Standard Model (MSSM) [45]. All of the known fundamental particles of the SM lie in supermultiplets, which can be classified into two types, namely *chiral* and *gauge* supermultiplets, and possess a superpartner with spin differing by 1/2 unit. The chiral supermultiplets contain SM fermions whose left–handed parts transform differently under the SU(2) gauge group than their right–handed parts. These left–handed and right–handed parts of quarks and leptons are thus separate two–component *Weyl* fermions so each must have its own complex scalar partner. They are called *squarks* and *sleptons*. A '$\sim$' is used on top of the symbol for an SM particle to denote its superpartner. The gauge interactions of each of these squark and slepton fields are the same as for the corresponding SM fermions; for instance, the left–handed squarks $\tilde{u}_L$ and $\tilde{d}_L$ couple to the W boson, while $\tilde{u}_R$ and $\tilde{d}_R$ do not.

Clearly, the Higgs boson must also reside in a chiral supermultiplet. However, one Higgs chiral supermultiplet does not turn out to be enough. Because of the structure of supersymmetric theories (analytic, as will be explained later), only a $Y = +1$ Higgs chiral supermultiplet can have the Yukawa couplings necessary to give masses to charge $+2/3$ up–type quarks (up, charm, top), and only a $Y = -1$ Higgs can have the Yukawa couplings necessary to give masses to charge $-1/3$ down–type quarks (down, strange, bottom) and to the charged leptons. Besides, two Higgs supermultiplets are also essential for the cancellation of gauge anomalies originating from triangular fermionic loops involving axial–vector current couplings [46]. The $SU(2)_L$–doublet complex scalar fields with $Y = +1$ and $Y = -1$ are referred to as H_u and H_d, respectively.

Names		spin 0	spin 1/2	$SU(3)_C$, $SU(2)_L$, $U(1)_Y$
squarks, quarks	Q	$(\tilde{u}_L \;\; \tilde{d}_L)$	$(u_L \;\; d_L)$	$(\mathbf{3}, \mathbf{2}, \frac{1}{6})$
(×3 families)	$\bar{u}$	$\tilde{u}_R^*$	$u_R^\dagger$	$(\overline{\mathbf{3}}, \mathbf{1}, -\frac{2}{3})$
	$\bar{d}$	$\tilde{d}_R^*$	$d_R^\dagger$	$(\overline{\mathbf{3}}, \mathbf{1}, \frac{1}{3})$
sleptons, leptons	L	$(\tilde{\nu} \;\; \tilde{e}_L)$	$(\nu \;\; e_L)$	$(\mathbf{1}, \mathbf{2}, -\frac{1}{2})$
(×3 families)	$\bar{e}$	$\tilde{e}_R^*$	$e_R^\dagger$	$(\mathbf{1}, \mathbf{1}, 1)$
Higgs, higgsinos	H_u	$(H_u^+ \;\; H_u^0)$	$(\tilde{H}_u^+ \;\; \tilde{H}_u^0)$	$(\mathbf{1}, \mathbf{2}, +1)$
	H_d	$(H_d^0 \;\; H_d^-)$	$(\tilde{H}_d^0 \;\; \tilde{H}_d^-)$	$(\mathbf{1}, \mathbf{2}, -1)$

Table 2.1: Chiral supermultiplets in the MSSM. The spin–0 fields are complex scalars while the spin–1/2 fields are left–handed two–component Weyl fermions.

The physical Higgs bosons emerge from linear combinations of H_u^0 and H_d^0. The fermionic partners of the Higgs scalars are called higgsinos. They are denoted by $\tilde{H}_u$, $\tilde{H}_d$ for the $SU(2)_L$-doublet left–handed Weyl spinor fields, with weak isospin components $\tilde{H}_u^+$, $\tilde{H}_u^0$ and $\tilde{H}_d^0$, $\tilde{H}_d^-$. All the chiral supermultiplets of the MSSM are listed in tab. 2.1, classified according to their transformation properties under the SM gauge group $SU(3)_C \times SU(2)_L \times U(1)_Y$, which combines u_L, d_L and ν, e_L degrees of freedom into $SU(2)_L$ doublets.

The vector bosons of the SM reside in gauge supermultiplets. Their fermionic superpartners are generically referred to as gauginos. The $SU(3)_C$ colour gauge interactions of QCD are mediated by the gluon, whose spin–1/2 colour–octet supersymmetric partner is the gluino. The symbols for the gluon and gluino are g and $\tilde{g}$ respectively. The $SU(2)_L \times U(1)_Y$ gauge symmetry is associated with the spin–1 gauge bosons W^+, W^0, W^- and B^0, with spin–1/2 superpartners $\tilde{W}^+, \tilde{W}^0, \tilde{W}^-$ and $\tilde{B}^0$, called *winos* and *bino*, respectively. After EWSB, the W^0, B^0 gauge eigenstates mix to give mass eigenstates Z and γ. The corresponding gaugino mixtures of $\tilde{W}^0$ and $\tilde{B}^0$ are called zino ($\tilde{Z}$) and photino ($\tilde{\gamma}$). The fermionic SUSY counterparts of Higgses are called *Higgsinos*, which also mix with the winos and the bino to give two chargino, $\chi^\pm$, and four

Names	spin 1/2	spin 1	$SU(3)_C$, $SU(2)_L$, $U(1)_Y$
gluino, gluon	$\tilde{g}$	g	(**8**, **1** , 0)
winos, W bosons	$\tilde{W}^{\pm}$ $\tilde{W}^0$	$W^{\pm}$ W^0	(**1**, **3** , 0)
bino, B boson	$\tilde{B}^0$	B^0	(**1**, **1** , 0)

Table 2.2: Gauge supermultiplets in the MSSM.

neutralino, $\chi^0_{1,2,3,4}$, mass eigenstates. Tab. 2.2 summarizes the gauge supermultiplets of the MSSM.

2.2.2 Soft SUSY Breaking

If SUSY were an exact symmetry of nature, there would be selectrons $\tilde{e}_L$ and $\tilde{e}_R$ with masses exactly equal to m_e, and likewise all other squarks, sleptons and gauginos with masses exactly equal to their SM counterparts. However, none of such superpartners of the SM particles have been discovered thus far. This means that SUSY cannot be an exact symmetry, and hence must be broken at some scale (at or) above the EW scale. But we need SUSY–breaking to occur in a way such that the supersymmetric particles are not too heavy as to reintroduce the hierarchy problem. Thus, if broken SUSY is still to provide a solution to the hierarchy problem, the relationships between dimensionless couplings (e.g., $\lambda_f = -\lambda_S$, as seen in sect. 2.1.2) which hold in the unbroken supersymmetric theory must be maintained. Also, in the breaking of SUSY we need to preserve the gauge invariance and the renormalisability of the theory.

Unfortunately, there is no completely satisfactory dynamical way to break SUSY, although there have been quite a few suggestions such as spontaneous SUSY breaking, gravity–mediated SUSY–breaking, and gauge–mediated SUSY–breaking [47, 44]. The most plausible way of breaking SUSY is to do it *softly*, that is, introducing in the MSSM Lagrangian mass terms and coupling parameters with positive mass dimension that

explicitly break SUSY. Such terms result only in logarithmic divergences in the radiative corrections to the scalar masses as the cancellation of quadratically divergent terms is maintained naturally to all orders in perturbation theory. In this way we parameterise our ignorance of the fundamental SUSY–breaking mechanism. The effective Lagrangian of the MSSM now has the form

$$\mathcal{L} = \mathcal{L}_{\text{SUSY}} + \mathcal{L}_{\text{soft}}, \tag{2.5}$$

where $\mathcal{L}_{\text{SUSY}}$ is the SUSY–preserving part containing the usual kinetic and potential terms for the various fields of the model, while $\mathcal{L}_{\text{soft}}$ contains the explicit soft SUSY–breaking terms that include

- mass terms for the gluinos, winos and binos:

$$-\mathcal{L}_{\text{gaugino}} = \frac{1}{2}\left[M_1\tilde{B}\tilde{B} + M_2\sum_{a=1}^{3}\tilde{W}^a\tilde{W}_a + M_3\sum_{a=1}^{8}\tilde{G}^a\tilde{G}_a \;+\; \text{h.c.}\right], \tag{2.6}$$

- mass terms for the scalar fermions:

$$-\mathcal{L}_{\text{sfermions}} = \sum_{i=gen} m^2_{\tilde{Q}_i}\tilde{Q}_i^\dagger\tilde{Q}_i + m^2_{\tilde{L}_i}\tilde{L}_i^\dagger\tilde{L}_i + m^2_{\tilde{u}_i}|\tilde{u}_{R_i}|^2 + m^2_{\tilde{d}_i}|\tilde{d}_{R_i}|^2 + m^2_{\tilde{\ell}_i}|\tilde{\ell}_{R_i}|^2, \tag{2.7}$$

- mass and bilinear terms for the Higgs bosons:

$$-\mathcal{L}_{\text{Higgs}} = m_1^2 H_d^\dagger H_d + m_2^2 H_u^\dagger H_u + B\mu(H_u\cdot H_d + \text{h.c.}), \tag{2.8}$$

- trilinear couplings between sfermions and Higgs bosons

$$-\mathcal{L}_{\text{tril.}} = \sum_{i,j=gen}\left[A^u_{ij}Y^u_{ij}\tilde{u}^*_{R_i}H_u\cdot\tilde{Q}_j + A^d_{ij}Y^d_{ij}\tilde{d}^*_{R_i}H_d\cdot\tilde{Q}_j + A^l_{ij}Y^\ell_{ij}\tilde{\ell}^*_{R_i}H_d\cdot\tilde{L}_j \;+\; \text{h.c.}\right]. \tag{2.9}$$

If the largest mass scale associated with the above soft terms is denoted $m_{\rm soft}$, then the additional non–supersymmetric corrections to M_H^2 must vanish in the $m_{\rm soft} \to 0$ limit, so by dimensional analysis they cannot be proportional to $\Lambda_{\rm UV}^2$. Such corrections cannot go like $\delta M_H^2 \sim m_{\rm soft}\Lambda_{\rm UV}$ either, because in general the loop integrals always diverge either quadratically or logarithmically, not linearly, as $\Lambda_{\rm UV} \to \infty$. However, $m_{\rm soft}$, and therefore the masses of at least the lightest few superpartners, should ideally be at the most about 1 TeV or so, in order for the MSSM scalar potential to provide a Higgs VEV resulting in m_W and m_Z equal to the experimentally observed values.

2.2.3 The Constrained MSSM

Unlike the supersymmetric part of the MSSM Lagrangian, $\mathcal{L}_{\rm soft}$ introduces many new parameters that are not present in the ordinary SM. With the inter–generational mixings and complex phases, one ends up with a huge number (105) of unknown parameters in addition to the 19 parameters of the SM [48]. Fortunately, most of these new parameters involve flavour mixing and CP–violation of the type which is already severely restricted by the experiment. Thus, a phenomenologically more viable MSSM can be defined by making the following assumptions:

1. All the soft SUSY–breaking parameters are real and therefore there is no new source of CP–violation generated, in addition to the one from the CKM matrix.

2. The matrices for the sfermion masses and for the trilinear couplings are all diagonal, implying the absence of FCNCs at the tree–level.

3. The soft SUSY–breaking masses and trilinear couplings of the first and second sfermion generations are the same at low energy to cope with the severe constraints from K^0–$\bar{K}^0$ mixing *etc.*

Making these three assumptions will lead to only 22 input parameters [41]:

$\tan\beta$: the ratio of the VEVs of the two Higgs doublet fields;

$M^2_{H_1}, M^2_{H_2}$: the Higgs mass parameters squared;

M_1, M_2, M_3: the bino, wino and gluino mass parameters;

$m_{\tilde{q}}, m_{\tilde{u}_R}, m_{\tilde{d}_R}, m_{\tilde{l}}, m_{\tilde{e}_R}$: the first/second generation sfermion mass parameters;

$A_{\tilde{u}}, A_{\tilde{d}}, A_{\tilde{e}}$: the first/second generation trilinear couplings;

$m_{\tilde{Q}}, m_{\tilde{t}_R}, m_{\tilde{b}_R}, m_{\tilde{L}}, m_{\tilde{\tau}_R}$: the third generation sfermion mass parameters;

$A_{\tilde{t}}, A_{\tilde{b}}, A_{\tilde{\tau}}$: the third generation trilinear couplings.

Such a model with relatively moderate number of parameters has much more predictability and is much easier to investigate phenomenologically, compared to the unconstrained MSSM, given the fact that in general only a small subset appears when one looks at a particular sector of the model. This model with 22 free input parameters is generally referred to as the 'phenomenological' MSSM or pMSSM [49].

Next, we assume that the soft SUSY–breaking parameters obey a set of universal boundary conditions at the GUT scale. We make use of the fact that all SUSY–breaking models are indicative of an underlying simplicity or symmetry of the Lagrangian at some very high energy scale Q_0. For example, if SUSY–breaking occurs in a hidden sector which communicates with the visible sector only through gravitational–strength interactions, as specified by *Supergravity*, universal soft breaking terms then emerge if these interactions are 'flavour–blind' (like ordinary gravitational interactions). This is assumed to be the case in the constrained MSSM (cMSSM) or minimal Supergravity (mSUGRA) model [50].

The unification condition for gauge coupling constants $g_{1,2,3}$ follows directly from their unification at a very high scale in the MSSM. The 1–loop renormalisation group (RG) equations for the gauge couplings g_1, g_2, g_3 in the SM and the MSSM are given

as

$$\beta_{g_a} \equiv \frac{d}{dt} g_a = \frac{1}{16\pi^2} b_a g_a^3, \qquad (b_1, b_2, b_3) = \begin{cases} (41/10,\ -19/6,\ -7) & \text{SM} \\ (33/5,\ 1,\ -3) & \text{MSSM} \end{cases}, \quad (2.10)$$

where $t = \ln(Q/Q_0)$, with Q being the RG scale. The MSSM coefficients are different because of the extra particles in the loops. Here the renormalisation for g_1 has been chosen to agree with the canonical covariant derivative for grand unification of the gauge group $SU(3)_C \times SU(2)_L \times U(1)_Y$ into SU(5) or SO(10). In terms of the conventional EW gauge couplings g and g' with $e = g \sin\theta_W = g' \cos\theta_W$, one has $g_2 = g$ and $g_1 = \sqrt{5/3} g'$. The reciprocal of $\alpha_a = g_a^2/4\pi$ in turn runs linearly with the RG scale at one–loop order:

$$\frac{d}{dt} \alpha_a^{-1} = -\frac{b_a}{2\pi} \quad (2.11)$$

Clearly, as fig. 2.2 shows, the MSSM includes just the right particle content to ensure that the gauge couplings can unify at a scale $M_U \sim 2 \times 10^{16}$ GeV below M_P, hinting at a grand unification theory (GUT) based on SUSY. Furthermore, a similar RG analysis can be expected to be reasonably applicable to other MSSM couplings and soft masses as well. Thus for the cMSSM we have:

- unification of the gaugino masses: $M_1 = M_2 = M_3 \equiv m_{1/2}$,
- universal sfermion masses: $m_{\tilde{Q}_i} = m_{\tilde{u}_{Ri}} = m_{\tilde{d}_{Ri}} = m_{\tilde{\ell}_{Li}} = m_{\tilde{\ell}_{Ri}} = m_0$ (i = generation),
- universal trilinear couplings: $A^u_{ij} = A^d_{ij} = A^\ell_{ij} \equiv A_0 \delta_{ij}$,

all defined at the GUT scale M_U.

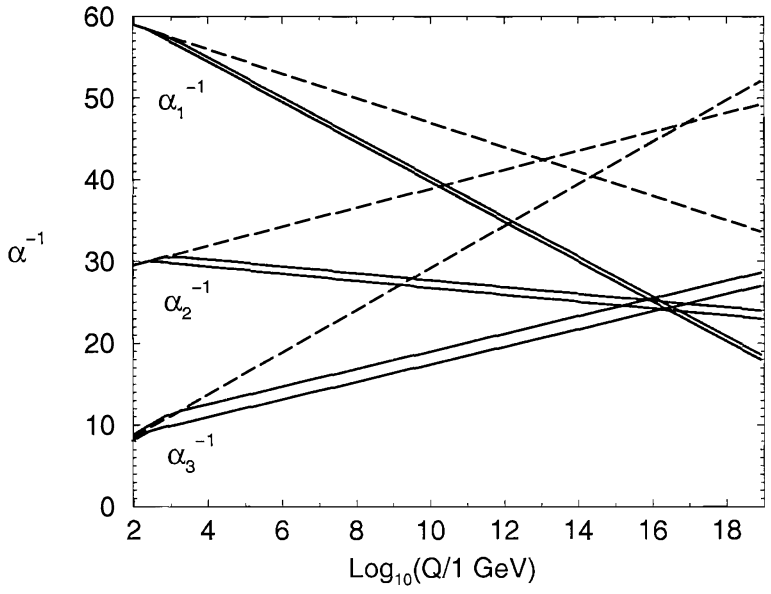

Figure 2.2: RG evolution of the inverse gauge couplings $\alpha_a^{-1}(Q)$ in the SM (dashed lines) and the MSSM (solid lines). In the MSSM case, the sparticle mass thresholds are varied between 250 GeV and 1 TeV, and $\alpha_3(m_Z)$ between 0.113 and 0.123. Two–loop effects are included.

Besides these three free parameters $m_{1/2}$, m_0 and A_0, the supersymmetric sector is described at the GUT scale by the bilinear coupling B and the supersymmetric Higgs(ino) mass parameter μ. However, EWSB results in two necessary minimization conditions of the two–Higgs doublet scalar potential which fix the values of μ^2 and $B\mu$ with the sign of μ not determined. Therefore, in the cMSSM, one is left with only four extra continuous free parameters, and an unknown sign:

$$\tan\beta \ , \ m_{1/2} \ , \ m_0 \ , \ A_0 \ , \ \ \mathrm{sign}(\mu). \tag{2.12}$$

The parameter $\tan\beta$ will be defined in the next subsection. Some of these parameters can be traded off for others belonging, in particular, to the Higgs sector of the MSSM[1]. All soft SUSY–breaking parameters at the weak scale are then obtained via RG equations [51].

[1]Hereafter, the acronym MSSM actually implies cMSSM.

2.3 Higgs sector of the MSSM

2.3.1 The Superpotential and R–Parity

In order to derive the scalar potential in the MSSM (or any other supersymmetric model) we first need to define a *superpotential* [44]. The superpotential is written in terms of the scalar fields ϕ_i treated as complex variables such that:

1. It must be a function of the superfields z_i only and not their conjugate z_i^*.

2. It should be an analytic function and, therefore, it has no derivative interaction.

3. It should have only terms of dimension 2 and 3 to keep the theory renormalisable.

The simplest possible MSSM superpotential satisfying the above conditions can be written as

$$W_{\rm MSSM} = \hat{Q}\hat{H}_u \mathbf{h_u} \hat{U}^C + \hat{H}_d \hat{Q} \mathbf{h_d} \hat{D}^C + \hat{H}_d \hat{L} \mathbf{h_e} \hat{E}^C + \mu \hat{H}_u \hat{H}_d. \tag{2.13}$$

where $\mathbf{h_u}$, $\mathbf{h_d}$ and $\mathbf{h_e}$ are dimensionless Yukawa coupling parameters. Notice, however, that the most general gauge-invariant and renormalisable superpotential could also include terms such as [44]:

$$W_{\Delta \rm L=1} = \frac{1}{2}\lambda^{ijk} L_i L_j \bar{e}_k + \lambda'^{ijk} L_i Q_j \bar{d}_k + \mu'^i L_i H_u \tag{2.14}$$

$$W_{\Delta \rm B=1} = \frac{1}{2}\lambda''^{ijk} \bar{u}_i \bar{d}_j \bar{d}_k \tag{2.15}$$

where $i = 1, 2, 3$ denote the family indices. The chiral supermultiplets carry baryon number assignments B= $+1/3$ for Q_i; B= $-1/3$ for $\bar{u}_i, \bar{d}_i$; and B= 0 for all others. The total lepton number (L) assignments are L= $+1$ for L_i, L= -1 for $\bar{e}_i$, and L= 0 for all others. Clearly, the terms in eq. (2.14) violate total lepton number by 1 unit (as

well as the individual lepton flavors) and those in eq. (2.15) violate baryon number by 1 unit. The problem is that the corresponding B– and L–violating processes have not been observed experimentally.

Therefore, one adds a new symmetry in the MSSM which has the effect of eliminating the possibility of B– and L– violating terms in the renormalisable superpotential, while allowing the good terms in eq. (2.13). This new symmetry is a discrete $\mathbb{Z}_2$ symmetry called 'R-parity' [52]. It is a multiplicatively conserved quantum number defined for each particle as

$$P_R = (-1)^{3(B-L)+2s} \tag{2.16}$$

where s is the spin of the particle. Evidently, all of the SM particles and the Higgs bosons have even R–parity ($P_R = +1$), while all of the squarks, sleptons, gauginos, and higgsinos have odd R-parity ($P_R = -1$). The symmetry principle to be enforced is that a candidate term in the Lagrangian (or in the superpotential) is allowed only if the product of P_R for all of the fields in it is $+1$. It is easy to see that each of the terms in eqs. (2.14) and (2.15) is thus forbidden, while the good and necessary terms in eq. (2.13) are allowed. The advantage of R–parity is that it can in principle be an *exact* and fundamental symmetry, which B and L themselves cannot, since they are known to be violated by non-perturbative EW effects.

The imposition of exact R-parity on the MSSM forbids any mixing between the sparticles and the $P_R = +1$ particles. Furthermore, every interaction vertex in the theory contains an even number of $P_R = -1$ sparticles. This has three extremely important phenomenological consequences:

- The lightest supersymmetric particle (LSP), with $P_R = -1$, must be absolutely

stable. If the LSP is electrically neutral, it interacts only weakly with ordinary matter, and so can make an attractive candidate [53] for non-baryonic dark matter required by cosmology.

- Each sparticle other than the LSP must eventually decay into a state that contains an odd number of LSPs (usually just one).

- In collider experiments, sparticles can only be produced in even numbers.

2.3.2 The Higgs Potential

As stated earlier, two doublets of complex scalar fields of opposite hypercharge are needed to break the EW symmetry in the MSSM:

$$H_u = \begin{pmatrix} H_u^+ \\ H_u^0 \end{pmatrix} \text{ with } Y_{H_u} = +1 \quad H_d = \begin{pmatrix} H_d^0 \\ H_d^- \end{pmatrix} \text{ with } Y_{H_d} = -1. \tag{2.17}$$

The so called 'F–terms' [54] in the scalar Higgs potential of the MSSM are obtained by taking the derivative of the superpotential with respect to all the scalar fields i.e., $|\partial W(\phi_i)/\partial\phi_i|^2$, thus giving, for the superpotential in eq. (2.13),

$$V_F = \mu^2(|H_d|^2 + |H_u|^2). \tag{2.18}$$

There are also the 'D–terms' [55] contributing to the Higgs potential. These terms include the quartic Higgs interactions and, for the two Higgs fields H_u and H_d, are given by

$$\begin{aligned} \mathrm{U(1)_Y} \quad &: \quad V_D^1 = \frac{1}{2}\left[\frac{g_1}{2}(|H_u|^2 - |H_d|^2)\right]^2, \\ \mathrm{SU(2)_L} \quad &: \quad V_D^2 = \frac{1}{2}\left[\frac{g_2}{2}(H_u^{i*}\tau_{ij}^a H_u^j + H_d^{i*}\tau_{ij}^a H_d^j)\right]^2, \end{aligned} \tag{2.19}$$

with $\tau^a = 2T^a$. Using the SU(2) identity $\tau^a_{ij}\tau^a_{kl} = 2\delta_{il}\delta_{jk} - \delta_{ij}\delta_{kl}$, one obtains the D-potential

$$V_D = \frac{g_2^2}{8}\left[(|H_u|^2)^2 + (|H_d|^2)^2 + 4|H_u \cdot H_d^\dagger|^2 - 2|H_u|^2|H_d|^2\right] + \frac{g_1^2}{8}(|H_u|^2 - |H_d|^2)^2. \quad (2.20)$$

Finally, there's a portion in the Lagrangian containing the soft SUSY–breaking scalar mass terms and the bilinear term

$$V_{\text{soft}} = m_1^2 H_d^\dagger H_d + m_2^2 H_u^\dagger H_u + B\mu(H_u \cdot H_d + \text{h.c.}). \quad (2.21)$$

The full scalar potential involving the Higgs fields is then the sum of the three terms, $V_H = V_F + V_D + V_{\text{soft}}$ [56], given as:

$$\begin{aligned} V_H &= \overline{m}_1^2|H_d|^2 + \overline{m}_2^2|H_u|^2 - \overline{m}_3^2\epsilon_{ij}(H_d^i H_u^j + \text{h.c.}) \\ &\quad + \frac{g_2^2 + g_1^2}{8}(|H_d|^2 - |H_u|^2)^2 + \frac{1}{2}g_2^2|H_d^\dagger H_u|^2, \end{aligned} \quad (2.22)$$

where the three mass squared terms are defined as

$$\overline{m}_1^2 = |\mu|^2 + m_1^2\,, \;\; \overline{m}_2^2 = |\mu|^2 + m_2^2\,, \;\; \overline{m}_3^2 = B\mu. \quad (2.23)$$

The minimum of the potential V_H breaks the SU(2)$_L\times$ U(1)$_Y$ symmetry for $\mu^2 < 0$ such that $\langle\frac{\partial V}{\partial H_u^0}\rangle = 0$ and $\langle\frac{\partial V}{\partial H_d^0}\rangle = 0$, and the neutral components of the two Higgs fields develop VEVs

$$\langle H_u^0\rangle = \frac{v_u}{\sqrt{2}} \;\; , \;\; \langle H_d^0\rangle = \frac{v_d}{\sqrt{2}}. \quad (2.24)$$

Just as in the SM, we chose the VEV of the field H_d^- to be zero, $\langle H_d^-\rangle$=0, making use

of the of SU(2) symmetry. At $\partial V/\partial H_d^-$=0, one then automatically obtains $\langle H_u^+ \rangle = 0$. Hence no breaking occurs in the charged directions and the QED symmetry is preserved. Here we define two important new SUSY parameters: $\tan\beta \equiv v_u/v_d$ and $v \equiv \sqrt{v_u^2 + v_d^2}$. The couplings of the MSSM Higgses to the particles and sparticles can be obtained from the kinetic terms in the Lagrangian in the usual way. For the SM fermions and bosons, these couplings, normalised to the corresponding SM couplings, are given in tab. 2.3.

	Φ	g_u^Φ	g_d^Φ	g_V^Φ
SM	H	1	1	1
MSSM	h	$\cos\alpha/\sin\beta$	$-\sin\alpha/\cos\beta$	$\sin(\beta-\alpha)$
	H	$\sin\alpha/\sin\beta$	$\cos\alpha/\cos\beta$	$\cos(\beta-\alpha)$
	A	$1/\tan\beta$	$\tan\beta$	0

Table 2.3: Higgs couplings to SM fermions and bosons in the MSSM.

2.3.3 Mass Spectrum

To obtain the physical Higgs fields and their masses, the complex scalar fields H_d and H_u are then developed around the vacuum, into real and imaginary parts

$$\begin{aligned} H_u = (H_u^+, H_u^0) &= \frac{1}{\sqrt{2}}\left(H_u^+ \ , \ v_u + H_u^0 + iP_u^0\right), \\ H_d = (H_d^0, H_d^-) &= \frac{1}{\sqrt{2}}\left(v_d + H_d^0 + iP_d^0 \ , \ H_d^-\right), \end{aligned} \tag{2.25}$$

where the real parts correspond to the CP–even Higgs bosons and the imaginary parts correspond to the CP–odd Higgs and the Goldstone bosons. The mass matrices are then evaluated as

$$\mathcal{M}_{ij}^2 = \frac{1}{2}\left.\frac{\partial^2 V_H}{\partial H_i \partial H_j}\right|_{\langle H_d^0\rangle=\frac{v_d}{\sqrt{2}},\langle H_u^0\rangle=\frac{v_u}{\sqrt{2}},\langle H_{1,2}^\pm\rangle=0}, \tag{2.26}$$

with $i, j = u, d$. In the case of the CP–even Higgs bosons, this gives a mass matrix of the form [41]

$$\mathcal{M}_R^2 = \begin{bmatrix} -\overline{m}_3^2 \tan\beta + m_Z^2 \cos^2\beta & \overline{m}_3^2 - m_Z^2 \sin\beta\cos\beta \\ \overline{m}_3^2 - m_Z^2 \sin\beta\cos\beta & -\overline{m}_3^2 \cot\beta + m_Z^2 \sin^2\beta \end{bmatrix}. \tag{2.27}$$

And the CP–odd mass matrix is obtained as

$$\mathcal{M}_I^2 = \begin{bmatrix} -\overline{m}_3^2 \tan\beta & \overline{m}_3^2 \\ \overline{m}_3^2 & -\overline{m}_3^2 \cot\beta \end{bmatrix}, \tag{2.28}$$

where $\mathrm{Det}\mathcal{M}_I^2 = 0$, and so the diagonalisation of this mass matrix results in a massless Goldstone state which makes up the longitudinal component of the Z boson. This rotation is carried out as

$$\begin{pmatrix} G^0 \\ A \end{pmatrix} = \begin{pmatrix} \cos\beta & \sin\beta \\ -\sin\beta & \cos\beta \end{pmatrix} \begin{pmatrix} P_d^0 \\ P_u^0 \end{pmatrix}, \tag{2.29}$$

resulting in one pseudoscalar Higgs boson with mass

$$M_A^2 = -\overline{m}_3^2(\tan\beta + \cot\beta) = -\frac{2\overline{m}_3^2}{\sin 2\beta}. \tag{2.30}$$

Similarly, one of the charged scalar fields can be rotated away as a Goldstone state to be eaten up by the W boson:

$$\begin{pmatrix} G^\pm \\ H^\pm \end{pmatrix} = \begin{pmatrix} \cos\beta & \sin\beta \\ -\sin\beta & \cos\beta \end{pmatrix} \begin{pmatrix} H_d^\pm \\ H_u^\pm \end{pmatrix}, \tag{2.31}$$

and we are left with a charged Higgs boson having mass

$$M_{H^\pm}^2 = M_A^2 + m_W^2. \tag{2.32}$$

The physical CP–even Higgs states are obtained with the help of angle α defined as

$$\alpha = \frac{1}{2}\arctan\left(\tan 2\beta \frac{M_A^2 + m_Z^2}{M_A^2 - m_Z^2}\right), \quad -\frac{\pi}{2} \leq \alpha \leq 0. \tag{2.33}$$

The rotation of the CP–even mass matrix through the angle α,

$$\begin{pmatrix} H \\ h \end{pmatrix} = \begin{pmatrix} \cos\alpha & \sin\alpha \\ -\sin\alpha & \cos\alpha \end{pmatrix} \begin{pmatrix} H_d^0 \\ H_u^0 \end{pmatrix}, \tag{2.34}$$

yields the masses of the two CP–even Higgs bosons of the MSSM,

$$M_{h,H}^2 = \frac{1}{2}\left[M_A^2 + m_Z^2 \mp \sqrt{(M_A^2 + m_Z^2)^2 - 4M_A^2 m_Z^2 \cos^2 2\beta}\right]. \tag{2.35}$$

where h (H) corresponds to the lighter (heavier) of the two CP–even Higgses. From these relations we obtain important constraints on the masses of the charged and the heavy CP–even Higgs boson as

$$M_H > \max(M_A, m_Z) \quad \text{and} \quad M_{H\pm} > m_W, \tag{2.36}$$

and, more crucially, an upper bound on the the lightest h boson mass at the tree–level,

$$M_h \leq \min(M_A, m_Z) \cdot |\cos 2\beta| \leq m_Z. \tag{2.37}$$

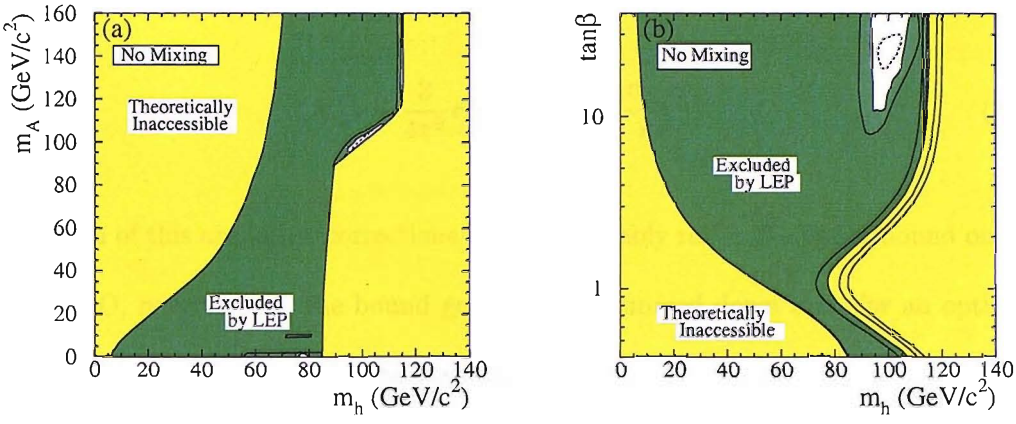

Figure 2.3: Exclusions in the MSSM parameter space from LEP2 in the case of the no–mixing benchmark scenario. Note the small domain at M_h between 75 and 80 GeV/c^2, small M_A and $\tan\beta < 0.7$ which is not excluded at the 95% C.L. [57]

However, the h mass eigenstate is subject to quite significant quantum corrections, with the largest one typically coming from the top and stop loops due to their large Yukawa and trilinear couplings, respectively, to h. A very important parameter in this regard, originating from the stop sector of the MSSM, is the stop mixing defined as $X_t = A_t - \mu \cot\beta$, which governs the mass splitting between the two stop mass eigenstates $\tilde{t}_1$ and $\tilde{t}_2$. The radiative corrections due to stop loops depend heavily on this parameter and this, in turn, causes notable variation of the upper limit on M_h. The bound is maximized when $X_t = \sqrt{6} M_{\mathrm{SUSY}}$, the 'maximal mixing scenario', and minimized when $X_t = 0$, the 'no–mixing scenario'. The latter scenario has been excluded by negative Higgs searches at LEP2 over almost the entire MSSM parameter space, as depicted by fig. 2.3. Therefore, we will concentrate on the maximal stop mixing scenario, also referred to as $M_h - max$ scenario, for the rest of this chapter.

In the limit of stop masses $m_{\tilde{t}_1}$, $m_{\tilde{t}_2}$ much greater than the top quark mass m_t, one

finds a one–loop radiative correction to eq. (2.37):

$$\delta(M_h^2) = \frac{3}{4\pi^2} v^2 h_t^4 \sin^4\beta \ln\left(\frac{m_{\tilde{t}_1\tilde{t}_2}}{m_t^2}\right). \tag{2.38}$$

Inclusion of this and other corrections [58] considerably raises the upper bound on M_h. At NNLO, nevertheless, the bound gets slightly trimmed down and (for an optimum choice of parameters) one obtains roughly

$$M_h \lesssim 130 \text{ GeV}. \tag{2.39}$$

2.4 Phenomenology of the MSSM Neutral Higgs sector

2.4.1 Production and Decay

The production modes of the neutral MSSM Higgses remain essentially the same as in the SM, described in sect. 1.4.2. The decay modes of the Higgses, on the other hand, are complemented by the tree–level decays, when kinematically allowed, into pairs of sparticles as well as into those of lighter Higgses. In the case of sparticles, such decays are strongly suppressed due to their small couplings to the Higgses. Sparticles are also generally considered to not contribute substantially to the loop induced decays of Higgs, such as $H \to \gamma\gamma/gg$, or to the higher order corrections in the production and decay processes, due to their heavy masses. However, some SUSY particles such as chargino, neutralinos and possibly sleptons and third generation squarks could, in principle, be light enough to play a non–negligible role in such decays [13, 41].

In addition to the effects of the new particles, Higgs phenomenology in the MSSM is also strongly manipulated by certain new parameters of the model. For example, the couplings of the lighter Higgs h to down–type fermions are strongly enhanced for large

values of the parameter $\tan\beta$. Fig. 2.4 shows the dependence of the Higgs prodction cross–section on the value of $\tan\beta$ at the LHC. Clearly, the gg production mode of h dominates except for large values of $\tan\beta$ and h mass of order 100 GeV, where $b\bar{b}$ takes over due to the enhanced coupling. For the case of H, gluon-fusion channel always remains dominant(subdominant) over(to) associated production with b-quarks for small(large) values of $\tan\beta$. The pseudoscalar A follows the same trend as h, as seen in fig. 2.5, owing to the enhanced $\bar{b}b$ coupling for large values of $\tan\beta$.

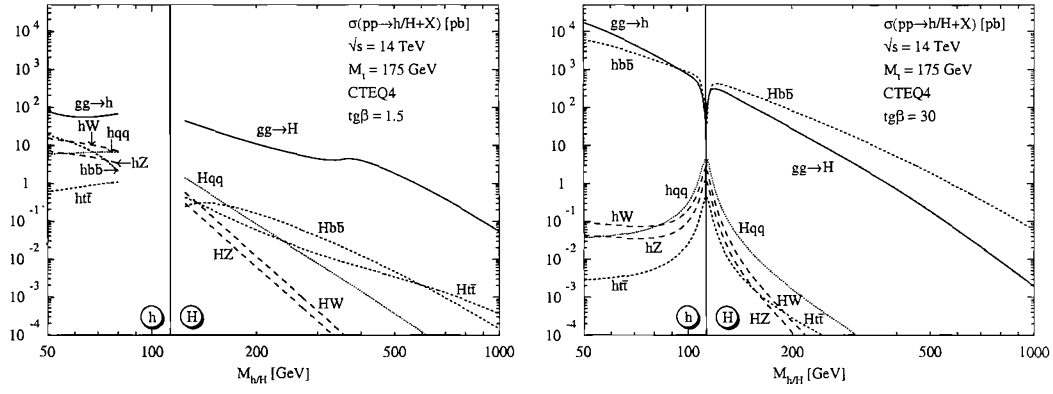

Figure 2.4: Production cross–sections of the MSSM CP–even Higgses at the LHC as a function of their masses, for $\tan\beta = 1.5$ (left) and 30 (right).

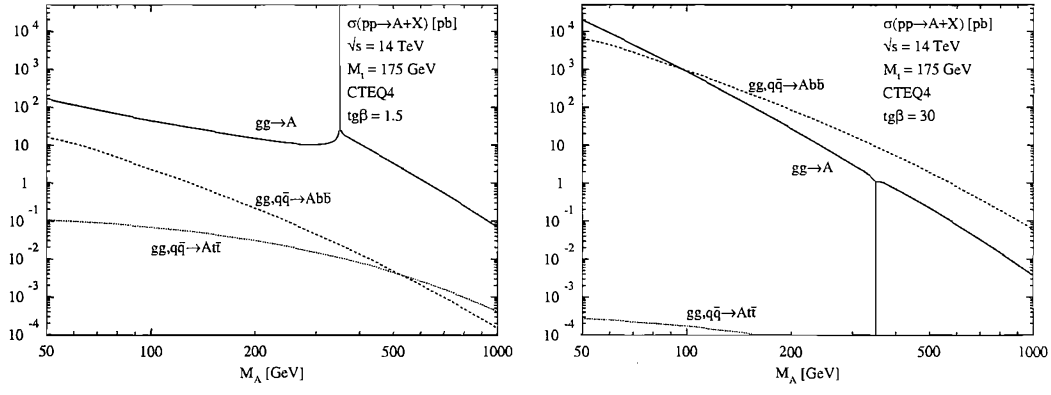

Figure 2.5: Production cross–section of the MSSM CP–odd Higgs at the LHC as a function of its mass, for $\tan\beta = 1.5$ (left) and 30 (right).

Along with $\tan\beta$, the mass of the CP–odd Higgs, M_A, which is generally taken as a free parameter of the model, plays a crucial role in the MSSM Higgs sector phe-

nomenology. Depending on the value of these two parameters, the MSSM Higgs sector can be divided into five regimes. These include:

i) The decoupling regime: When $M_A >> m_Z$, for large values of $\tan\beta$, the masses of H and $H^{\pm}$ are almost degenerate with M_A, and h is SM–like.

ii) The anti–decoupling regime: If the pseudoscalar is very light, $M_A << m_Z$, the situation is exactly opposite to the decoupling regime and at large values of $\tan\beta$, h and H are degenerate in mass with A and the Z boson, respectively.

iii) The intense coupling regime: When M_A is close to m_Z at tree–level, at large $\tan\beta$ all the Higgses will have comparable masses, i.e., $M_h \sim M_H \sim M_A \sim M_h^{\max}$.

iv) The intermediate coupling regime: For low $\tan\beta$ and a not too heavy M_A, the H, A and $H^{\pm}$ bosons, even though relatively heavy, are not completely decoupled from the the theory, thus triggering some interesting decays such as $H \to hh$ and $A \to hZ$ etc.

v) The vanishing–coupling regime: When M_A and $\tan\beta$ are fairly large, there occur regions in the MSSM parameter space where g_{hdd} can vanish owing to certain cancellations between tree–level couplings and higher–order corrections.

The decays of the MSSM Higgses then essentially rely on the regime being exploited. In the decoupling regime, for example, the couplings of the lightest Higgs to the down–type fermions is maximized resulting in $b\bar{b}$ as the dominant decay channel, followed closely by $\tau^+\tau^-$. But since h decay into t–pairs is kinematically closed due to very high value of m_t, even for small values of $\tan\beta$, no significant variation occurs in the BR trends of h. For the heavier Higgses, however, the BRs vary formidably with $\tan\beta$, so that for lower values of the latter, the $t\bar{t}$ BR takes over when kinematically allowed. BRs of the MSSM Higgses into various particles are shown in figs. 2.6a–c.

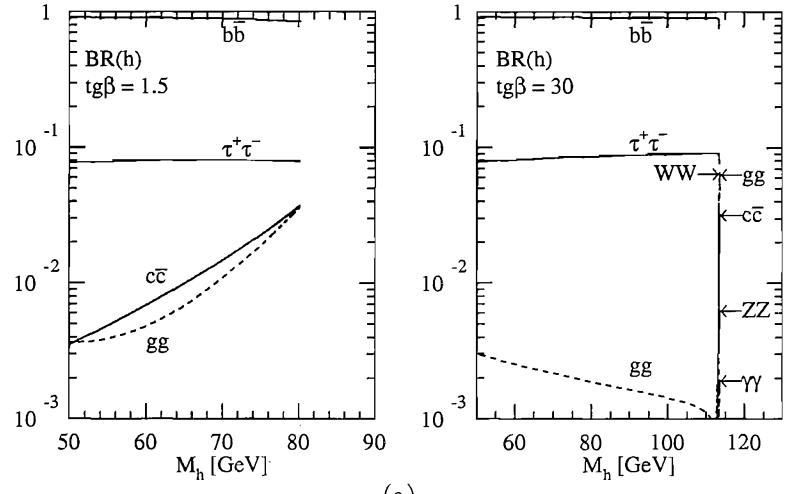

(a)

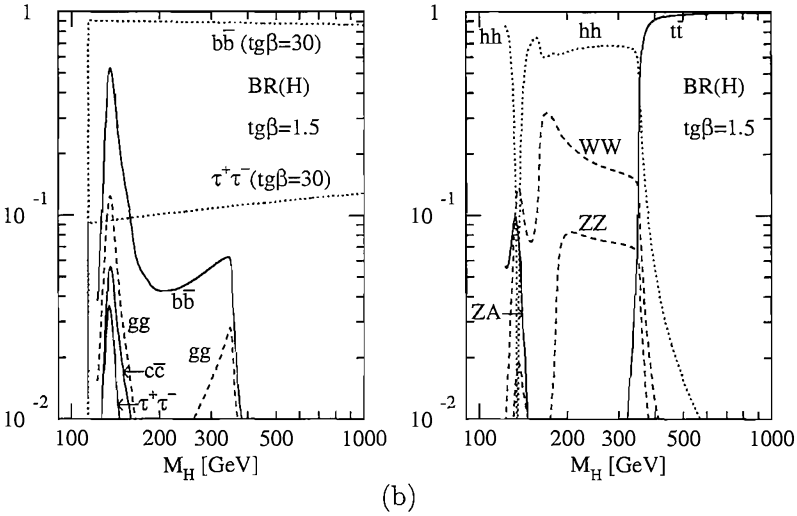

(b)

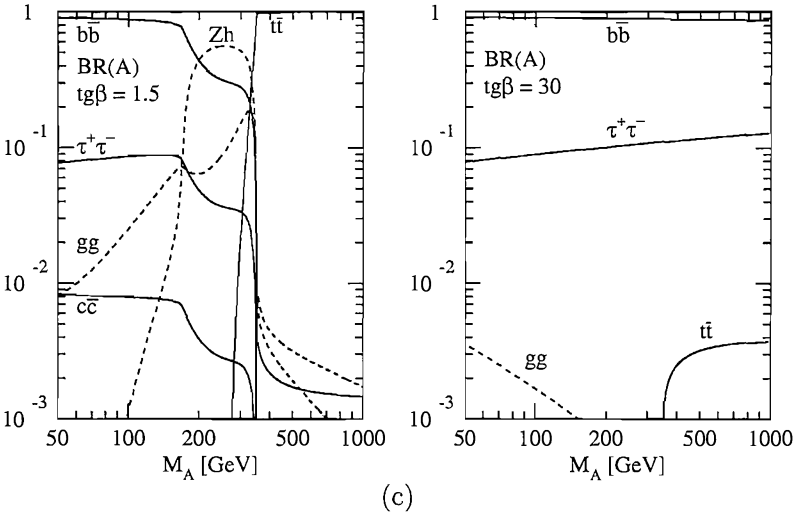

(c)

Figure 2.6: BRs of h (a), H (b) and A (c) for $\tan\beta = 1.5$ and 30 as functions of their masses [13].

2.4.2 Collider Signatures

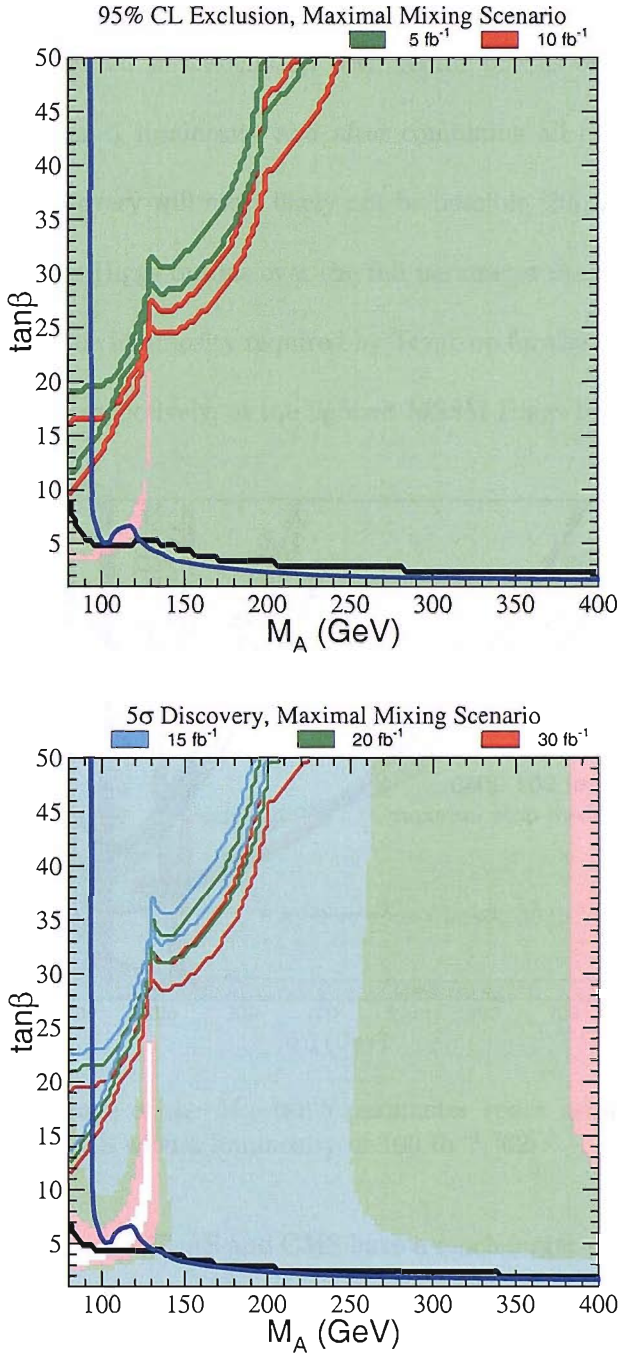

Figure 2.7: Luminosity required by Tevatron for exclusion at 95% C.L. (top) and for 5σ discovery (bottom) of an MSSM Higgs boson as a function of M_A and $\tan\beta$ for the $M_h - max$ scenario with initial (lower lines) and modified (corresponding upper lines) LEP2 limits. Shaded regions indicate the reach of WH and ZH searches, the region above the diagonal lines are accessible to searches for Higgs–strahlung, the dark line indicates the LEP2 limit [20].

At the Tevatron Run II, with an integrated luminosity of the order 8 fb^{-1}, most of the MSSM parameter space can be tested at 95% C.L. by a combination of searches for Higgs bosons produced in association with vector bosons or b–quarks. However, even with the full Run II luminosity and after combining all channels and both the experiments, a 5σ discovery will most likely not be possible [20], leaving it to the LHC to explore and discover Higgs bosons over the full parameter range of the MSSM. Figs. 2.7 a and b illustrate the luminosity required by Tevatron for the exclusion at 95% C.L. and for 5σ discovery, respectively, of the lightest MSSM Higgs boson.

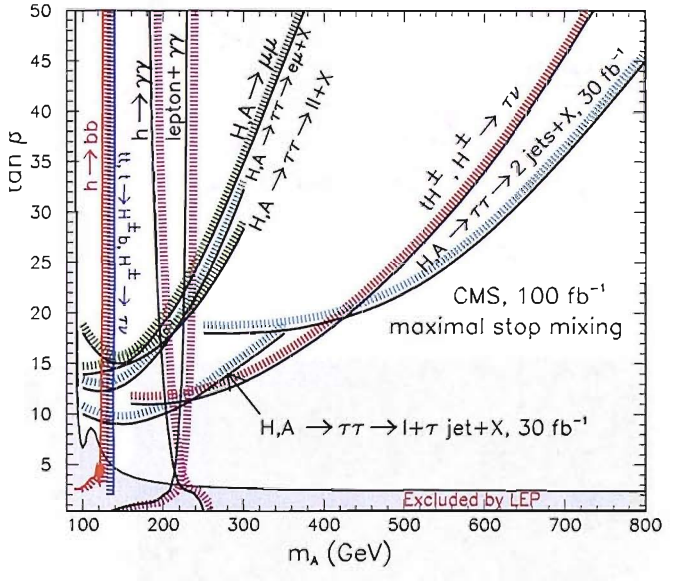

Figure 2.8: The coverage of the M_A–tanβ parameter space using various Higgs production channels in CMS with a luminosity of 100 fb^{-1} [62].

The LHC experiments ATLAS and CMS have a much larger potential for the investigation of the MSSM Higgs sector. The experimental searches carried out at LEP and presently continued at Tevatron can be extended to much larger Higgs boson masses. Therefore at least one (light) neutral MSSM Higgs boson should be observed over the entire parameter space through various production and decay modes if the expected levels of luminosity ($\sim$ 100 fb^{-1}/year) are obtained [60]. However, heavier Higgses can

only be observed for large ($\gtrsim 10$) and small ($\lesssim 3$) values of $\tan\beta$ [61], even if a large integrated luminosity of 300 fb^{-1} is assumed. This fact is evident from fig. 2.8 for the CMS [62] and from fig. 2.9 for the ATLAS [30] experiments at the LHC.

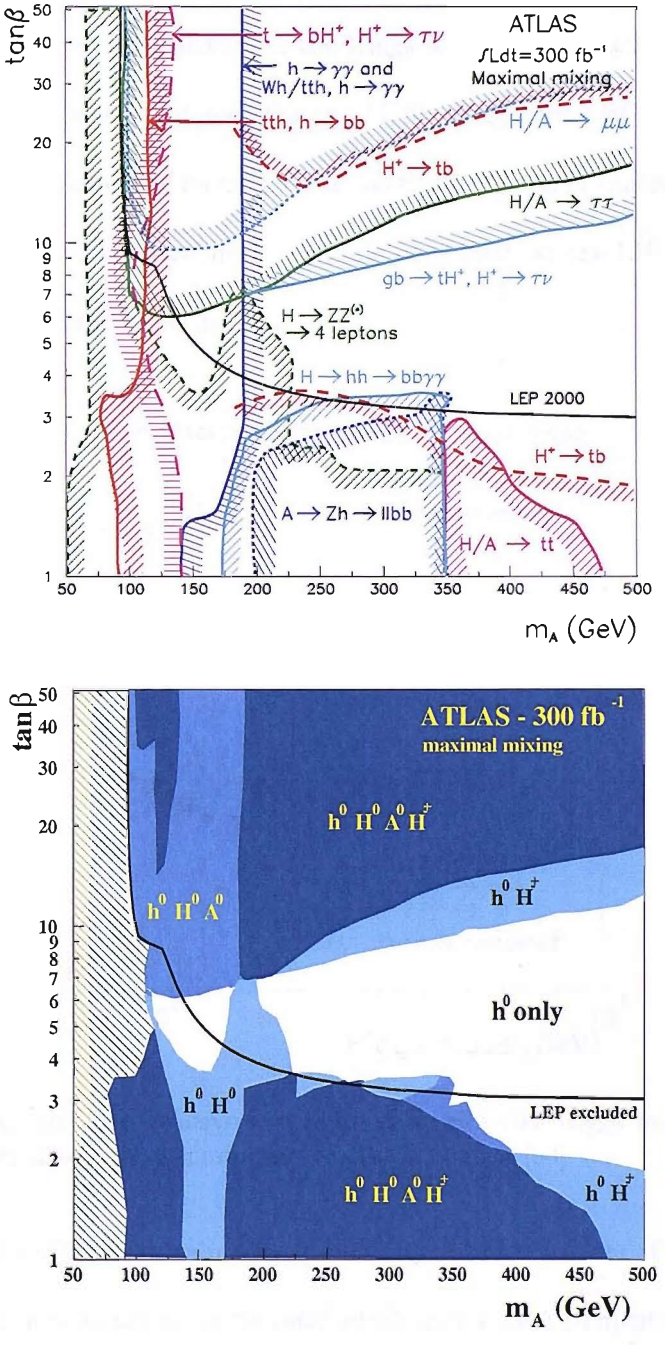

Figure 2.9: The coverage of the M_A–$\tan\beta$ parameter space though various Higgs production channels in ATLAS (above) and the number of MSSM Higgs bosons that can be observed in ATLAS (below), with a luminosity of 300 fb^{-1} [30].

If only a single Higgs boson is observed with decays and production rates that suggest it is SM–like, it will be crucial to search for any deviations of its properties from those predicted in the SM. These deviations would be a direct indication that the SM–like Higgs boson observed is part of an extended Higgs sector. In any case, the LHC would yield a first qualitative picture of the Higgs sector once a significant amount of integrated luminosity is accumulated. For an SM–like Higgs, the LHC should be able to make a precise measurement of its mass. The relative precision in this measurement for the various production channels (individual and combined) at the LHC, as a function of the Higgs mass, is illustrated in fig. 2.10 [63].

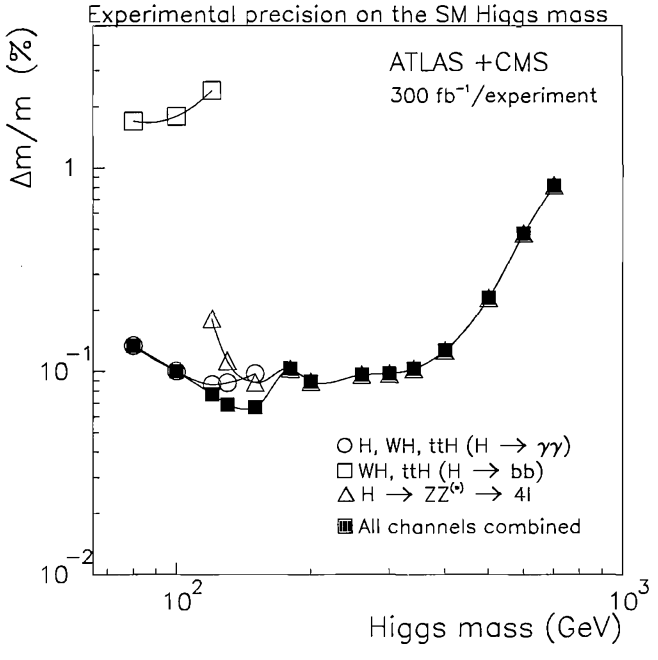

Figure 2.10: The combined relative precision on an SM–like Higgs mass at the CMS and ATLAS experiments for a luminosity of 300 fb^{-1} each [63].

Along with the mass, constraints on spin and quantum numbers of a light Higgs, a model dependent determination of its total width and a measurement of its couplings to the EW gauge bosons should also be possible. The relative precision with which these Higgs couplings can be measured is shown in fig. 2.11. In case heavier Higgses

are also observed, only their masses up to several hundred GeV can be measured [61].

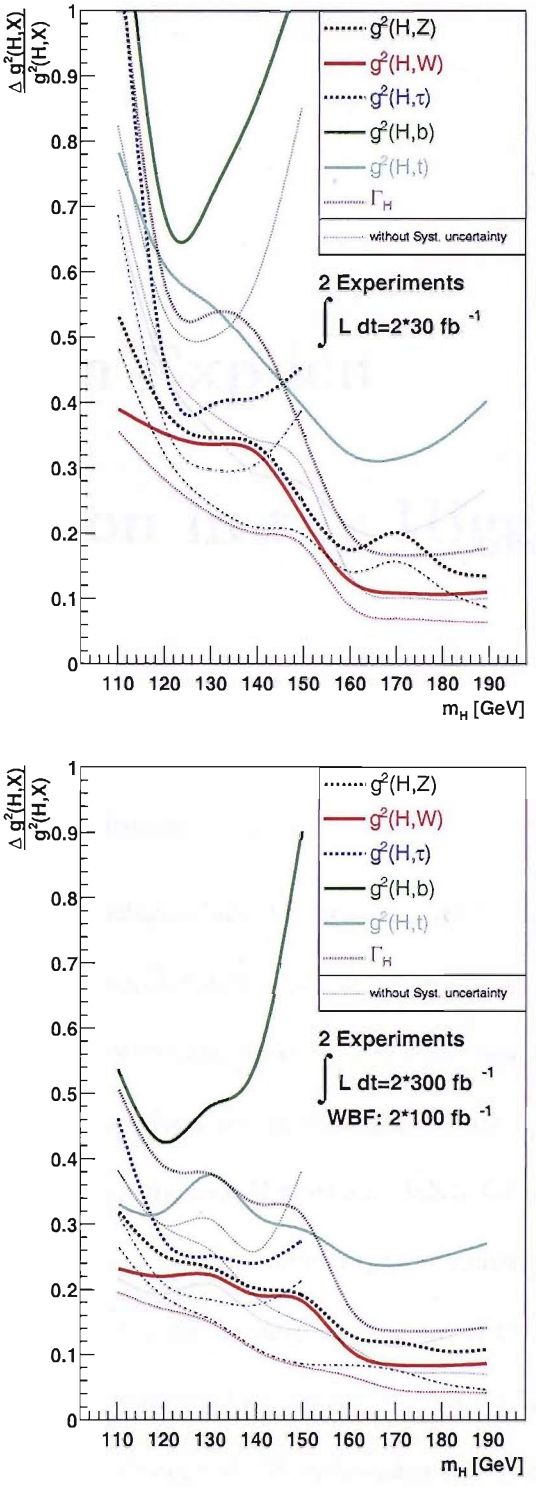

Figure 2.11: Relative precision of fitted Higgs couplings–squared as a function of the Higgs boson mass for 2×30 fb^{-1} (above) and $2\times300 + 2\times100$ fb^{-1} (below) luminosity scenarios for SM rates [64].

Chapter 3

MSSM with Explicit CP–Violation in the Higgs Sector

3.1 The Model

3.1.1 Non–SM CP–Violation

Despite physicists' continuous efforts since the discovery of CP–violation in the neutral kaons system in 1964, a deep understanding of the origin of CP asymmetry in nature remains elusive thus far. Nevertheless, most of the scenarios predicted in existing literature [65]-[80] indicate that Higgs interactions play a key role in mediating CP–violation. The scalar potential of the MSSM does not violate CP at tree level [10]. The reason is that SUSY imposes an additional *holomorphic* symmetry on the Higgs sector (by requiring the superpotential to be an analytic function of the scalar fields, as seen in sect. 2.3.2) of a general two–Higgs doublet model, that entails flavour conservation in tree–level neutral currents and absence of CP–violating scalar–pseudoscalar mixings in the Born approximation. Beyond the Born approximation, recent studies have shown that CP invariance of the Higgs potential may in principle be broken by radiative

corrections [81], as the VEVs of the two Higgs doublets develop a relative phase [65]. This type of CP–violation is generally referred to as spontaneous CP–violation and it requires the CP–odd Higgs scalar to be sufficiently light as a result of the Georgi–Pais theorem [82], but the possibility of the latter has now been ruled out by experiment [83, 84].

CP–violation can also be explicitly induced in the MSSM, in much the same way as it is done in the SM by complex Yukawa couplings of the Higgs bosons to quarks [66]. As seen earlier, there are several new parameters in the supersymmetric theory which are absent in the SM that could well be complex and thus possess CP–odd phases. Such parameters include: (i) the higgsino mass parameter μ, (ii) the soft SUSY–breaking gaugino masses M_a $(a = 1, 2, 3)$, the soft bilinear term $B\mu$ and (iv) the soft trilinear Yukawa couplings $A_{\tilde{f}}$ of the Higgs particles to scalar fermion of flavour $\tilde{f}$. If the universality condition is imposed on all gaugino masses at the unification scale M_X, the gaugino masses M_a have a common phase. Likewise, the different trilinear couplings $A_{\tilde{f}}$ are all equal at M_X. Here, one may slightly deviate from exact universality by assuming that $A_{\tilde{f}}$ is a diagonal matrix in the flavour space [67].

However, the conformal–invariant part of the MSSM Lagrangian has two global U(1) symmetries; the PQ symmetry and the $\mathrm{U}(1)_R$ symmetry acting on the Grassman–valued co–ordinates. As a consequence, not all CP–violating phases of the four complex parameters $\{\mu, B\mu, M_a, A_{\tilde{f}}\}$ turn out to be physical. Employing these two global symmetries, one of the Higgs doublets and the gaugino fields can be rephased such that M_a and $B\mu$ become real [85]. As a result, $arg(\mu)$ and $arg(A_{\tilde{f}})$ are the only physical CP–violating phases in the low energy MSSM supplemented by universal boundary conditions at the GUT scale [68].

The CP–violating phases associated with the sfermions of the first and, to a lesser

extent, second generations are severely constrained by bounds on the EDMs of the electron, neutron, and muon. However, there have been several suggestions [86]–[88] to evade these constraints without suppressing the CP–violating phases. One possibility is to arrange for partial cancellations among various contributions to the electron and neutron EDMs [88], in which case the CP–violating phases turn out to be rather correlated. Another option is to make the first two generations of sfermions rather heavy, of order a few TeV, so that the one–loop EDM constraints are automatically evaded. In fact, one can consider so–called effective SUSY models [87] where decouplings of the first and second generation sfemions are invoked to solve the SUSY flavour changing neutral current (FCNC) and CP problems without spoiling the naturalness condition. We adopted the latter version of a CP–violating MSSM for our analysis.

3.1.2 MSSM Higgs Sector with Explicit CP–Violation

The CP–violating phases $arg(\mu)$ and $arg(A_{\tilde{f}})$ discussed in the previous section could in principle be measured directly in the production cross–sections and decay widths of (s)particles in high energy colliders [76]–[72] or indirectly via their radiative effect on the Higgs sector [66]. These phases introduce non–vanishing off–diagonal mixing terms in the neutral Higgs mass matrix, which in the weak basis (ϕ_1, ϕ_2, a), where $\phi_{1,2}$ are the CP–even states and a is the CP–odd state, may schematically be written as [67, 73]

$$\mathcal{M}_N^2 = \begin{pmatrix} \mathcal{M}_S^2 & \mathcal{M}_{SP}^2 \\ \mathcal{M}_{PS}^2 & \mathcal{M}_P^2 \end{pmatrix}. \tag{3.1}$$

$$\text{where} \qquad \mathcal{M}_{PS}^2 = (\mathcal{M}_{SP}^2)^T \propto \frac{\mathcal{I}(\mu A_{\tilde{f}})}{M_{\text{SUSY}}^2}, \tag{3.2}$$

in the $\xi = 0$ renormalisation scheme [65, 73] (see Appendix A). It is a 1×2 matrix describing the mixing between the CP–even and CP–odd states, and is dominated by loops involving the top squarks. $\mathcal{M}_S^2$ is a 2×2 matrix describing the transition between the CP–even states whilst $\mathcal{M}_P^2$ gives the mass term of the CP–odd state. As a result, Higgs bosons of the MSSM no longer carry any definite CP–parities and rotation from the EW states to the mass eigenstates,

$$(\phi_1, \phi_2, a)^T = O(H_1, H_2, H_3)^T,$$

is now carried out by a 3×3 real orthogonal matrix O, such that

$$O^T \mathcal{M}_N^2 O = diag(M_{H_1}, M_{H_2}, M_{H_3}), \tag{3.3}$$

with $M_{H_1} \leq M_{H_2} \leq M_{H_3}$, instead of the usual 2×2 one, and the angle α resulting from the singling out of the Goldstone state as in the CP–conserving case, as seen in sect. 2.3.3. As a consequence, it is now inappropriate to parameterise the MSSM Higgs sector in terms of M_A as is the case for a CP–conserving MSSM. Instead, the mass of the charged Higgs boson, $M_{H^\pm}$, remains an observable parameter in terms of which the Higgs sector of the model can be parameterised. For a detailed formulation of the MSSM Higgs sector with explicit CP–violation see Appendix A.

3.2 CPV Signatures

3.2.1 The Di–photon Decay Channel

In order to study the effects of the CP–violating phases we focussed on the di–photon decay mode of a neutral Higgs boson. The reason is twofold. Firstly, the di–photon

decay mode is the most promising channel for the discovery of a light, say 80–130 GeV, neutral Higgs at the LHC [30], as pointed out in sect. 1.4.3. Secondly, the dominant CP–violating terms dependent on μ and $A_{\tilde{f}}$ (hereafter, $\tilde{f} = \tilde{t}, \tilde{b}, \tilde{\tau}$) enter the perturbative calculation of the di–photon decay width with a coupling strength that is of the same order as that of the CP–conserving ones (of $\mathcal{O}(\alpha^3)$).

Furthermore, on the technical side, thanks to the narrow width of such a light Higgs state (of 10 MeV at the most), the entire $gg/qq \to H_1 \to \gamma\gamma$ process can be factorised in the narrow width approximation into three parts up to corrections of order Γ_{H_1}/M_{H_1}): the production process, the Higgs propagator and the decay channel. Effects of CP violation can show up in this process through the aforementioned couplings in the production, through a possible mixing of Higgs states at one-loop and above in the propagator and through the same couplings in the decay.

CP violation entering the production of a neutral Higgs state in gluon-gluon fusion process at hadron colliders has already been analysed a few times with varying constraints on the parameter space [76, 69, 77]. Effects of CP-mixing in the propagator have also been discussed separately in great detail [72]. A thorough study of the other MSSM Higgs decay channels in the presence of CP-violation has also been carried out [68]-[80]. Here, we will concentrate on the decay of the lightest physical Higgs particle, H_1, which is now a CP–mixed state, into two photons.

In the MSSM, a Higgs state decays into two photons through loops of fermions, sfermions, gauge bosons, charged Higgs as well as charginos, as shown in fig. 3.1. In the presence of non–trivial CP–violating phases, the couplings of the decaying Higgses to all the particles in the loops are strongly modified with respect to the CP–conserving

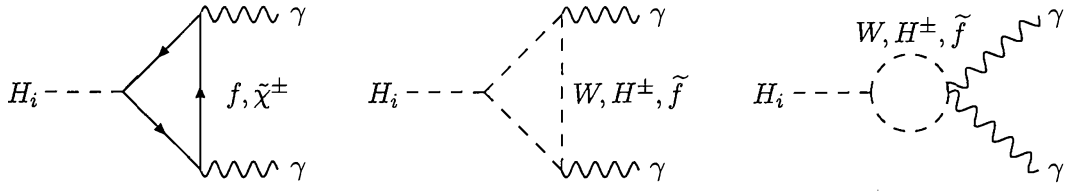

Figure 3.1: Higgs decay into $\gamma\gamma$ pair in the CP–violating MSSM. $f \equiv t,\, b$; $\tilde{f} \equiv \tilde{t}_{1,2}, \tilde{b}_{1,2}, \tilde{\tau}_{1,2}$.

MSSM. The amplitude for the decay process $H_i \to \gamma\gamma$ can be written as [90]

$$\mathcal{M}_{\gamma\gamma H_i} = -\frac{\alpha M_{H_i}^2}{4\pi\, v}\left\{ S_i^\gamma(M_{H_i})\ (\epsilon_{1\perp}^* \cdot \epsilon_{2\perp}^*) - P_i^\gamma(M_{H_i}) \frac{2}{M_{H_i}^2} \langle \epsilon_1^* \epsilon_2^* k_1 k_2 \rangle \right\}, \tag{3.4}$$

where $k_{1,2}$ are the momenta of the two photons and $\epsilon_{1,2}$ the wave vectors of the corresponding photons, $\epsilon_{1\perp}^\mu = \epsilon_1^\mu - 2k_1^\mu (k_2 \cdot \epsilon_1)/M_{H_i}^2$, $\epsilon_{2\perp}^\mu = \epsilon_2^\mu - 2k_2^\mu (k_1 \cdot \epsilon_2)/M_{H_i}^2$ and $\langle \epsilon_1 \epsilon_2 k_1 k_2 \rangle \equiv \epsilon_{\mu\nu\rho\sigma}\, \epsilon_1^\mu \epsilon_2^\nu k_1^\rho k_2^\sigma$. The gauge boson loops in the CP–even amplitude are calculated in the Feynman gauge [91]or equivalently in a non-linear R_ξ gauge [92].

The scalar and pseudoscalar form–factors, retaining only the dominant loop contributions from the third–generation (s)fermions (for reasons pointed out in sect. 3.1.1), charginos, $W^\pm$ and charged Higgs bosons, are given by

$$\begin{aligned}
S_i^\gamma(M_{H_i}) &= 2 \sum_{f=b,t,\tilde{\chi}_1^\pm,\tilde{\chi}_2^\pm} N_C\, Q_f^2\, g_f g_{H_i \bar{f} f}^S \frac{v}{m_f} F_{sf}(\tau_{if}) \\
&\quad - \sum_{\tilde{f}_j=\tilde{t}_1,\tilde{t}_2,\tilde{b}_1,\tilde{b}_2,\tilde{\tau}_1,\tilde{\tau}_2} N_C\, Q_{\tilde{f}}^2 g_{H_i \tilde{f}_j^* \tilde{f}_j} \frac{v^2}{2m_{\tilde{f}_j}^2} F_0(\tau_{i\tilde{f}_j}) \\
&\quad - g_{H_i WW} F_1(\tau_{iW}) - g_{H_i H^+ H^-} \frac{v^2}{2M_{H^\pm}^2} F_0(\tau_{iH^\pm}), \\
P_i^\gamma(M_{H_i}) &= 2 \sum_{f=b,t,\tilde{\chi}_1^\pm,\tilde{\chi}_2^\pm} N_C\, Q_f^2\, g_f g_{H_i \bar{f} f}^P \frac{v}{m_f} F_{pf}(\tau_{if}),
\end{aligned} \tag{3.5}$$

where $\tau_{ix} = M_{H_i}^2/4m_x^2$, $N_C = 3$ for (s)quarks and 1 for staus and charginos, respectively.

The form–factors F_{sf}, F_{pf}, F_0, and F_1 can be expressed as

$$\begin{aligned} F_{sf}(\tau) &= \tau^{-1}\left[1+(1-\tau^{-1})f(\tau)\right], \quad F_{pf}(\tau) = \tau^{-1} f(\tau), \\ F_0(\tau) &= \tau^{-1}\left[-1+\tau^{-1}f(\tau)\right], \qquad F_1(\tau) = 2+3\tau^{-1}+3\tau^{-1}(2-\tau^{-1})f(\tau), \end{aligned} \tag{3.6}$$

where $f(\tau)$ stands for the integrated function

$$f(\tau) = -\frac{1}{2}\int_0^1 \frac{\mathrm{d}y}{y}\ln\left[1-4\tau y(1-y)\right] = \begin{cases} \arcsin^2(\sqrt{\tau}) & \tau \le 1, \\ -\frac{1}{4}\left[\ln\left(\frac{\sqrt{\tau}+\sqrt{\tau-1}}{\sqrt{\tau}-\sqrt{\tau-1}}\right) - i\pi\right]^2 & \tau \ge 1. \end{cases} \tag{3.7}$$

It is clear that imaginary parts of the form–factors appear for Higgs boson masses greater than twice the mass of the charged particle running in the loop, i.e., $\tau \ge 1$. In the limit $\tau \to 0$, $F_{sf}(0) = 2/3$, $F_{pf}(0) = 1$, $F_0(0) = 1/3$, and $F_1(0) = 7$. Finally, the decay width is given by

$$\Gamma(H_i \to \gamma\gamma) = \frac{M_{H_i}^3 \alpha^2}{256\pi^3 v^2}\left[\left|S_i^\gamma(M_{H_i})\right|^2 + \left|P_i^\gamma(M_{H_i})\right|^2\right]. \tag{3.8}$$

The modified couplings g_f, $g^S_{H_i\bar{f}f}$, $g^P_{H_i\bar{f}f}$, $g_{H_i\tilde{f}_j^*\tilde{f}_j}$, g_{H_iVV} and $g_{H_iH^+H^-}$ mentioned above are given in Appendix B.

3.2.2 Numerical Procedures

We used the publicly available `Fortran` code `CPsuperH` [90] v2.0 for our study. `CPsuperH` calculates the mass spectrum and decay widths of the neutral and charged Higgs bosons in the most general MSSM including explicitly CP–violating phases. In addition it computes all the couplings of the neutral Higgs bosons $H_{1,2,3}$ and the charged Higgs boson $H^\pm$. The program is based on the results obtained in Refs. [68]–[70] and the most

recent RG improved effective–potential approach at next-to-leading-order, which includes dominant higher–order logarithmic and threshold corrections, b–quark Yukawa coupling resummation effects and Higgs boson pole–mass shifts [73, 74]. `CPsuperH` efficiently computes the neutral and charged Higgs boson couplings and masses with equally high levels of precision in the CP–conserving case as well [93].

The free non–SM parameters of the model now include: $|\mu|$, phase of μ (ϕ_μ), charged Higgs mass ($M_{H^\pm}$), soft gaugino masses (M_a), soft sfermion masses of the third generation ($M_{(\tilde{Q}_3,\tilde{U}_3,\tilde{D}_3,\tilde{L}_3,\tilde{E}_3)}$), (unified) soft trilinear couplings of the third generation ($|A_{\tilde{f}}|$), phase of the trilinear coupling ($\phi_{A_{\tilde{f}}}$). We chose the following very extensive parameter ranges:

- $\tan\beta$: 1–60;
- $|\mu|$: 100–2000 GeV;
- ϕ_μ: 0°–180°;
- $M_{H^\pm}$: 100–400 GeV;
- M_2: 100–500 GeV;
- $M_{(\tilde{Q}_3,\tilde{U}_3,\tilde{D}_3,\tilde{L}_3,\tilde{E}_3)}$: 100–2000 GeV;
- $|A_{\tilde{f}}|$: 100–2000 GeV,

We aimed at searching regions in the supersymmetric parameter space where the variation in BR($H_1 \to \gamma\gamma$) due to the CP–violating phases is maximized compared to the CP–conserving case. As stated earlier, the CPV effects are proportional to $arg(\mu A_{\tilde{f}})$, so we opted to fix $\phi_{A_{\tilde{f}}}$ to 0 and varied only ϕ_μ in the above range. M_1 and M_3 were kept fixed as their variation is of no significance here. Also, no unification of the soft sfermion masses was assumed so that, even though they are taken in the same

range, they might have different numeric values. Finally, we switched off the threshold corrections induced by the exchange of gluinos and charginos in the Higgs–quark–antiquark vertices [94, 95].

We modified `CPsuperH` slightly to make it scan over the above range of input parameters instead of giving a single output for a given set of the same. We scanned the above parameter space for 100,000 randomly selected points and for each of these we have taken values of ϕ_μ increasing from 0° to 180° in steps of 20°. Notice that $\phi_\mu = 0°(180)°$ corresponds to the CP-conserving MSSM point with $\mu = +|\mu|(-|\mu|)$, while any other non-trivial ϕ_μ shows the effect of CP violation. The following experimental constraints from LEP2 and Tevatron [96, 97] were imposed during the scan:

$$\begin{aligned} m_{\chi_1^\pm} &\geq 104 \text{ GeV (LEP2)}, \\ m_{\tilde{f}} &\gtrsim 100 \text{ GeV for } \tilde{f} = \tilde{l}, \tilde{\nu}, \tilde{t}_1 \text{ (LEP2)}, \\ m_{\tilde{b}} &\gtrsim 300 \text{ GeV (Tevatron)}. \end{aligned}$$

The parameter space points violating these constraints were discarded. Notice that `CPsuperH` intrinsically takes care of the positivity of the mass–squared entries in the various mass matrices. As for the Higgs, we only kept points with lightest Higgs mass (M_{H_1}) between 90 and 130 GeV, the range in which the $H_1 \to \gamma\gamma$ decay is relevant.

3.2.3 Estimating CPV

We now describe the methodology of our analysis. For each point in the scans that survives the various constraints discussed above we asked `CPSuperH` to print out the mass and $\gamma\gamma$ BR of the lightest Higgs H_1. In order to have an idea of the overall trend followed by the BR for different phases, we first looked at the average behaviour

at specific M_{H_1} values. To do this we divided the mass range into bins of width 4 GeV. To find the average sensitivity within each mass bin, we defined the percentage deviation

$$R^i_{\phi_\mu} = \frac{\sum_n \left(\mathrm{BR}^{(i,n)}_{\phi} - \mathrm{BR}^{(i,n)}_{0}\right)}{\sum_n \mathrm{BR}^{(i,n)}_{0}} \times 100, \tag{3.9}$$

where the summation is over the number of random points (n) within a particular bin i. We denote the BR in the CP-conserving case by BR_0 (specifically, the latter corresponds to the case $\phi_\mu = 0°$, however, without any loss or gain of information, we could alternatively have used the limit $\phi_\mu = 180°$) and that with a non-vanishing ϕ_μ (different from 180°) by BR_ϕ. This average percentage deviation is plotted in fig. 3.2 for the different values of ϕ_μ taken in each bin.

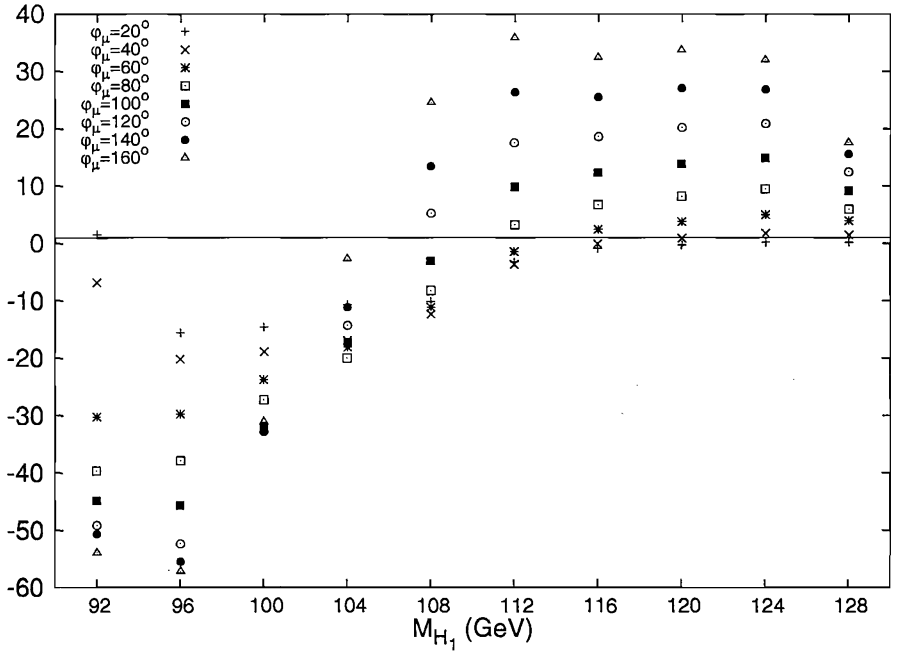

Figure 3.2: $R^i_{\phi_\mu}$, defined in eq. (3.9), plotted as a function of H_1 mass for values of ϕ_μ increasing in steps of 20°.

The number of points falling in each bin varies with the Higgs mass value that bin

is centered around. It reaches an averaged (over all values of ϕ_μ) maximum of around 20,000 points for M_{H_1} lying between 118–122 GeV, and around 15,000 for M_{H_1} in the range 114–118 GeV. The minimum number of points occurs for very light and very heavy H_1 mass, i.e., for the ranges 90–94 GeV and 126–130 GeV, where it is reduced to an average of a few hundreds. Clearly, there is an enhancement of about 20% in the BR for M_{H_1} larger than 110 GeV for moderate values of $\phi_\mu \sim 100°$, while there is a suppression of about $40 - 50\%$ for M_{H_1} around $90 - 98$ GeV. This change-over from enhancement to suppression for lower M_{H_1} values shows the diminishing role of sparticles in the loop as the difference between $2m_{\tilde{f}}$ and M_{H_1} increases and the dependence on a non–zero ϕ_μ effectively relies more and more on the changed H_1WW coupling.

Notice that in 3.2, in the mass region of $100 - 110$ GeV, the effect of a non–zero $\phi_m u$ is apparently very small. However, this is an artifact of the binned averaging,

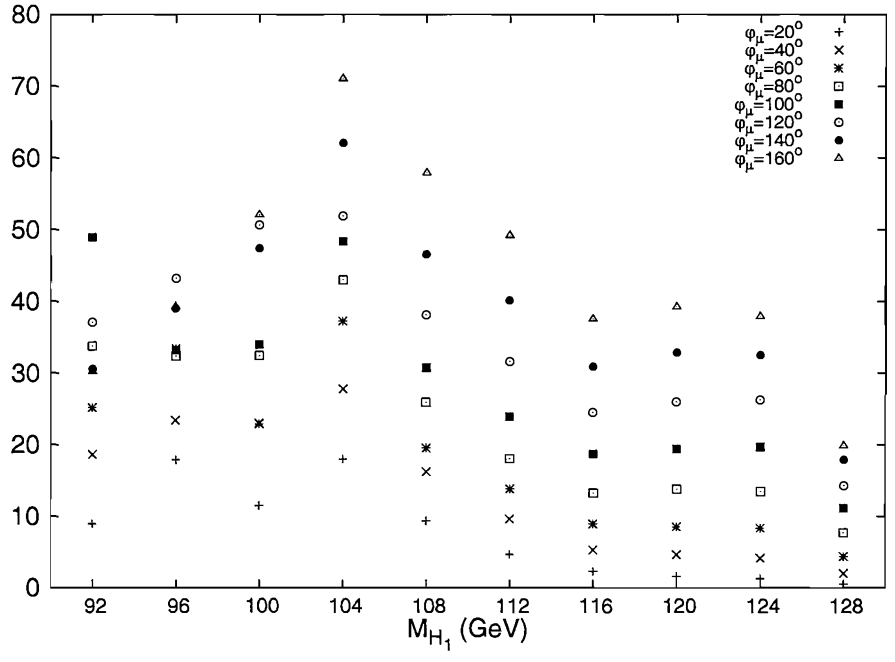

Figure 3.3: $R^i_{\phi_\mu}$, defined in eq. (3.9), but with averaged absolute value of the numerator, plotted as a function of H_1 mass for values of ϕ_μ increasing in steps of 20°.

where points with enhanced and suppressed BRs falling in the same mass bin cancel each other. This cancellation is nullified by taking the absolute value of the difference in the numerator of Eq. (3.9), i.e., $\sum_n |\mathrm{BR}_\phi^{(i,n)} - \mathrm{BR}_0^{(i,n)}|$. The result is plotted in fig. 3.3. More than 50% deviation is seen for $\phi_\mu = 100°$ for M_{H_1} around 104 GeV. Now, it should be noted that these figures represent only the average behaviour. It is therefore possible to find regions of parameter space where the differences are larger (or smaller, for that matter). We did indeed find points with difference in the BR larger than 50 times in our scan in either direction. Some such sample points are listed below.

1. $\frac{\mathrm{BR}_\phi}{\mathrm{BR}_0} = 55$:

   $\phi_\mu = 40°$, $\tan\beta = 25.56$, $M_{H^\pm} = 286.04$ GeV, $|\mu| = 1882.85$ GeV, $M_2 = 327.64$ GeV, $M_{\tilde{Q}_3} = 509.57$ GeV, $M_{\tilde{U}_3} = 1033.11$ GeV, $M_{\tilde{D}_3} = 1933.03$ GeV, $M_{\tilde{L}_3} = 370.31$ GeV, $M_{\tilde{E}_3} = 1933.50$ GeV, $|A_{\tilde{t}}| = 1848.97$ GeV, $|A_{\tilde{b}}| = 530.36$ GeV, $|A_{\tilde{\tau}}| = 1016.04$ GeV.

2. $\frac{\mathrm{BR}_\phi}{\mathrm{BR}_0} = 80$:

   $\phi_\mu = 100°$, $\tan\beta = 57.71$, $M_{H^\pm} = 284.13$ GeV, $|\mu| = 1257.55$ GeV, $M_2 = 324.30$ GeV, $M_{\tilde{Q}_3} = 121.95$ GeV, $M_{\tilde{U}_3} = 531.62$ GeV, $M_{\tilde{D}_3} = 1894.15$ GeV, $M_{\tilde{L}_3} = 1451.41$ GeV, $M_{\tilde{E}_3} = 578.66$ GeV, $|A_{\tilde{t}}| = 1483.55$ GeV, $|A_{\tilde{b}}| = 1504.37$ GeV, $|A_{\tilde{\tau}}| = 1724.46$ GeV.

3. $\frac{\mathrm{BR}_\phi}{\mathrm{BR}_0} = \frac{1}{93}$:

   $\phi_\mu = 100°$, $\tan\beta = 50.07$, $M_{H^\pm} = 184.03$ GeV, $|\mu| = 1510.54$ GeV, $M_2 = 203.83$ GeV, $M_{\tilde{Q}_3} = 545.59$ GeV, $M_{\tilde{U}_3} = 702.27$ GeV, $M_{\tilde{D}_3} = 721.39$ GeV, $M_{\tilde{L}_3} = 1664.65$ GeV, $M_{\tilde{E}_3} = 1947.71$ GeV, $|A_{\tilde{t}}| = 1035.22$ GeV, $|A_{\tilde{b}}| = 1214.54$ GeV, $|A_{\tilde{\tau}}| = 1163.69$ GeV.

4. $\frac{\mathrm{BR}_\phi}{\mathrm{BR}_0} = 60$:

$\phi_\mu = 160°$, $\tan\beta = 55.52$, $M_{H^\pm} = 199.70$ GeV, $|\mu| = 1558.47$ GeV, $M_2 = 391.16$ GeV, $M_{\tilde{Q}_3} = 1680.03$ GeV, $M_{\tilde{U}_3} = 710.55$ GeV, $M_{\tilde{D}_3} = 1802.08$ GeV, $M_{\tilde{L}_3} = 833.35$ GeV, $M_{\tilde{E}_3} = 465.01$ GeV, $|A_{\tilde{t}}| = 1300.28$ GeV, $|A_{\tilde{b}}| = 1296.45$ GeV, $|A_{\tilde{\tau}}| = 129.02$ GeV.

5. $\frac{\mathrm{BR}_\phi}{\mathrm{BR}_0} = \frac{1}{62}$:

$\phi_\mu = 160°$, $\tan\beta = 48.75$, $M_{H^\pm} = 187.22$ GeV, $|\mu| = 1462.18$ GeV, $M_2 = 198.49$ GeV, $M_{\tilde{Q}_3} = 913.02$ GeV, $M_{\tilde{U}_3} = 854.55$ GeV, $M_{\tilde{D}_3} = 457.48$ GeV, $M_{\tilde{L}_3} = 805.43$ GeV, $M_{\tilde{E}_3} = 1207.83$ GeV, $|A_{\tilde{t}}| = 1118.37$ GeV, $|A_{\tilde{b}}| = 1708.16$ GeV, $|A_{\tilde{\tau}}| = 900.21$ GeV.

However, a subtlety should be noted in this context, concerning the derived MSSM masses that also depend on ϕ_μ and enter the decay $H_1 \to \gamma\gamma$ (M_{H_1}, $m_{\tilde{b},\tilde{t},\tilde{\tau}}$, $M_{\chi^\pm_{1,2}}$). In fact, all the latter change when going from the CP–conserving case to the CP–violating one. The most crucial one in this respect is M_{H_1}. However, fig 3.4 verifies that for the same parameter point (apart from a different ϕ_μ), the change in M_{H_1} is less than 2 GeV for the two MSSM configurations. Hence, our 4 GeV wide bins do capture percentage

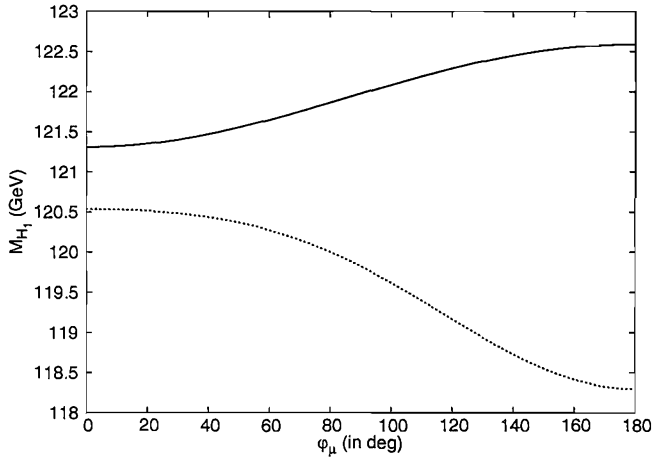

Figure 3.4: Mass of H_1 as a function of ϕ_μ. Solid line corresponds to the case when none of the sparticles going into the loops is light while dashed line represents the case when the $\tilde{t}_1$ is light (of order 200 GeV), see text.

corrections to the BR consistently between the two MSSMs as a function of the lightest Higgs boson mass. (Rare borderline cases are also correctly assigned to the right bin.) Besides, 2 GeV is roughly the di–photon mass resolution in ATLAS [30] (while in CMS it is somewhat better [98]).

In short, we imagine an experimental situation in which a Higgs resonance is extracted in $\gamma\gamma X$ samples with the above mass resolution at a time when the other SUSY masses and mixing (including $\tan\beta$) entering the loops of the $H_1 \to \gamma\gamma$ mode have already been measured in real sparticle production with a resolution that does not allow one to distinguish between a CP–conserving and a CP–violating MSSM scenario. Under these conditions, for large enough differences of BRs, a simple measurement of the normalisation of the $\gamma\gamma$ resonance (after background subtraction) may suffice to distinguish between the two envisaged CP scenarios, independently of whether the di–photon signal is established in inclusive (i.e., via gluon–fusion) or exclusive (i.e., accompanied by high transverse momentum leptons from Higgs–strahlung) mode.

To illustrate the validity of the above argument, we singled out some benchmark points that showed significant deviations from the CP–conserving MSSM case with an intention to study the contribution of various parameters to the $H_1 \to \gamma\gamma$ BR. Fig. 3.5 gives the change in BR for one such point with respect to the H_1 mass for three values of $\phi_\mu = 0°, 90°$ and $180°$, where $0°$ and $180°$ represent the CP–conserving cases (corresponding to a change in the sign of the parameter μ). This point corresponds to a randomly generated parameter set where all the sparticles are heavy (order 1 TeV). Clearly, there is a reasonable shift in BR between the three cases despite large sparticle masses. This follows from eqs. (3.4) and (3.5), which indicate that the decay amplitude is sensitive also to the Higgs couplings to various (s)particles which now get modified by an entry from the matrix O that diagonalizes the CP–violating Higgs mass matrix

(see Appendix B), apart from the loop particle masses. Also the trilinear couplings of the sfermions to the Higgs boson are proportional to the Yukawa couplings of their fermionic counterparts. Notice that in fig. 3.5, BR(180°) is larger than BR(0°) even though both these value of ϕ_μ correspond to the CP–conserving case. This is due to the fact that these are physically two different points giving out the same H_1 mass depending on the values of other parameters such as $M_{H^\pm}$ which are not fixed for this plot. Also M_{H_1} saturates around 120 GeV for the range of $M_{H^\pm}$ scanned over here, hence the plot has been cut–off at this value.

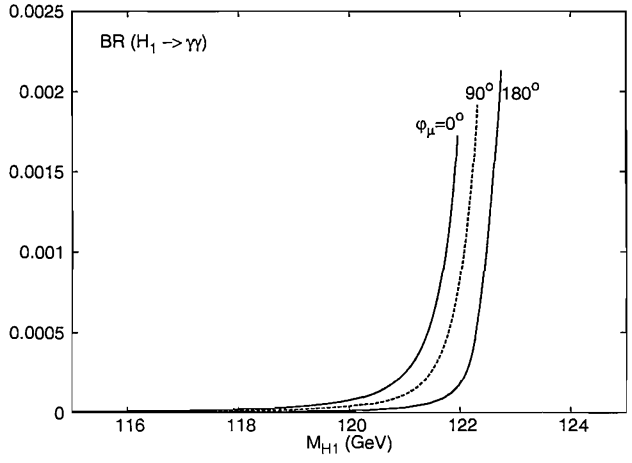

Figure 3.5: BR of Higgs into two photons for three values of ϕ_μ = 0° (solid, left), 90° (dashed) and 180° (solid, right) plotted against its mass. Here $M_{Q_3} = 1$ TeV, $|A_{\tilde{f}}| = 1.5$ TeV, $|\mu| = 1$ TeV, $\tan\beta = 20$ and this point corresponds to a scenario in the parameter space when none of the sparticles is light.

It should be pointed out here that this result is in agreement with an earlier one [77] where the production of Higgses through gluon–fusion and its decay via di–photon mode in the MSSM with explicit CP–violation was studied. It was concluded there that the CP–violating phases could result in a suppression of the signal cross-section for a light H_1 owing to a decrease in the strength of $H_1W^+W^-$ couplings due to CP–mixing of the three neutral Higgs states. The scenarios discussed therein were the ones where

none of the sparticles is light enough to contribute substantially in the loops which, therefore, correspond to the one presented above.

We then headed on to examine the dependence of BR($H_1 \to \gamma\gamma$) on the masses of the sparticles going into the loops and their subsequent dependence on the CP–violating phases. We generated points such that for every particular combination of soft–masses, only one out of $\tilde{t}_1$, $\tilde{b}_1$, $\tilde{\tau}_1$ and $\chi_1^{\pm}$ has a mass very close to the experimental lower bound, while all others remained considerably heavy (the mass of the charged Higges boson is varied between 100 GeV and 400 GeV, but for the interesting region $M_{H_1} > 115$ GeV it is heavier than 300 GeV). We expected to see the effect due only to the exchange of this light sparticle, alongside the one due to standard matter, t, b and $W^{\pm}$.

As fig. 3.6 illustrates, the most dominant change in BR occurs when the $\tilde{t}_1$ is light, around 200 GeV, despite the large value of $\tan\beta$ involved. Such behaviour could also be attributed to the fact that the mass of the stop going into the loop itself varies notably with the value of ϕ_μ, as seen in fig. 3.7. This added to the fact that the Yukawa coupling of t–quark is the largest among SM particles for small to moderate $\tan\beta$. Notice that

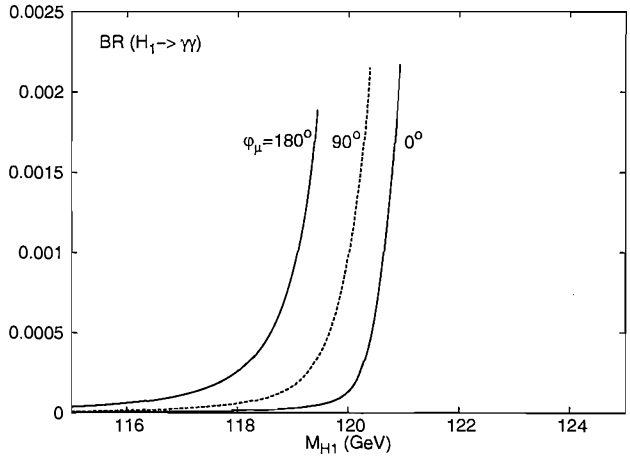

Figure 3.6: BR of Higgs into two photons for three values of $\phi_\mu = 0°$ (solid, right), $90°$ (dashed) and $180°$ (solid, left), plotted against its mass. Here $M_{Q_3} = 1$ TeV, $|A_{\tilde{f}}| = 1.5$ TeV, $|\mu| = 1$ TeV, $\tan\beta = 20$, $M_{\tilde{U}_3} = 250$ GeV and this point corresponds to the scenario when the $\tilde{t}_1$ is light, $\mathcal{O}(250$ GeV), while all the other loop sparticles are heavy.

the variation in $m_{\tilde{t}_1}$ itself is of the same order as the expected experimental resolution [30, 98], so that it may not be possible to confirm CP-violating effects directly in the stop sector.

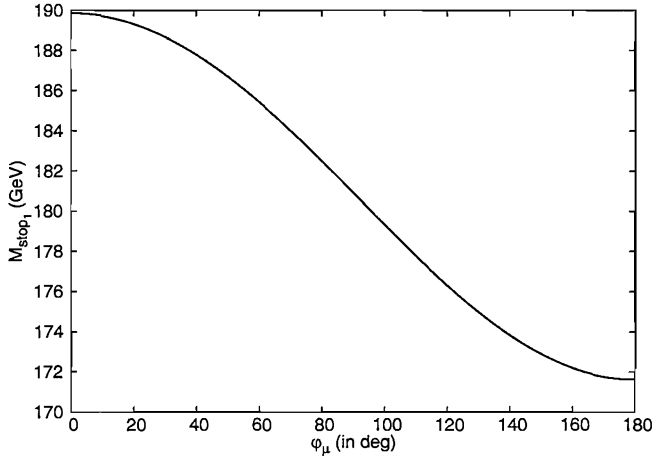

Figure 3.7: Mass of $\tilde{t}_1$ as a function of ϕ_μ.

As for the remaining sparticles, by comparing figs. 3.8 a, b and c which correspond to the points where a light $\tilde{b}_1$, a light $\tilde{\tau}_1$ and a light $\tilde{\chi}_1^\pm$ is produced, respectively, to fig. 3.5, one can safely say that their light masses have negligible effect on the BR. The reason, evidently, being the fact that the mass of these sparticles get only marginally rescaled with variations in ϕ_μ in the first place. This fact is illustrated in fig. 3.9, where we see that the maximum drop in the mass of $\tilde{b}_1$ due to non–zero ϕ_μ is roughly 1.5 GeV, as opposed to the case of $\tilde{t}_1$ where it gets dropped by tens of GeVs. Also, as pointed earlier, the Yukawa couplings of all the corresponding SM–partners are fairly small compared to that of the t–quark. Due to identical couplings, $\tilde{\tau}_1$ and $\tilde{\chi}_1^\pm$ follow the same trend as $\tilde{b}_1$, so we will overlook the ϕ_μ dependence of their masses here.

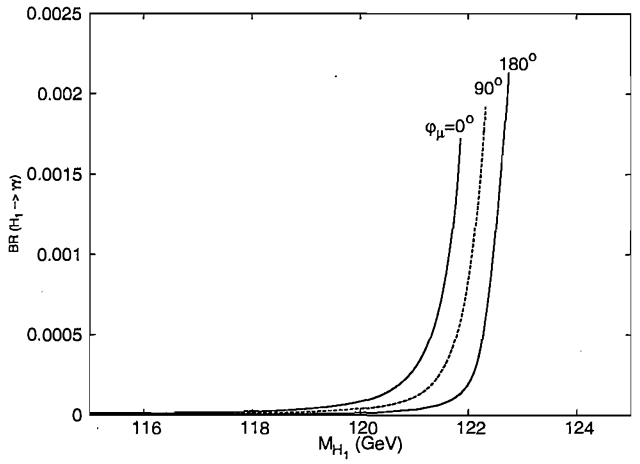

(a)

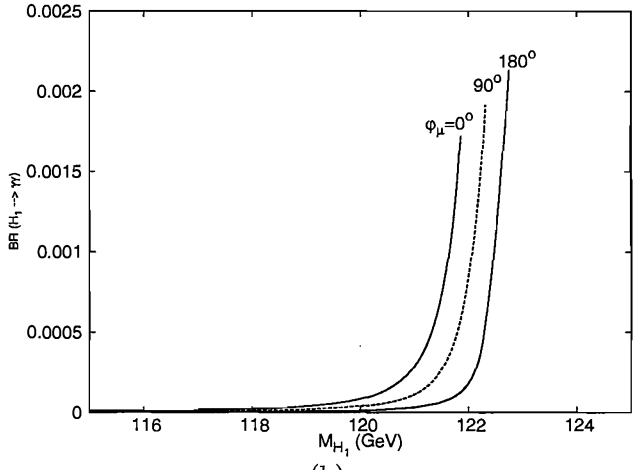

(b)

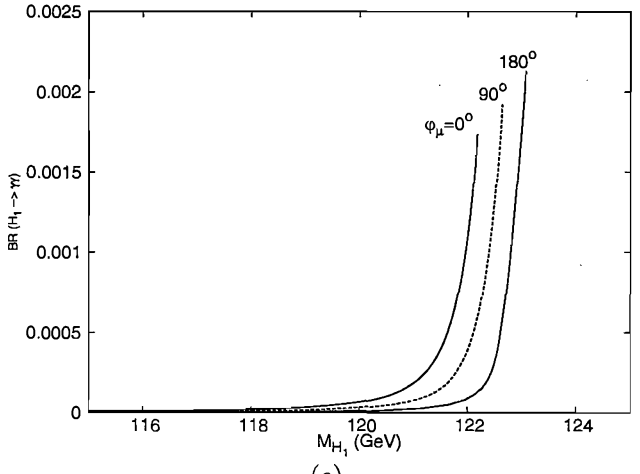

(c)

Figure 3.8: BR of H_1 into two photons for three values of ϕ_μ = 0° (solid), 90° (dashed) and 180° (dotted), plotted against the H_1 mass, for the scenarios when (a) $M_{\tilde{D}_3} = 300$ GeV giving a light $\tilde{b}_1$, $\mathcal{O}(300$ GeV) (b) $M_{\tilde{L}_3} = 300$ giving $\tilde{\tau}_1$ of $\mathcal{O}(300$ GeV), and (c) $M_2 = 150$ giving $\tilde{\chi}_1^\pm$ of $\mathcal{O}(120$ GeV), while all the remaining sparticles are heavy. The values of the other input parameters for all these scenarios are identical: $M_{Q_3} = 1$ TeV, $|A_{\tilde{f}}| = 1.5$ TeV, $|\mu| = 1$ TeV, $\tan\beta = 20$.

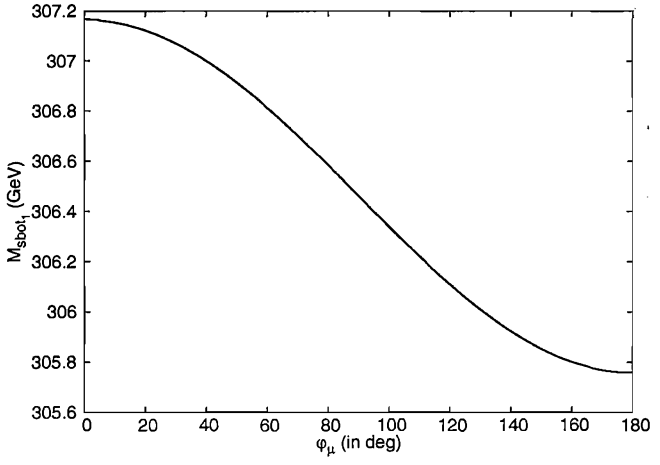

Figure 3.9: Mass of $\tilde{b}_1$ as a function of ϕ_μ.

Our statement regarding sparticle contributions becomes more convincing if we perform a form–factor level analysis of the cases mentioned above. Plotted in fig. 3.10a,b is the (individual and combined) contribution to the real part of $S_i^\gamma(M_{H_i})$ given in eq. (3.5), from SM particles (a) versus that from $\tilde{t}_1$ (b) in the scenario when it is the only light sparticle. We see that the former is roughly twice the size of the latter at the maximum. The scenario with a light $\tilde{b}_1$ is presented in fig. 3.11a,b, where clearly the maximum $\tilde{b}_1$ contribution is at least two orders of magnitude smaller than the SM one. Although not shown here, it can be verified that the contributions from $\tilde{\tau}_1$ and $\tilde{\chi}_1^\pm$ are also of the same order as $\tilde{b}_1$.

3.3 Conclusion

In summary, while a full study incorporating the production processes and detector dependent aspects are needed to have a clear quantitative picture, our preliminary analyses indicate that the di–photon channel of the lightest Higgs boson may enable one

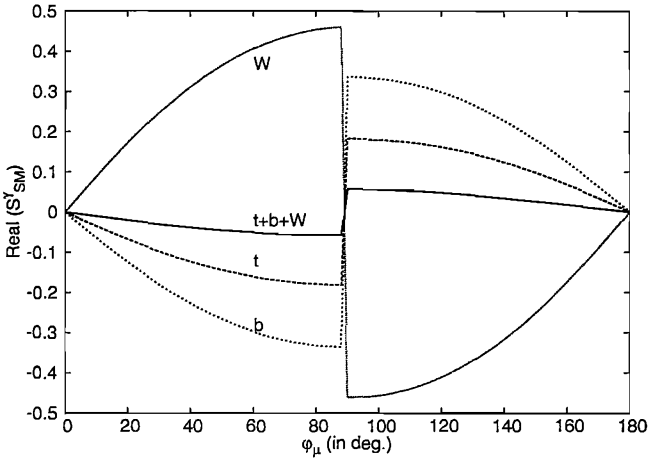

(a)

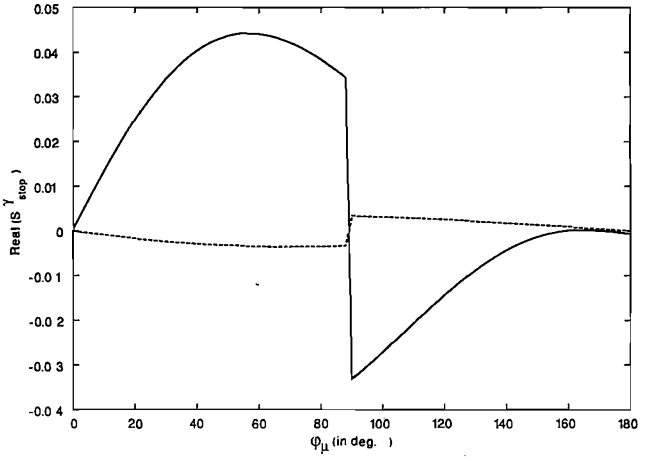

(b)

Figure 3.10: Contribution to the real part of $S_i^{\gamma}(M_{H_i})$ from (a) SM particles individually (dashed lines) and combined (solid line), and (b) $\tilde{t}_1$ (solid line) and $\tilde{t}_2$ (dotted line), as a function of ϕ_μ.

to distinguish the CP–violating MSSM from the CP–conserving one, so long that some SUSY parameters are measured elsewhere, even if the precision on these measurements is as low as about 10 % or so. This is not phenomenologically inconceivable, as the $H_1 \to \gamma\gamma$ detection mode requires a very high luminosity, unlike the discovery of those sparticles (and the measurement of their masses and couplings which are in turn determined in terms of the SUSY parameters once some SUSY signals have been established [30]) that impinge on the Higgs process studied here. We have also presented

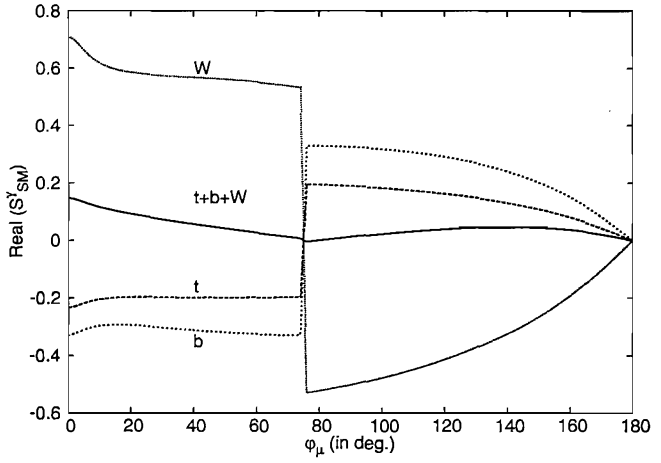

(a)

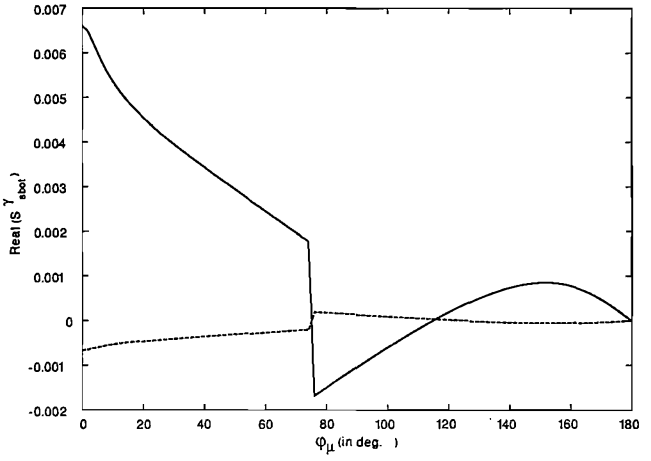

(b)

Figure 3.11: Contribution to the real part of $S_i^{\gamma}(M_{H_i})$ from (a) SM particles individually (dashed lines) and combined (solid line), and (b) $\tilde{b}_1$ (solid line) and $\tilde{b}_2$ (dashed line), as a function of ϕ_μ.

a detailed analysis of the factors contribution to CP–violation in the $H_1 \to \gamma\gamma$ decay and shown that the modified couplings as well as the stop mass account for maximal variation in its BR in the MSSM with explicit CP–violation compared to the one with CP conserved. A complete analysis will eventually require to fold the decay process with propagator effects and the appropriate production mode (gluon-gluon fusion and Higgs-strahlung in this case), where similar CP-violating effects may enter.

Chapter 4

The Next-to-Minimal Supersymmetric Standard Model

4.1 Beyond the MSSM

4.1.1 Problem with the MSSM

The MSSM, though efficiently solves the hierarchy and naturalness issues of the SM and is attractive due to the small number of parameters required to fully specify the theory in its constrained version at least, is itself faced by a problem of phenomenological significance. As seen in sect. 2.3.2, the MSSM superpotential can be written as

$$W_{\rm MSSM} = \hat{Q}\hat{H}_u \mathbf{h_u} \hat{U}^C + \hat{H}_d \hat{Q} \mathbf{h_d} \hat{D}^C + \hat{H}_d \hat{L} \mathbf{h_e} \hat{E}^C + \mu \hat{H}_u \hat{H}_d. \tag{4.1}$$

The last term in the above equation contains a dimensionful parameter μ. A corresponding bilinear SUSY–breaking term of the form

$$V_1 = B\mu H_u H_d + h.c., \tag{4.2}$$

where B is of the order M_{SUSY} like the rest of the soft SUSY–breaking parameters since they are all assumed to have a common origin, also appears in the effective scalar potential. This bilinear term is essential if the pseudoscalar P is to avoid being a phenomenologically unacceptable EW axion in the MSSM with $v_u, v_d \neq 0$. The value of the (arbitrary) parameter μ is thus, also phenomenologically constrained to be close to M_{SUSY} or m_W [99]. However, since μ is present before SUSY is broken, one would naturally expect its value to be either 0 or the Planck mass M_P. On one hand, if $\mu = 0$, the form of the RG equations [100] implies that the mixing between Higgs doublets is not generated at any scale and the minimum of the Higgs potential occurs for $\langle H_d \rangle = 0$, and that would in turn result in massless down–type fermions and leptons after $\text{SU}(2)_L$ symmetry breaking. On the other hand, $\mu \approx M_P$ would reintroduce the fine–tuning problem in the MSSM since the Higgs scalars would acquire a huge contribution $\sim \mu^2$ to their squared masses (thus impairing the justification of SUSY, which is invoked to effectively remove such quadratically divergent contributions to the Higgs mass from SM particles). This is the so–called μ–problem of the MSSM.

4.1.2 The Next–to–Minimal Supersymmetric Standard Model

There have been a couple of suggestions on countering the μ–problem. One approach is known as the Giudice–Masiero mechanism [102], in which μ automatically arises from the general couplings of broken supergravity and hence all low energy mass parameters arise from supergravity breaking. A more general and more elegant solution, however, is to introduce a new singlet scalar field S into the theory and replace the μ–term in the MSSM superpotential by an interaction term $\sim \lambda \hat{S} \hat{H}_u \hat{H}_d$. At the same time, also the soft term $B\mu H_u H_d$ in the Lagrangian gets replaced by the term $\sim \lambda A_\lambda S H_u H_d$. When the extra scalar field S acquires a VEV, an effective μ term, naturally of the EW scale,

is generated automatically. Such a mechanism operates in many superstring models based on $\mathbb{E}_6$ [101] and SU(5) $\times$ U(1) GUT groups [103], in which the renormalisable superpotential is purely trilinear and automatically contains a coupling of the form in eq. (4.2) to some singlet field N.

The implementation of such an idea in the MSSM results in a model known as the Next–to–Minimal Supersymmetric Standard Model (NMSSM) [104], described by the superpotential

$$W_{\text{NMSSM}} = \hat{Q}\hat{H}_u\mathbf{h_u}\hat{U}^C + \hat{H}_d\hat{Q}\mathbf{h_d}\hat{D}^C + \hat{H}_d\hat{L}\mathbf{h_e}\hat{E}^C + \lambda\hat{S}(\hat{H}_u\hat{H}_d) + \frac{1}{3}\kappa\hat{S}^3 + \ldots, \quad (4.3)$$

where $\hat{S}$ is an extra Higgs isosinglet superfield, λ and κ are dimensionless couplings and the last term results from the $\mathbb{Z}_3$ symmetry which is imposed to forbid the dangerous PQ symmetry (which is broken in the MSSM by the μ–term itself). The spontaneous breaking of this symmetry would lead to the appearance of the PQ–axion (as seen in sect. 1.5), ruling out most of the model's parameter space [105]. The ellipses stand for possible renormalisable terms that can be safely neglected when considering low–energy processes if there are no intermediate mass scales between m_W and M_P (as we assume here). Moreover, this form of the superpotential is scale independent, so that if bilinear terms are absent at tree–level, they cannot be generated by renormalisation.

As stated, the NMSSM superpotential given above is still invariant under a discrete $\mathbb{Z}_3$ symmetry [106], which is spontaneously broken at the EW scale when the Higgs fields acquire a non–zero VEV. It is well known, however, that the spontaneous breaking of such a discrete symmetry results in disastrous cosmological domain walls [107], unless it is explicitly broken by the nonrenormalisable sector of the theory. In order to break this $\mathbb{Z}_3$ symmetry, operators suppressed by powers of the Planck scale can

be introduced. However, these operators in general give rise to quadratically divergent tadpole contributions, which once again lead to a destablisation of mass hierarchy [108].

This problem can be circumvented by introducing new discrete symmetries (such as $\mathbb{Z}_{5R}$ of the $\mathrm{U}(1)_{R'}$ combination $R' = 3R+PQ$) to forbid or loop–suppress the dangerous tadpole contributions. In this case the breaking of the $\mathbb{Z}_3$ symmetry should be small enough to not upset the mass hierarchy but large enough to prevent the problematic domain walls [109]. Thus the surviving tadpole terms are sufficiently suppressed so that the low–energy phenomenology of the model is not affected. Alternative formulations to the NMSSM – known as the Minimal Non–minimal Supersymmetric Standard Model (MNSSM) and new Minimally–extended Supersymmetric Standard Model or nearly–Minimal Supersymmetric Standard Model (nMSSM) – also exist [110].

Upon EWSB, a VEV will be generated in the superpotential, eq. (4.3), for the real scalar component of $\hat{S}$ (the singlet Higgs field), $\langle S \rangle$, alongside those of the two doublets, $\langle H_u \rangle$ and $\langle H_d \rangle$. In the absence of fine–tuning, one should expect these three VEVs to be of the order of M_{SUSY} or m_W (nevertheless, the mechanism generating the common scale of order 100 GeV to 1 TeV is left unexplained). Since λ is also in the perturbative regime now, one has an 'effective μ–parameter', $\mu_{\mathrm{eff}} = \lambda\langle S \rangle$, naturally of the required size, thus solving the μ–problem. Once such a term is present in the superpotential, evolution from M_P to M_{SUSY} or m_W will, in general, automatically generate a contribution to the soft SUSY–breaking potential of the form

$$V_1 = -\lambda A_\lambda S H_u H_d + h.c. \tag{4.4}$$

Besides effectively eradicating the μ–problem, there are some other added features of non–minimal SUSY models. For instance, all such models predict the existence of a

(quasi–)stable singlet–type neutralino (the singlino) that could be responsible for the dark matter of the universe [111]. Also, in these extended SUSY models, the singlet superfield $\hat{S}$ has no SM gauge group charge (so that MSSM gauge coupling unification is preserved) and one can comfortably explain the baryon asymmetry of the universe by means of a strong first order EW phase transition [112] (unlike the MSSM, which would require a light top squark and Higgs boson barely compatible with current experimental bounds [113]).

4.1.3 Higgs Phenomenology in the NMSSM

In the NMSSM, the soft SUSY–breaking Higgs sector is described by [114]:

$$V_{\rm NMSSM} = m_{H_u}^2 H_u^\dagger H_d + m_{H_d} H_d^\dagger H_d + m_S^2 |S|^2 - \left(\epsilon_{ij} \lambda A_\lambda S H_d^i H_u^j + \frac{1}{3} \kappa A_\kappa S^3 + h.c. \right), \tag{4.5}$$

where A_λ and A_κ are dimensionful parameters of order $M_{\rm SUSY}$. As a result of the introduction of an extra complex singlet scalar field, the Higgs sector of the NMSSM comprises of a total of seven mass eigenstates: a charged pair $H^\pm$, three CP–even Higgses $H_{1,2,3}$ ($M_{H_1} < M_{H_2} < M_{H_3}$) and two CP–odd Higgses $A_{1,2}$ ($M_{A_1} < M_{A_2}$). The detailed formulation of the NMSSM Higgs sector is given in Appendix C.

The extended Higgs sector of the NMSSM hints at a phenomenology that could be plausibly different from that in the MSSM. As an indication, the mass expressions for the CP–even Higgses in the NMSSM can be translated into a modified upper bound on the lightest Higgs mass as

$$M_{H_1}^2 \leq m_Z^2 \cos^2 2\beta + \frac{\lambda^2}{2} \nu^2 \sin^2 2\beta + \Delta, \tag{4.6}$$

where the first term on the RHS describes the MSSM upper limit while the second term

is specific to the NMSSM (Δ represents the higher order corrections which are similar in both models due to similar particle content). This expression dictates a slightly elevated upper bound on the lightest Higgs boson in the NMSSM from the one in the MSSM, reaching 135–140 GeV, for maximal stop mixing and $\tan\beta = 2$ [115, 116] (a configuration indeed excluded in the MSSM by LEP data).

4.2 The No–Lose Theorem for NMSSM Higgses

4.2.1 Theorem Revisited

As stated earlier, the NMSSM Higgs sector bears a lot of promise for new physics signals. The raised upper bound on the lightest Higgs mass provides a reasonably enhanced window to the experimentalists in which to search for such a Higgs boson, since the lower limit set by the LEP2 on the Higgs mass is short by only a few GeV of the theoretical upper limit on the lightest Higgs mass in the MSSM for small values of $\tan\beta$. Incidentally, such small values of $\tan\beta$ turn out to be of greater significance to our NMSSM analysis. As for future machines, chiefly the LHC, quite some work has been dedicated to probing the NMSSM Higgs sector over recent years. Primarily, there have been attempts to establish a so–called 'No–lose theorem' for the NMSSM Higgses. The theorem was originally formulated for the MSSM Higgs sector and states that at least one MSSM Higgs boson should be observed via the usual SM–like production and decay channels at the LHC throughout the MSSM parameter space [60].

For the case of the NMSSM, the theorem [117, 118] can only be tested for the portion of the parameter space that does not allow any Higgs–to–Higgs decay. However, when the only light non–singlet (and, therefore, potentially visible) CP–even Higgs boson,

H_1 or H_2, decays mainly through one of the channels:

$$i)\ H \to \acute{H}\acute{H}, \quad ii)\ H \to AA, \quad iii)\ H \to H^{\pm}H^{\mp}, \quad iv)\ H \to AZ,$$

$$v)\ H \to H^{\pm}W^{\pm}, \quad vi)\ \acute{A} \to HA, \quad vii)\ A \to HZ, \quad viii)\ A \to H^{\pm}W^{\mp},$$

where $H(A)$ and $\acute{H}(\acute{A})$ refer to the heavier and lighter of two CP–even(odd) Higgses, respectively, one may not have a Higgs signal of statistical significance at the LHC [119, 120]. In fact, further violations to the theorem may occur if one enables Higgs–to–SUSY decays (e.g., into neutralino pairs, yielding invisible Higgs signals). Fortunately though, the regions violating the theorem account for a very tiny fraction ($\sim 1\%$) of the entire (allowed) NMSSM parameter space [121].

From preliminary studies [118] it appeared that using the $qq \to qqW^+W^-, qqZZ \to qqH_{1,2} \to qqA_1A_1$ detection mode, i.e., via VBF, may lead to the possibility of establishing a no–lose theorem in the NMSSM, particularly if the lightest CP–odd Higgs mass is such that there can happen abundant $A_1A_1 \to b\bar{b}\tau^+\tau^-$ decays, with both τ–leptons being detected via their e, μ leptonic decays[1]. At high luminosity, this signal may be detectable at the LHC as a bump in the tail of a rapidly falling mass distribution. However, this procedure relies on the background shape to be accurately predictable. These analyses were based on Monte Carlo (MC) event generation (chiefly, via the SUSY routines of the `HERWIG` v6.4 code [122]) and a toy detector simulation (`GETJET`, based on UA1 software). Further analyses based on `PYTHIA` v6.2 [123] and a more proper ATLAS detector simulation (`ATLFAST`) [119] found that the original selection procedures may need improvement in order to extract a signal [120].

In an attempt to reassess the theorem, we decided to investigate the possibilities

[1]The scope of other decays, $A_1A_1 \to jjjj$, $A_1A_1 \to jj\tau^+\tau^-$ (where j represents a light quark jet) or $A_1A_1 \to \tau^+\tau^-\tau^+\tau^-$ is very minute in comparison.

offered by exploiting Higgs–strahlung (HS) off gauge bosons ($q\bar{q}' \to W^{\pm *} \to W^{\pm} H_{1,2}$, with a subleading component from $q\bar{q} \to Z^{0*} \to Z^0 H_{1,2}$) and, more marginally, off heavy quark pairs (chiefly top quarks, $q\bar{q}, gg \to t\bar{t}H$, because of the small $\tan\beta$ values involved in the scenarios outlined in [118]) as the underlying Higgs production modes with the Higgs decaying into a pair of pseudoscalars, in place of or – better – alongside VBF.

4.2.2 NMSSM Parameter Space

As the first step for our analysis, we needed to outline the parameter space that we intended to explore. The choice of the parameter space largely depends on the version of the NMSSM under consideration, or more specifically, on the implication of unification of parameters at some very high scale in the model. This, in turn, leans on the technique adopted for the breaking of SUSY, as seen in sect. 2.2.2.

In order to render our very preliminary analysis reasonably general, instead of postulating unification and without taking into account the SUSY breaking mechanism, we fixed the soft SUSY breaking terms to a very high value, so that they had little or no contribution to the outputs of the parameter space scans. Consequently, we were left with six free parameters; the trilinear couplings λ and κ, the soft trilinear terms A_λ and A_κ, $\tan\beta$ and $\mu_{\text{eff}} = \lambda\langle S\rangle$.

We used the publicly available `Fortran` code `NMHDECAY` v1.1 [124]. This program computes the masses, couplings and decay widths of all the Higgs bosons of the NMSSM in terms of its parameters at the EW scale. The computation of the spectrum by `NMHDECAY` includes leading two loop terms, EW corrections and propagator corrections. The decay widths, however, do not include three body decays. `NMHDECAY` also takes into account theoretical as well as experimental constraints from negative Higgs searches at

LEP along with the unconventional channels relevant for the NMSSM and eliminates parameter points which violate such constraints. We used the (slightly modified) code to scan over the NMSSM parameter space defined through the aforementioned six parameters taken in the following intervals:

$$\lambda : 0.0001 - 0.75, \quad \kappa : -0.65 - +0.65, \quad \tan\beta : 1.6 - 54,$$

$$\mu_{\text{eff}},\, A_\lambda,\, A_\kappa : -1000 - +1000 \text{ GeV}.$$

Remaining soft terms which were fixed in the scan include:

- $m_{\tilde{Q}_3} = m_{\tilde{U}_3} = m_{\tilde{D}_3} = m_{\tilde{L}_3} = m_{\tilde{E}_3} = 2$ TeV,
- $A_{\tilde{U}_3} = A_{\tilde{D}_3} = A_{\tilde{E}_3} = 1.5$ TeV,
- $\tilde{m}_Q = \tilde{m}_U = \tilde{m}_D = \tilde{m}_L = \tilde{m}_E = 2$ TeV,
- $M_1 = M_2 = M_3 = 3$ TeV.

The above ranges of parameters was specified through the condition of positivity of the following tests [121]:

1. Squark/slepton masses–squared are positive.

2. The running Yukawa coupling does not encounter a Landau sigularity below the GUT scale.

3. The scalar potential is deeper than the local unphysical minima with vanishing $\langle H_u \rangle = v_u$, $\langle H_d \rangle = v_d$ or $\langle S \rangle = v_s$, and so the minimum with all VEVs non–zero is the true minimum.

4.2.3 Spectrum Configuration and Scan

The allowed decay modes for neutral NMSSM Higgs bosons included[2]:

$$H, A \to gg, \quad H, A \to \mu^+\mu^-, \quad H, A \to \tau^+\tau^-, \quad H, A \to b\bar{b}, \quad H, A \to t\bar{t},$$

$$H, A \to s\bar{s}, \quad H, A \to c\bar{c}, \quad H \to W^+W^-, \quad H \to ZZ,$$

$$H, A \to \gamma\gamma, \quad H, A \to Z\gamma, \quad H, A \to \text{Higgses}, \quad H, A \to \text{sparticles}.$$

(Notice that for the pseudoscalar Higgses, the decay into vector boson pairs is not allowed due to CP–conservation.) Here, 'Higgses' refers to any final state involving all possible combinations of two Higgs bosons (neutral and/or charged) or of one Higgs boson and a gauge vector.

We performed our scan over several millions of randomly selected points in the specified parameter space. The output contained masses, BRs and couplings of the NMSSM Higgses for all the points which were not forbidden by the various constraints imposed within the code. These surviving data points were then used to determine the cross–section for NMSSM Higgs hadro–production by using an adapted version of the codes described in [14]. As the SUSY mass scales have been arbitrarily set well above the EW one, the NMSSM Higgs production modes exploitable in simulations at the LHC are those involving couplings to heavy ordinary matter only, i.e., the direct production modes described in sect. 1.4.2. The production and decay rates for NMSSM neutral Higgs bosons were then multiplied together to yield inclusive event rates, assuming a LHC luminosity of 100 fb^{-1} throughout.

[2]Here, the label $H(A)$ signifies any of the neutral CP–even(odd) Higgs bosons of the NMSSM.

4.2.4 Complementary Higgs Production modes at the LHC

As the study aims at comparing the yield of VBF, $qq \to qqH$, against HS off W bosons (W–HS), $qq \to WH$, and off $t\bar{t}$ pairs (tt–HS), $gg \to ttH$, it is of relevance to examine in fig. 4.1 the light Higgs hadro–production cross–section at the LHC in the SM, as the NMSSM rates would be obtained from these (for a given Higgs mass) by rescaling the VVH and ttH couplings. We see that in the SM W–HS dominates for Higgs masses below 80 GeV while VBF becomes the leading channel above such a value (in the NMSSM these two processes are rescaled by the same amount). The case tt–HS is generally subleading (even in the presence of appropriate NMSSM couplings), but not negligible at low Higgs masses. Besides, notice that HS off a Z boson is always very small, and hence we ignored it for the remainder of our analysis. It is also worth recalling that gluon–fusion, despite being the mode with largest production rates, plays no role in our case, as $H_{1,2} \to A_1 A_1$ decay channels would not be extractable in this case from the background because because in the 4–jet decay of the pseudoscalar Higgses produced through this channel, the background is overwhelming while in the case of τ–decay, triggers may not be possible. (Notice in the figure the normalisation via NLO QCD throughout.)

As a second step we computed the NMSSM total cross–section times BR into $A_1 A_1$ pairs for VBF and W–HS + tt–HS for each of the two lightest neutral Higgs bosons, H_1 and H_2. We display these rates in fig. 4.2 as a function of M_{H_1} and M_{H_2}. Here, one can appreciate that there exist more possibilities of establishing a H_1 signal than one due to H_2, since even though the decay rates and patterns are the same for both the Higgses, the normalisation is different. Whereas the potential to detect the heavier of these two Higgs states is confined to masses above 115 GeV or so and probably below 140 GeV, when VBF is largely dominant with respect to W–HS + tt–HS, in the case

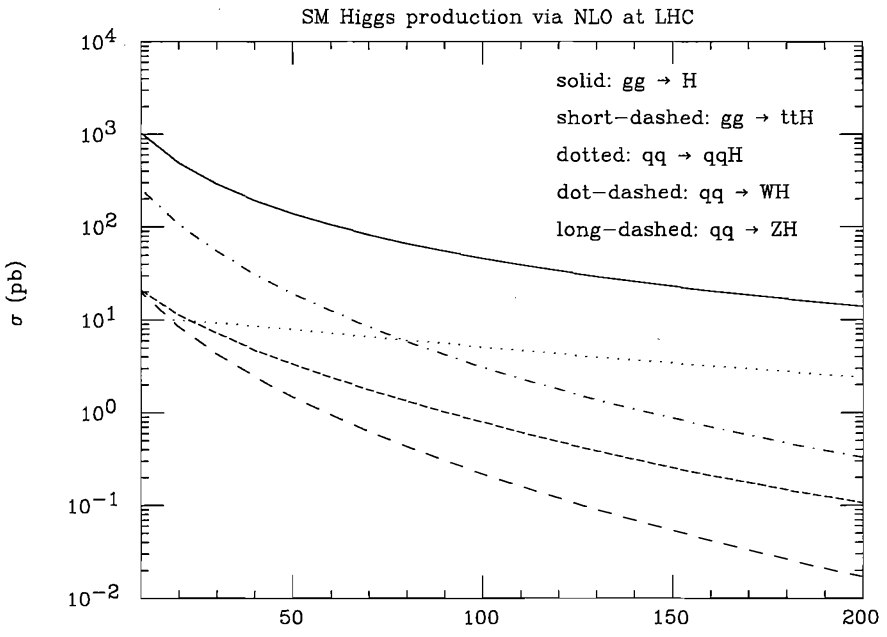

Figure 4.1: The Higgs production cross–section through NLO QCD in the SM at the LHC [13].

of the light state there exists a low mass window where production rates via the latter two processes combined are comparable to those from the former, most often within 10–20% of each other. In fact, at times, W–HS + tt–HS rates are larger than those for VBF, the more so the lower the H_1 mass. Recall that all parameter points examined here are compliant with collider bounds, even those at very low Higgs mass, as these correspond to reduced Higgs couplings to gauge bosons which are compensated by the large LHC luminosity.

Now, one should bear in mind that the rates in fig. 4.2 do not include yet the efficiency to trigger on the signal. In the case of VBF, one triggers on one forward and one backward jet, with transverse momentum $p_T > 20$ GeV, pseudorapidity $|\eta| < 5$ and $\eta(\text{fwd}) \cdot \eta(\text{bwd}) < 0$. The efficiency is here about 60%. In the case of W–HS, one triggers on a high transverse momentum lepton (electron or muon), with $p_T > 20$ GeV and $|\eta| < 2.5$. In this case the efficiency is lower, about 19%, primarily due to the fact that a W boson decays into electron/muons only about 20% of the times.

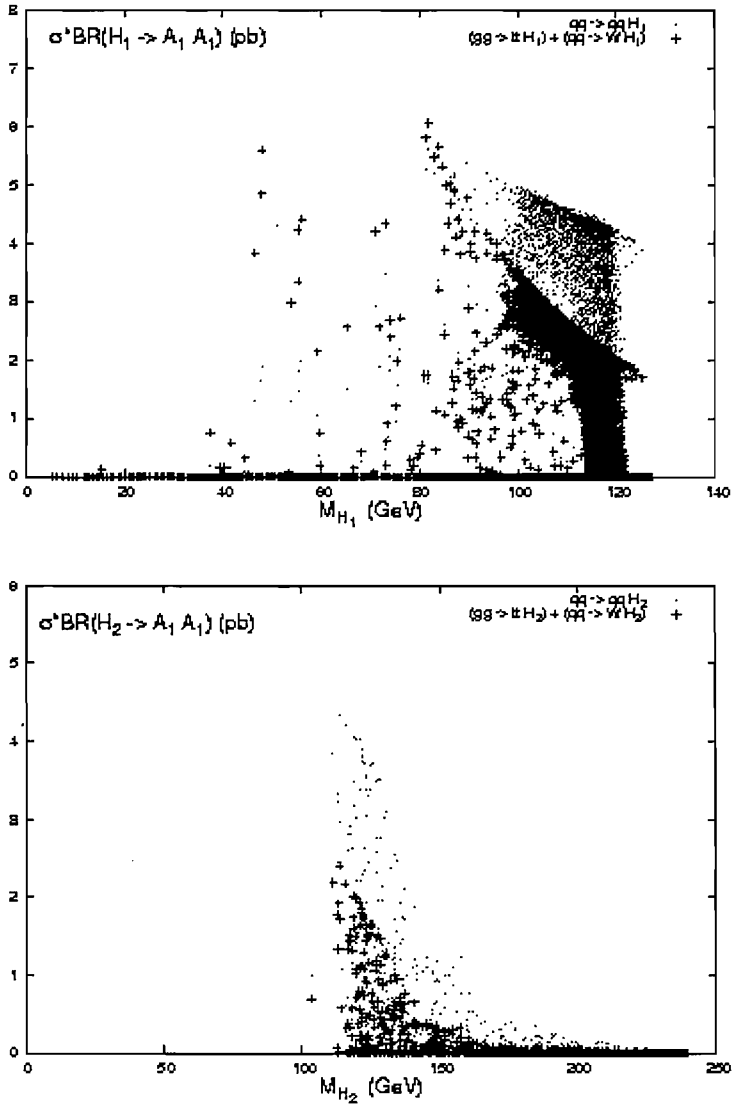

Figure 4.2: Cross–section times BR of H_1 (top) and H_2 (bottom) plotted against their respective masses. The symbol '·' refers to VBF while '+' to W–HS + tt–HS.

The efficiency for tt–HS is 14%, as one top is required to decay hadronically and the other leptonically. These efficiency values are basically independent of the Higgs mass. Even so, the W–HS component, aided by the tt–HS one, would make a sizable addition to the production rates of VBF. As we expect the efficiency of extracting whichever $H_{1,2} \to H_1 A_1$ decays to be the same in both processes[3], we see a potential in improving

[3]If anything, since no actual b–tagging was enforced in the earlier analyses [118, 119], whenever $A_1 A_1$ hadronic decays are present, we would expect the efficiency to worsen for the case of VBF, because of jet combinatorics.

the signal yield by using all mentioned channels beyond what is achieved by using VBF alone.

By recalling that the efficiency to trigger on VBF is at least three times the one to isolate W–HS + tt–HS, it is of particular interest to estimate the proportion of points where the latter gives more cross–section than the former. Despite the fact that W–HS + tt–HS very rarely exceeds VBF by more than a factor of three, there are clear zones of NMSSM parameters space where W–HS + tt–HS is consistently larger than VBF, those producing M_{H_1} values below 80 GeV, indeed the SM crossing point seen in fig. 4.1. Evidently, this mass range is of relevance to $H_1 \to A_1 A_1$ decays only, see fig. 4.2. For the case of $H_2 \to A_1 A_1$, cross–sections are much smaller in comparison and VBF is always very dominant, as – for potentially detectable rates – M_{H_2} is above ≈ 115 GeV and below ≈ 140 GeV. Finally, notice that $H_2 \to H_1 H_1$ decays very often compete with $H_2 \to A_1 A_1$ [121]. In fact the former occur almost as often as the latter over the NMSSM parameter space investigated here. In this respect, it is also interesting to see how the masses of the decaying Higgs bosons, H_1 and H_2, relate to that of the light A_1 state. This is illustrated in fig. 4.3.

Even after accounting for the trigger efficiencies, the VBF cross–sections plotted in fig. 4.2 are in the same range as those probed in the original formulation of the no–lose theorem[4] [118], so that, for similar H_1 and H_2 masses, we would expect to obtain the same overall detection efficiencies seen back then also for all our points falling in the mass range, say, 50 to 120 GeV. Crucially, NMSSM parameter points giving the highest cross–sections for VBF are the same yielding the largest rates for W–HS + tt–HS. More in general, from figs. 4.4a–b, one can also gather where the regions of highest

[4]We were in fact able to reproduce most of the points discussed therein.

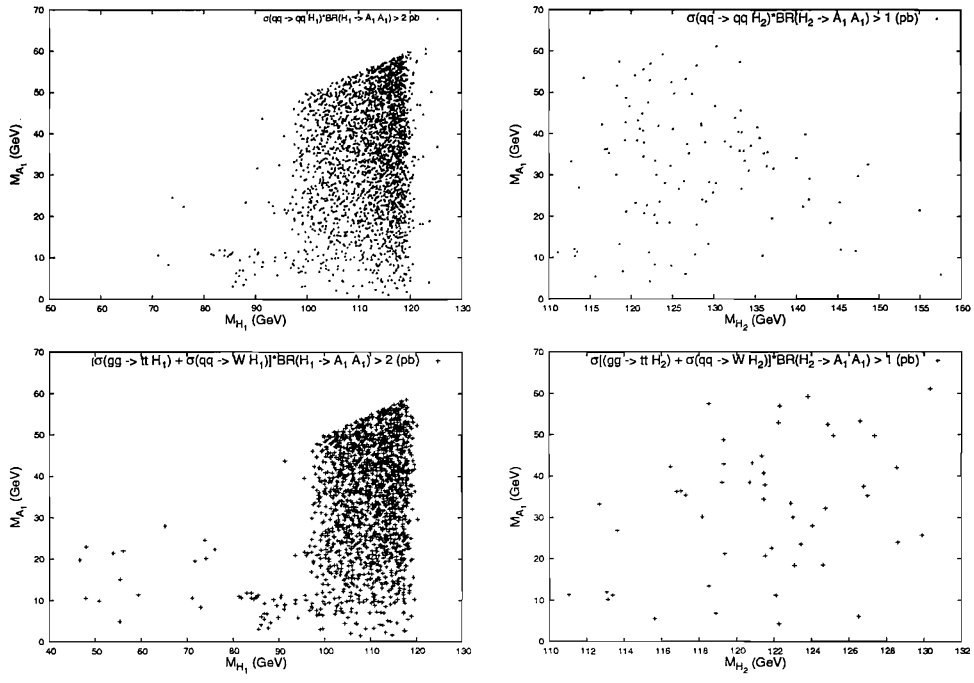

Figure 4.3: Distribution of the H_1 (left) and H_2 (right) masses with respect to that of A_1, when they are potentially visible in VBF (top) and W–HS + tt–HS (bottom), i.e., limited to those NMSSM parameter points for which cross–section times BR are larger than 2(1) pb (see text) for $H_1(H_2)$.

cross–sections, for both channels (VBF and W–HS + tt–HS) and Higgs flavours (H_1 and H_2), lie in the NMSSM parameter space. In particular, their distribution is quite homogeneous as they are not located in some specific areas (i.e., in a sense, not 'fine–tuned'), except for A_κ which is generally small in order to keep M_{A_1}, which is directly proportional to it, in the range relevant here. Altogether, the proportion of parameter space where the two production modes yield potentially detectable Higgs signals (at least according to the analysis in [118]), say, above 1–2 pb (prior to including tagging efficiencies and A_1 decay rates), is 0.21% for VBF and 0.13% for W–HS + tt–HS. However, if production cross–sections of 4 pb or upwards are required to render the $H_1 \to A_1 A_1$ signal visible, then the rates reduce to 0.096% and 0.0019%, respectively. For the case of $H_2 \to A_1 A_1$, the numbers are typically 20 and 10 times smaller for VBF and W–HS + tt–HS, respectively.

Clearly, while the production cross–sections (after triggering), the selection procedures and efficiencies to extract the Higgs decays may well be the same in both samples, the background will differ. In fact, whilst in the case of VBF the latter is dominated by top–antitop pair production and decay, for V–HS and tt–HS we expect that (more manageable) WZ + jets events will be the largest noise, assuming the most promising Higgs signature discussed above (i.e., $b\bar{b}\tau^+\tau^-$).

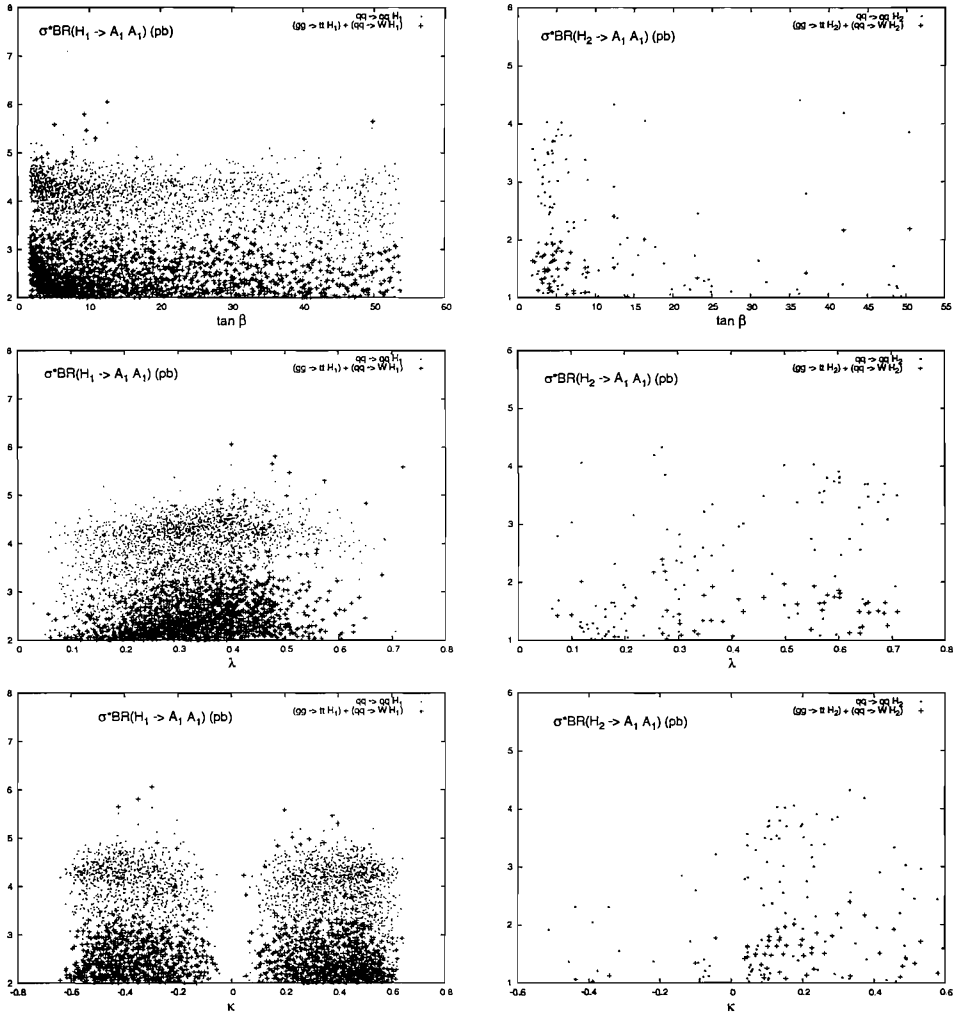

(a)

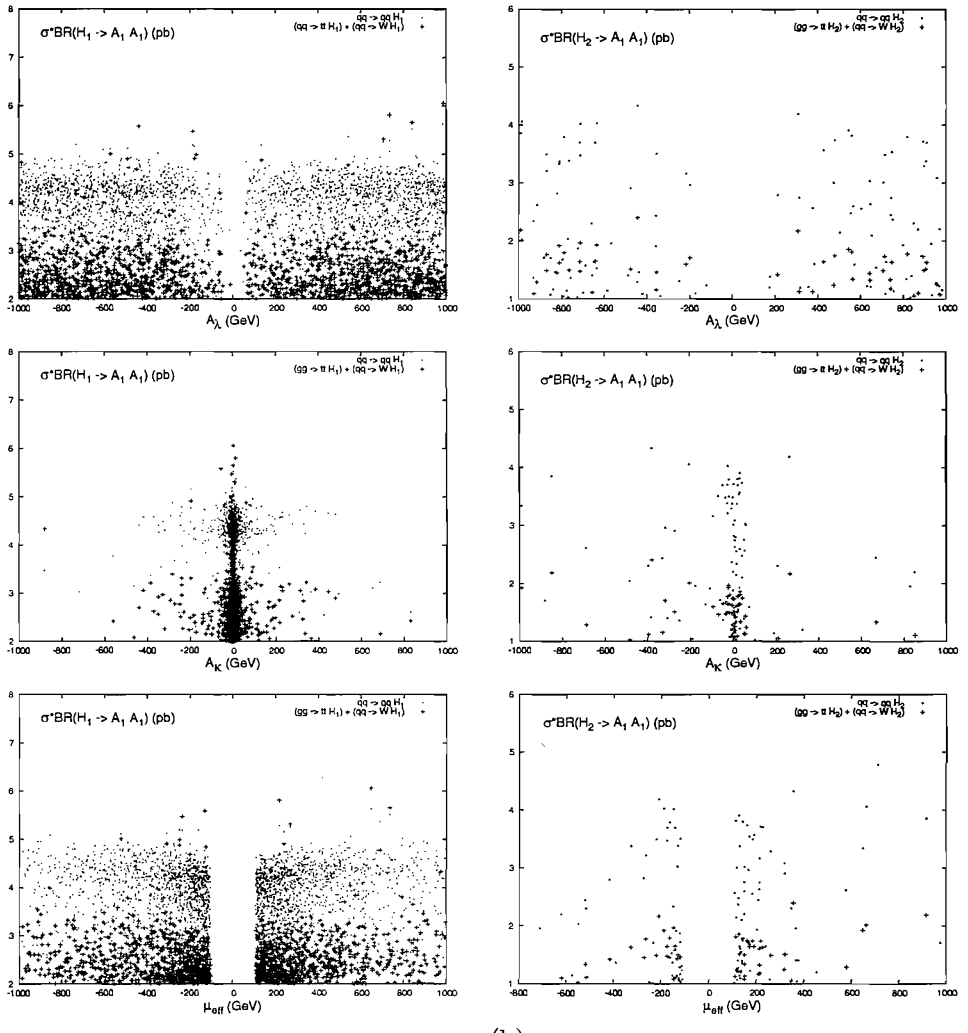

(b)

Figure 4.4: Cross–section times BR of H_1 (left) and H_2 (right) when potentially visible, i.e., limited to those NMSSM parameter points for which cross–section × BR is larger than 2(1) pb for $H_1(H_2)$, plotted against the following parameters: (a) $\tan\beta$, λ and κ; (b) A_λ, A_κ and $\mu_{\rm eff}$.

4.3 Establishing a More–to–Gain Theorem

4.3.1 Outline

In addition to reassessing the no–lose theorem by thoroughly exploiting the NMSSM Higgs sector, we embarked on an orthogonal approach also: an attempt to formulate a so–to–speak 'More–to–gain theorem' for the NMSSM. We intended to explore whether there exist regions in the NMSSM parameter space where more Higgs states of the NMSSM are visible at the LHC than those available within the MSSM, and thus highlight the best case scenarios for the former that would not only endorse the existence of the Higgs boson but also validate non–minimal SUSY beyond the SM. In our attempt to overview all such possibilities, we started by considering the case of the di–photon decay channel of neutral Higgs bosons. Notice that, for the NMSSM, there is another crucial factor that made us thrive on the $\gamma\gamma$ decay mode primarily besides its being the one of the most auspicious candidates for Higgs discovery at the LHC.

As opposed to the MSSM, where only a single (lightest) Higgs scenario can be realised in this particular decay mode, in the NMSSM, due to the rapidly falling tail of the $\gamma\gamma$ background with increasing invariant mass of the di–photon pair and owing to the fact that the photon detection efficiency grows with the Higgs mass [29], signal peaks for heavier Higgses could also be visible in addition to (or instead of) the lightest one, although the cross–section for these processes is relatively very low [41, 20]. This scenarios, while infeasible in the MSSM, are made possible in the NMSSM by the fact that larger number of Higgs states means that the splitting between their masses could be much smaller as compared to the MSSM, so that the intermediate state between the lightest and heaviest Higgses is also very likely to possess a mass well within the reach of the LHC. Also mixing amongst more Higgs states may favour some BRs, as there

are cancellations between fermions and bosons in the loop.

4.3.2 Inclusive Event Rates

We started, again, by computing the total cross–section times BR of decays into $\gamma\gamma$ pairs against each of the six parameters of the NMSSM, for each Higgs boson. We adopted the scan outputs described in sect. 4.2.2 and, employing all the direct production modes, started by computing total (i.e., fully inclusive) rates[5]. Based on the ATLAS analysis [30], we concluded that cross–section times BR rates of 10 fb or so are potentially interesting from a phenomenological point of view, in the sense that they may yield visible signal events, the more so the heavier the decaying Higgs state.

Tab. 4.1 recaps the potential observability of one or more NMSSM Higgs states in the di–photon decay mode at the LHC, under the above assumptions. It is obvious from the table that one light CP–even Higgs should be observable almost throughout the NMSSM parameter space, thus reaffirming the no–lose theorem. However, there is also a fair number of points where two Higgses may be visible simultaneously (H_1 and H_2 or – more rarely – H_1 and A_1), while production and decay of the three lightest Higgses (H_1, H_2 and A_1) at the same time, although possible, occurs for only a very small number of points in the parameter space. Furthermore, the percentage of points for which only the second lightest Higgs state is visible is also non–negligible. These last two conditions are clearly specific to the NMSSM, as they are never realised in the MSSM.

Importantly, while the lone detection of the lightest CP–even NMSSM Higgs boson may mimic a similar signal from the corresponding state in the MSSM, the reconstructed mass may well be beyond the upper mass limit in the MSSM, this possibility

[5]After verifying that the bulk of the signal rates is due to gluon–gluon fusion (even at large Higgs masses), we eventually decided – for simplicity – to limit ourselves to emulate only this channel. Hence, all the results quoted hereafter suffer from a slight underestimate of the signal rates.

Higgs Flavor	Points Visible		Percentage
H_1	Total:	1345884	99.7468
	Alone:	1345199	99.6961
	With H_2:	528	0.0391
	With A_1:	152	0.0113
	With H_2 and A_1:	5	0.0004
H_2	Total:	1253	0.0929
	Alone:	717	0.0531
	With H_1:	528	0.0391
	With A_1:	3	0.0002
	With A_1 and A_1:	5	0.0004
H_3	Total:	0	0
A_1	Total:	165	0.0122
	Alone:	5	0.0004
	With H_1:	152	0.0113
	With H_2:	3	0.0002
	With H_1 and H_2:	5	0.0004
A_2	Total:	0	0

Table 4.1: Higgs events potentially visible in the NMSSM at the LHC through the $\gamma\gamma$ decay mode (i.e., those yielding cross–section time BR rates of order 10 fb or upwards). Percentage refers to the portion of NMSSM parameter space involved for each discovery scenario.

also pointing towards an NMSSM Higgs sector. Finally, none of the two heaviest NMSSM neutral Higgs states (H_3 and A_2) will be visible in the di–photon channel at the LHC (given their large masses and hence tiny cross–sections).

4.3.3 Signatures for Non–Minimal Physics

We plotted the cross–section times BR for the three potentially observable Higgses against the various NMSSM parameters. These plots, shown in figs. 4.5–4.7, reveal that the distribution of possibly visible points (i.e., of those yielding cross–section times BR rates in excess of 10 fb) is quite homogeneous over the NMSSM parameter space

and not confined to some specific areas (i.e., again, not fine–tuned). The cross–section times BR for the same points as a function of the corresponding Higgs masses can be found in fig. 4.8.

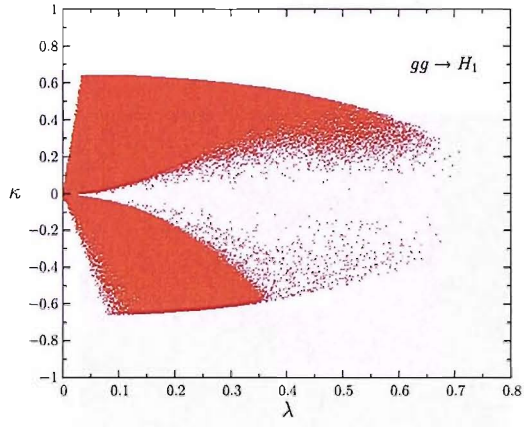

(a)

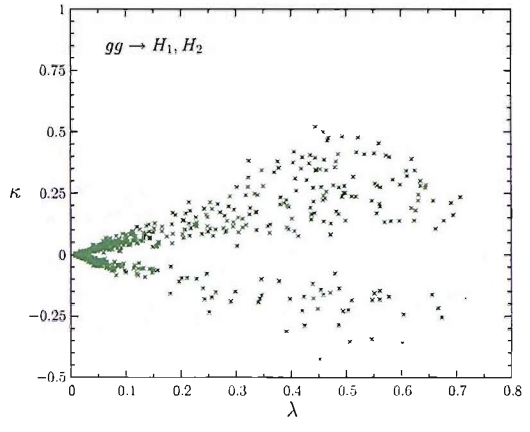

(b)

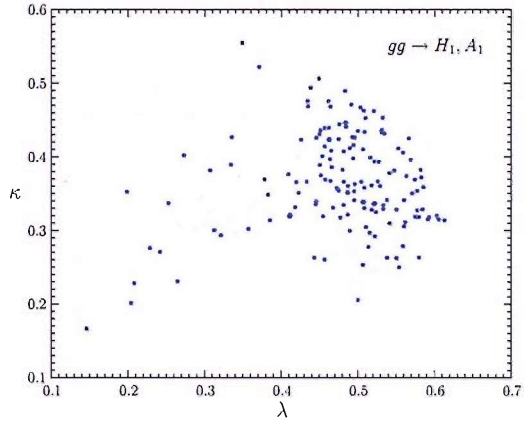

(c)

Figure 4.5: The NMSSM parameter space when (a) H_1 (red/dots) is potentially visible alone; (b) H_1 is potentially visible simultaneously with H_2 (green/crosses); and (c) H_1 is potentially visible simultaneously with A_1 (blue/stars); λ plotted against κ.

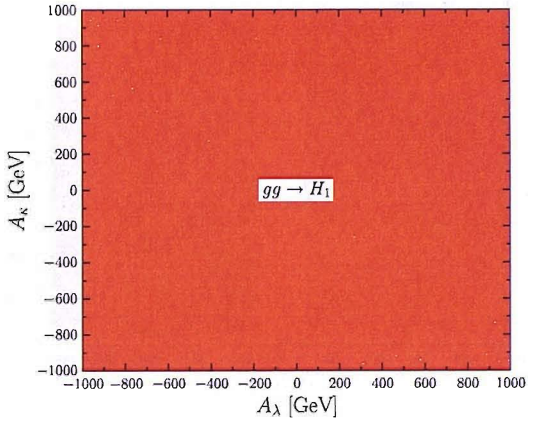

(a)

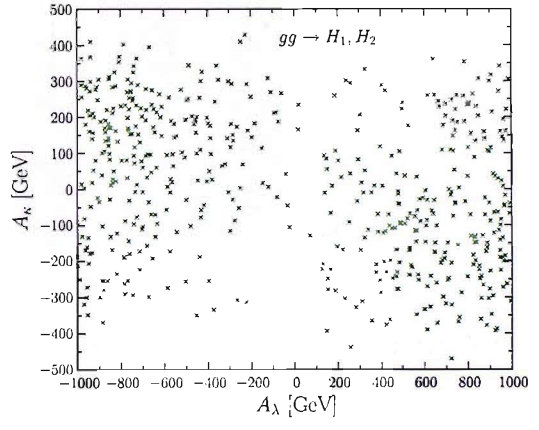

(b)

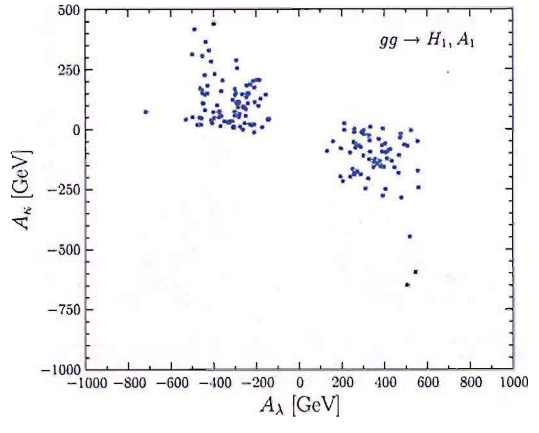

(c)

Figure 4.6: As fig. 4.5; A_λ plotted against A_κ.

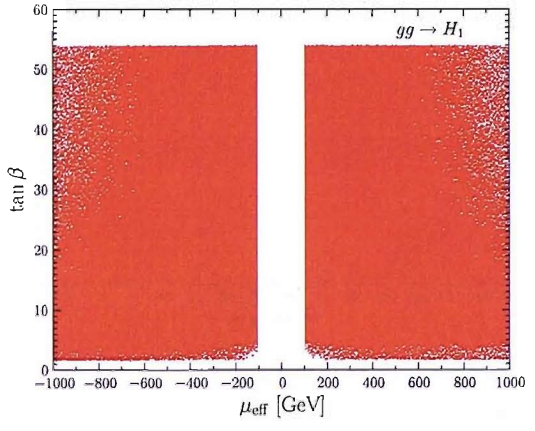

(a)

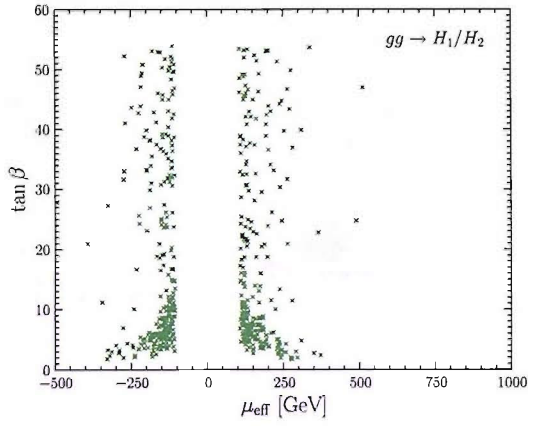

(b)

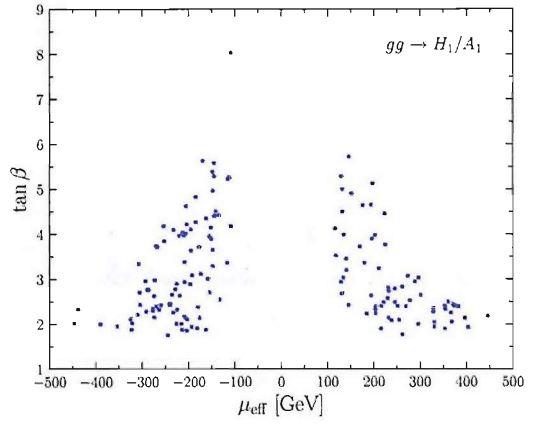

(c)

Figure 4.7: As fig. 4.5; $\mu_{\rm eff}$ plotted against $\tan\beta$.

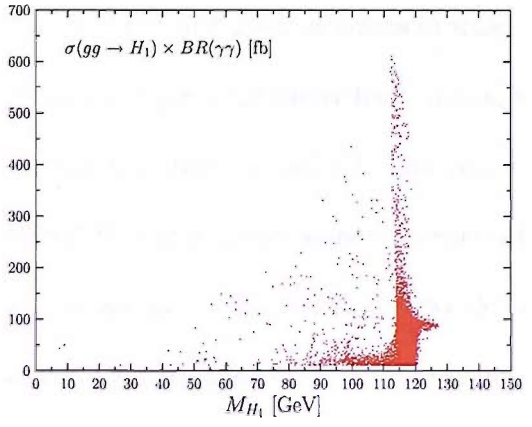

(a)

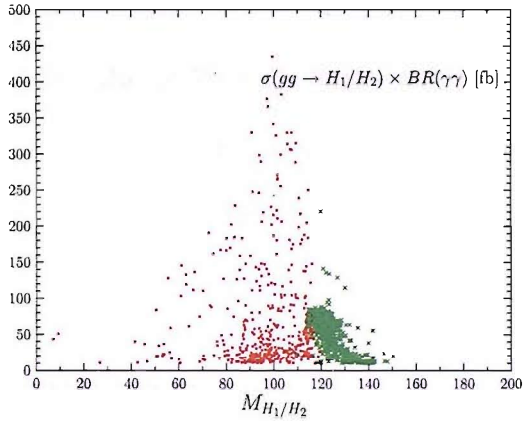

(b)

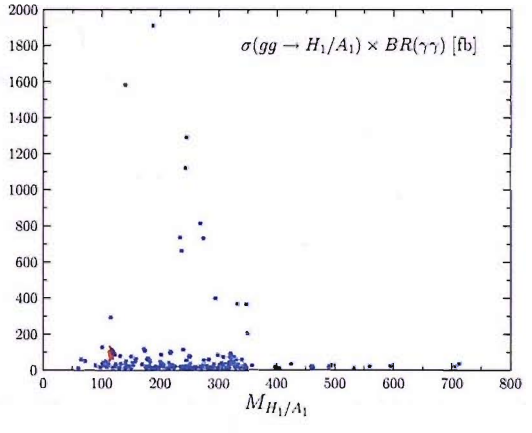

(c)

Figure 4.8: Cross–section times BR, (a) for H_1 (red/dots) when it is potentially visible alone; (b) for H_1 and H_2 (green/crosses) when both are potentially visible simultaneously; and (c) for $H1$ and A_1 (blue/stars) when both are potentially visible simultaneously, plotted against their respective masses.

Of particular relevance is the distribution of points in which only the NMSSM H_1 state is visible, when its mass is beyond the upper limit on the corresponding CP–even MSSM Higgs state mass, which is shown in fig. 4.9. This plot reveals that the masses of about 93% of the NMSSM H_1 states visible alone are expected to be within 2–3 GeV beyond the MSSM upper bound, hence the two models would be indistinguishable by and large[6]. Nonetheless, there is a fraction of a percent of such points with M_{H_1} values even beyond 125 GeV or so (the higher the mass the smaller the density, though), which should indeed allow one to distinguish between the two models. It must be pointed out here that we have used the value of 120 GeV (which is obtained at the same level of accuracy, i.e. second order leading log in perturbation theory) as the upper mass limit on the lightest CP–even Higgs boson of the MSSM instead of the one quoted generally ($\sim$ 130 GeV).

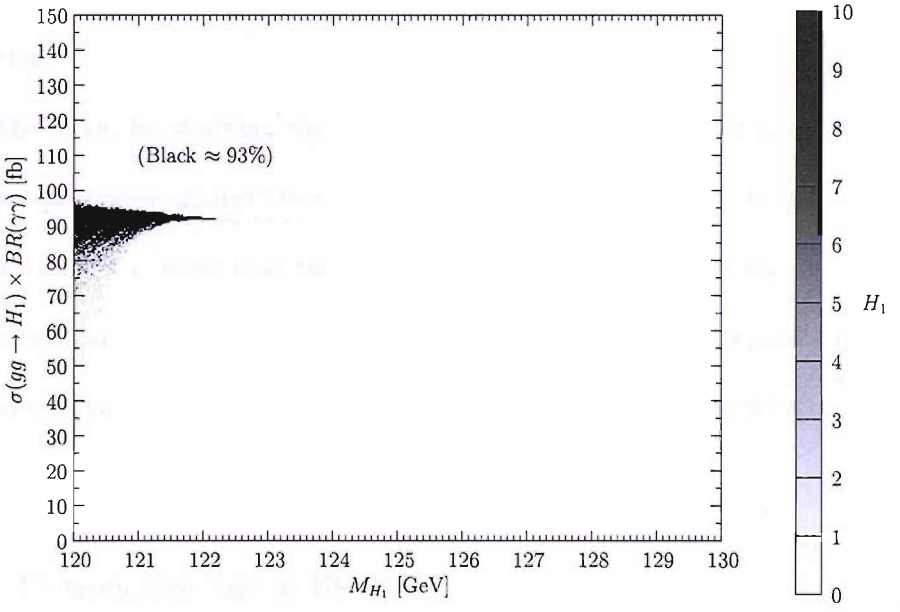

Figure 4.9: The distribution of points with potentially visible NMSSM H_1 state with mass beyond the MSSM upper limit on the corresponding Higgs state mass. The scale on the right represents a measure of point density.

[6]Other than an experimental di–photon mass resolution of 2 GeV or so [30] one should also bear in mind here that the mass bounds in both models come with a theoretical error of comparable size.

Notice here that the value obtained for $M_{H_1}^{\max}$ from NMHDECAY v1.1 and used in fig. 4.9, of $\sim$ 127 GeV, based on the leading two–loop approximations described in [124], is a few GeV lower than the value declared in sect. 4.1.3. This can be ascribed to the fact that we have assigned very high values to the SUSY masses while SUSY trilinear terms have been fixed to relatively smaller values. Performing a check with slightly lowered values of the SUSY masses and raised values of the trilinear couplings (which maximises the Higgs masses) easily reveals an upper limit complying with that quoted in sect. 4.1.3 [125]. But for the sake of consistency with the earlier analyses, we opted for the fixed SUSY parameters implemented herein. (Indeed, as we checked, a slightly modified $M_{H_1}^{\max}$ value is obtained for the NMSSM from NMHDECAY v2.1 [126], because of the improved mass approximations and loop corrections with respect to the earlier version of the program adopted here.) Eventually, when the LHC is online, the exercise that we are proposing can be performed with the then state–of–the–art calculations.

Furthermore, by studying the cross–section times BR of the Higgses when two of them are observable against their respective mass differences, figs. 4.10–4.12, one sees that the former are larger than the typical mass resolution in the di–photon channel, so that the two decaying objects should indeed appear in the data as separate resonances. (We also verified that their decay widths are small compared to the detector resolution in the $\gamma\gamma$ invariant mass.)

4.3.4 Prospective Signal Events

Next, we proceeded to a dedicated parton level analysis of signal and background processes, the latter involving both tree–level $q\bar{q} \to \gamma\gamma$ and one–loop $gg \to \gamma\gamma$ contributions. We have adopted standard cuts on the two photons [30]: $p_T^\gamma > 25$ GeV

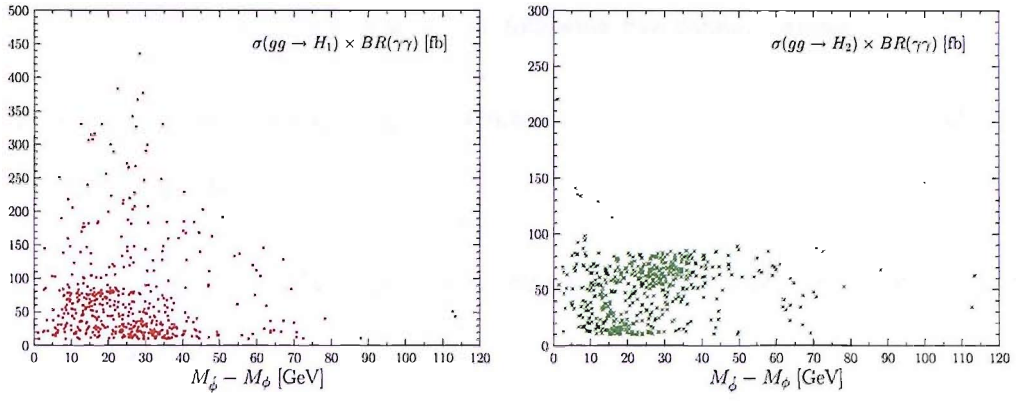

Figure 4.10: Cross–section times BR of H_1 (red/dots) and H_2 (green/crosses) plotted against their mass differences when the two are potentially visible simultaneously.

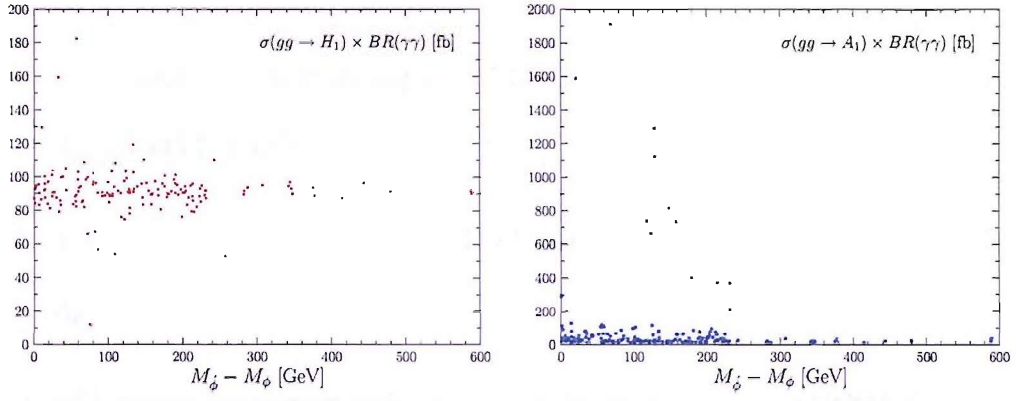

Figure 4.11: Cross–section times BR of H_1 (red/dots) and A_1 (blue/stars) plotted against their mass differences when the two are potentially visible simultaneously.

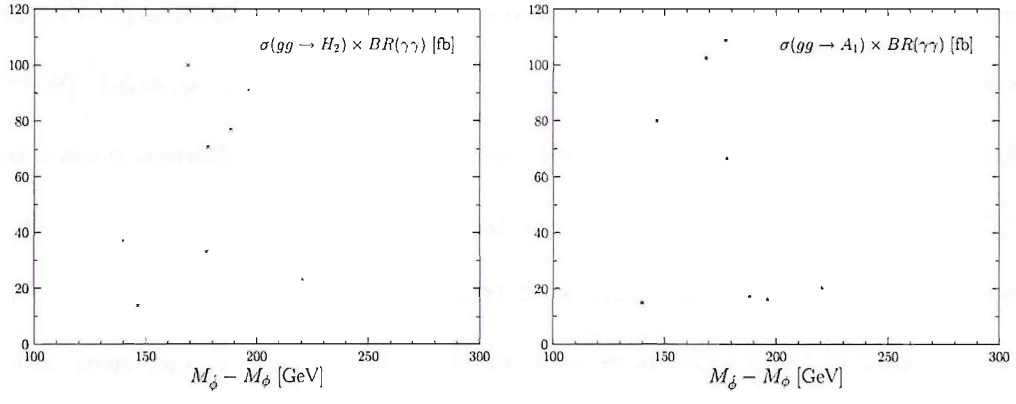

Figure 4.12: Cross–section times BR of H_2 (green/crosses) and A_1 (blue/stars) plotted against their mass differences when the two are potentially visible simultaneously.

and $|\eta^{\gamma}| < 2.4$ on transverse energy and pseudorapidity, respectively. As illustrative examples of a possible NMSSM Higgs phenomenology appearing at the LHC in the

di–photon channel, we have picked up the following five configurations:

1. $\lambda = 0.6554$, $\kappa = 0.2672$, $\mu_{\rm eff} = -426.48$ GeV, $\tan\beta = 2.68$, $A_\lambda = -963.30$ GeV, $A_\kappa = 30.48$ GeV;

2. $\lambda = 0.6445$, $\kappa = 0.2714$, $\mu_{\rm eff} = -167.82$ GeV, $\tan\beta = 2.62$, $A_\lambda = -391.16$ GeV, $A_\kappa = 50.02$ GeV;

3. $\lambda = 0.4751$, $\kappa = 0.354$, $\mu_{\rm eff} = -152.72$ GeV, $\tan\beta = 2.72$, $A_\lambda = -235.17$ GeV, $A_\kappa = 148.38$ GeV;

4. $\lambda = 0.4865$, $\kappa = 0.3516$, $\mu_{\rm eff} = 355.63$ GeV, $\tan\beta = 2.35$, $A_\lambda = 519.72$ GeV, $A_\kappa = -445.71$ GeV;

5. $\lambda = 0.5157$, $\kappa = 0.2967$, $\mu_{\rm eff} = -319.14$ GeV, $\tan\beta = 2.04$, $A_\lambda = -355.67$ GeV, $A_\kappa = 203.28$ GeV.

Configuration 1 is representative of the case in which only the NMSSM H_1 boson is visible, but with mass larger than the MSSM upper limit on the corresponding Higgs state. Configurations 2 and 3 refer instead to the case when also the H_2 is visible along with H_1. Likewise, points 4 and 5 correspond to the scenarios when the H_1 and the A_1 states are potentially visible simultaneously. The final results for the points 1, 2 and 4 above are given in fig. 4.13. The corresponding mass resonances are clearly visible above the continuum di–photon background and discoverable beyond the 5σ level. Indeed, similar situations can be found for each of the combinations listed in table. 4.1 and most of these correspond to phenomenological scenarios which are distinctive of the NMSSM and that cannot be reproduced in the MSSM.

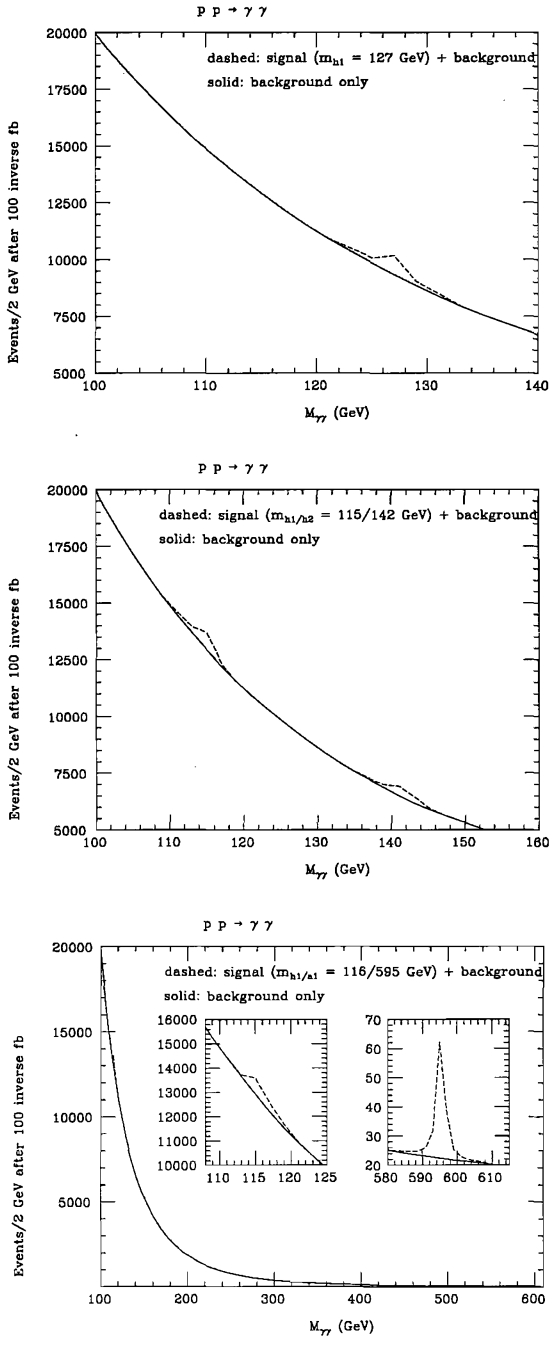

Figure 4.13: The differential distribution in invariant mass of the di–photon pair after the cuts in p_T^γ and η^γ mentioned in the text, with 100 fb^{-1} of luminosity at the LHC, in the case of the background (solid) and the sum of signal and background (dashed), for the example points 1–3. described in the text, in the same correspondence.

4.4 Conclusion

We have concluded that the chances of establishing a 'no–lose theorem' in the NMSSM at the LHC via the aforementioned Higgs–to–Higgs decay mode might improve considerably if the Higgs state strongly coupled to gauge bosons is the lightest one, although a detailed phenomenological study, based upon parton shower, hadronisation and detector simulation (like in Refs. [118, 119]), is obviously in order before drawing any firm conclusions from our very preliminary study. Nonetheless, we find it worthwhile to alert the LHC experiments to the possibility of supplementing the search for $H_{1,2} \to A_1 A_1$ signals via VBF with that through W–HS + tt–HS, as such Higgs decays are relevant in a region of NMSSM parameter space where the two production modes are competitive. Whilst the efficiency of tagging two forward/backward jets in VBF is three times higher than that to trigger on a high transverse momentum electron/muon in W–HS + tt–HS (mainly in virtue of the leptonic BR suppression in the second case), the combination of the latter two remains competitive with the former over the Higgs mass range relevant to these decays, 50 to 120 GeV or so, the more so the lighter the mass of the decaying Higgs state.

In our opinion such a low mass scenario is the one alleviating the so–called 'little fine–tuning problem' of the MSSM, resulting in LEP failing to detect a light CP–even Higgs boson, predicted over most of the MSSM parameter space, as in the NMSSM the mixing among more numerous CP–even or CP–odd Higgs fields would have enabled the production of light mass states at LEP yet they remained undetected because of their reduced couplings to Z bosons [116].

We have also remarked that there exists the possibility of establishing a 'more–to–gain theorem' within the NMSSM, as compared to what is expected in the MSSM, in

terms of novel Higgs signals appearing in the di–photon discovery channel which can be ascribed to the former but not to the latter. We have shown this to be the case for a few selected NMSSM parameter points, by performing a proper signal–to–background analysis at the partonic level. However, a similar numerical study can easily be extended to encompass sizable regions of the NMSSM parameter space. While the bulk of the latter is in a configuration degenerate with the MSSM case (as far as di–photon signals at the LHC are concerned), non–negligible areas exist where further phenomenological studies have the potential to unveil a non–minimal nature of the underlying SUSY model.

Our analyses were based on a fairly extensive scan of the NMSSM parameter space incorporating the latest experimental constraints. To this end, NMSSM benchmark scenarios, amenable to experimental investigation in the context of full MC analyses, based on event generation and detector simulation, are currently being devised [127]. Also, an upgraded version of HERWIG [122], suitable for MC event generation in the context of non–minimal SUSY models, is in preparation.

Chapter 5

Conclusions

As the SM era approaches an end, plenty of new physics seems to be in store beyond it. Even the MSSM appears to be a work in progress as there are still many loopholes in its basic structure. The mere invocation of extra CP–violating phases shows remarkable deviations from the phenomenology of the model in its CP–conserving limit as we have testified. We have seen a rise of about 80% in the BR of the lightest Higgs into two photons for certain values of the ϕ_μ phase. In fact, several points emerged in our scans for which the BR showed an increase by an order of magnitude, but such points were very rare and can not be generalised to the entire parameter space.

We have also tried to analyse the behaviour of the $H_1 \to \gamma\gamma$ decay by probing its dependence on the various parameters as well as individual form–factors. In this context, the masses of the sparticles going into the loops do not appear to have sufficient influence on the BR of H_1, apart from that of the stop. Instead, the modified couplings of all the (s)particles resulting from a CP–mixed Higgs mass matrix seem to play a very crucial role. As indicated earlier, for the purpose of this study we have only focussed on the di-photon decay mode, but eventually this study is to be extended to the process shown below:

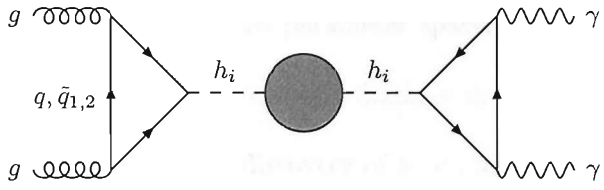

This process incorporates CP-violating couplings in the production as well as the decay modes at the LO, and in the Higgs propagator at NLO. Again, we expect to observe significant variation in the cross-section of the entire process with respect to the CP–conserving case. It remains to be seen whether the CP–violating effects at each stage of the process tend to enhance each other or do they cancel each other out, thus diminishing the overall effect.

As for the NMSSM, we have reasserted that at least one Higgs state should remain potentially visible at the LHC over the entire NMSSM parameter space - as per the no-lose theorem - if the complementarity of the various Higgs production modes is exploited for its decay into two light CP–odd Higgses, although, as we have remarked, a dedicated detector-level analysis is in order before drawing any firm conclusions. Such an analysis will follow soon. Meanwhile a detailed study of other decay modes of the Higgs in the relevant mass range may help further in enhancing its observability in current 'no-go' regions of the NMSSM parameter space.

We have also shown that as many as three NMSSM Higgses could be simultaneously detectable at the LHC if the desired level of luminosity is reached. It is these signals which will help us draw a clear distinction between the MSSM and the NMSSM, as such scenarios have been ruled out in the former. Actually, the probability of finding as many as two Higgses in a single decay mode is very minute in the MSSM, irrespective of the masses of the Higgses. In addition, a considerable number of single di-photon resonances beyond the MSSM upper bound on the lightest Higgs mass have been observed over

a fairly extensive region of the NMSSM parameter space, which also provide a clear signature of non-minimal physics. Thus, our findings in the di-photon Higgs decay channel carry a lot of promise for the discovery of a non-minimal Higgs sector.

In short, the new physics signatures in the NMSSM, coupled with its ability to efficiently circumvent the μ-problem of the MSSM, make it a very interesting candidate as a SUSY model for the LHC to base its extrapolations on.

Appendix A

MSSM Higgs sector with explicit CP–Violation

The most general CP–violating Higgs potential of the MSSM can conveniently be described by the effective Lagrangian [67]:

$$\begin{aligned}
\mathcal{L}_V &= \overline{m}_1^2(H_d^\dagger H_d) + \overline{m}_2^2(H_u^\dagger H_u) + B\mu(H_d^\dagger H_u) + (B\mu)^*(H_u^\dagger H_d) \\
&\quad +\lambda_1(H_d^\dagger H_d)^2 + \lambda_2(H_u^\dagger H_u)^2 + \lambda_3(H_d^\dagger H_d)(H_u^\dagger H_u) + \lambda_4(H_d^\dagger H_u)(H_u^\dagger H_d) \\
&\quad +\lambda_5(H_d^\dagger H_u)^2 + \lambda_5^*(H_u^\dagger H_d)^2 + \lambda_6(H_d^\dagger H_d)(H_d^\dagger H_u) + \lambda_6^*(H_d^\dagger H_d)(H_u^\dagger H_d) \\
&\quad +\lambda_7(H_u^\dagger H_u)(H_d^\dagger H_u) + \lambda_7^*(H_u^\dagger H_u)(H_u^\dagger H_d)\,. \qquad \text{(A.1)}
\end{aligned}$$

At the tree level, the kinematic mass parameters are given by $\overline{m}_1^2 = -m_1^2 - |\mu|^2$ and $\overline{m}_2^2 = -m_2^2 - |\mu|^2$, and the quartic couplings in terms of the SM gauge couplings as

$$\begin{aligned}
&\lambda_1 = \lambda_2 = -\frac{1}{8}(g_2^2 + g_1^2)\,, \quad \lambda_3 = -\frac{1}{4}(g_2^2 - g_1^2)\,, \\
&\lambda_4 = \frac{1}{2}g_2^2\,, \qquad \lambda_5 = \lambda_6 = \lambda_7 = 0\,. \qquad \text{(A.2)}
\end{aligned}$$

Here, m_1^2, m_2^2, and $B\mu$ are soft SUSY–breaking parameters related to the Higgs sector. As remarked in the text, $B\mu$ could generally be complex (but its phase can be rotated away), and beyond the Born approximation, the quartic couplings λ_5, λ_6, λ_7 receive significant radiative corrections from trilinear Yukawa couplings of the Higgs fields to third generation squarks (in the decoupling limit of the first two generations), rendering them complex. The analytic expressions for these quartic couplings are given as:

$$
\begin{aligned}
\lambda_1 \;=\; & -\frac{g_2^2+g_1^2}{8}\left(1-\frac{3}{8\pi^2}\,h_b^2\,t\right) \\
& -\frac{3}{16\pi^2}\,h_b^4\left[t+\frac{1}{2}\,X_b+\frac{1}{16\pi^2}\left(\frac{3}{2}\,h_b^2+\frac{1}{2}\,h_t^2-8g_3^2\right)(X_b t+t^2)\right] \\
& +\frac{3}{192\pi^2}\,h_t^4\,\frac{|\mu|^4}{M_{\rm SUSY}^4}\left[1+\frac{1}{16\pi^2}\,(9h_t^2-5h_b^2-16g_3^2)t\right], \qquad \text{(A.3)} \\
\lambda_2 \;=\; & -\frac{g_2^2+g_1^2}{8}\left(1-\frac{3}{8\pi^2}\,h_t^2\,t\right) \\
& -\frac{3}{16\pi^2}\,h_t^4\left[t+\frac{1}{2}\,X_t+\frac{1}{16\pi^2}\left(\frac{3}{2}\,h_t^2+\frac{1}{2}\,h_b^2-8g_3^2\right)(X_t t+t^2)\right] \\
& +\frac{3}{192\pi^2}\,h_b^4\,\frac{|\mu|^4}{M_{\rm SUSY}^4}\left[1+\frac{1}{16\pi^2}\,(9h_b^2-5h_t^2-16g_3^2)t\right], \qquad \text{(A.4)} \\
\lambda_3 \;=\; & -\frac{g_2^2-g_1^2}{4}\left[1-\frac{3}{16\pi^2}\,(h_t^2+h_b^2)\,t\right] \\
& -\frac{3}{8\pi^2}\,h_t^2h_b^2\left[t+\frac{1}{2}\,X_{tb}+\frac{1}{16\pi^2}\,(h_t^2+h_b^2-8g_3^2)\,(X_{tb}t+t^2)\right] \\
& -\frac{3}{96\pi^2}\,h_t^4\left(\frac{3|\mu|^2}{M_{\rm SUSY}^2}-\frac{|\mu|^2|A_t|^2}{M_{\rm SUSY}^4}\right)\left[1+\frac{1}{16\pi^2}\,(6h_t^2-2h_b^2-16g_3^2)t\right] \\
& -\frac{3}{96\pi^2}\,h_b^4\left(\frac{3|\mu|^2}{M_{\rm SUSY}^2}-\frac{|\mu|^2|A_b|^2}{M_{\rm SUSY}^4}\right)\left[1+\frac{1}{16\pi^2}\,(6h_b^2-2h_t^2-16g_3^2)t\right], \qquad \text{(A.5)} \\
\lambda_4 \;=\; & \frac{g_2^2}{2}\left[1-\frac{3}{16\pi^2}\,(h_t^2+h_b^2)\,t\right] \\
& +\frac{3}{8\pi^2}\,h_t^2h_b^2\left[t+\frac{1}{2}\,X_{tb}+\frac{1}{16\pi^2}\,(h_t^2+h_b^2-8g_3^2)\,(X_{tb}t+t^2)\right] \\
& -\frac{3}{96\pi^2}\,h_t^4\left(\frac{3|\mu|^2}{M_{\rm SUSY}^2}-\frac{|\mu|^2|A_t|^2}{M_{\rm SUSY}^4}\right)\left[1+\frac{1}{16\pi^2}\,(6h_t^2-2h_b^2-16g_3^2)t\right] \\
& -\frac{3}{96\pi^2}\,h_b^4\left(\frac{3|\mu|^2}{M_{\rm SUSY}^2}-\frac{|\mu|^2|A_b|^2}{M_{\rm SUSY}^4}\right)\left[1+\frac{1}{16\pi^2}\,(6h_b^2-2h_t^2-16g_3^2)t\right], \qquad \text{(A.6)} \\
\lambda_5 \;=\; & \frac{3}{192\pi^2}\,h_t^4\,\frac{\mu^2A_t^2}{M_{\rm SUSY}^4}\left[1-\frac{1}{16\pi^2}\,(2h_b^2-6h_t^2+16g_3^2)t\right] \\
& +\frac{3}{192\pi^2}\,h_b^4\,\frac{\mu^2A_b^2}{M_{\rm SUSY}^4}\left[1-\frac{1}{16\pi^2}\,(2h_t^2-6h_b^2+16g_3^2)t\right], \qquad \text{(A.7)}
\end{aligned}
$$

$$\lambda_6 = -\frac{3}{96\pi^2}\,h_t^4\,\frac{|\mu|^2\mu A_t}{M_{\rm SUSY}^4}\Big[1-\frac{1}{16\pi^2}\Big(\frac{7}{2}\,h_b^2-\frac{15}{2}\,h_t^2+16g_3^2\Big)\,t\Big]$$
$$+\frac{3}{96\pi^2}\,h_b^4\,\frac{\mu}{M_{\rm SUSY}}\Big(\frac{6A_b}{M_{\rm SUSY}}-\frac{|A_b|^2A_b}{M_{\rm SUSY}^3}\Big)\Big[1-\frac{1}{16\pi^2}\Big(\frac{1}{2}\,h_t^2-\frac{9}{2}\,h_b^2+16g_3^2\Big)\,t\Big], \quad \text{(A.8)}$$

$$\lambda_7 = -\frac{3}{96\pi^2}\,h_b^4\,\frac{|\mu|^2\mu A_b}{M_{\rm SUSY}^4}\Big[1-\frac{1}{16\pi^2}\Big(\frac{7}{2}\,h_t^2-\frac{15}{2}\,h_b^2+16g_3^2\Big)\,t\Big]$$
$$+\frac{3}{96\pi^2}\,h_t^4\,\frac{\mu}{M_{\rm SUSY}}\Big(\frac{6A_t}{M_{\rm SUSY}}-\frac{|A_t|^2A_t}{M_{\rm SUSY}^3}\Big)\Big[1-\frac{1}{16\pi^2}\Big(\frac{1}{2}\,h_b^2-\frac{9}{2}\,h_t^2+16g_3^2\Big)\,t\Big], \quad \text{(A.9)}$$

with $t=\ln(M_{\rm SUSY}^2/\overline{m}_t^2)$ and

$$h_t = \frac{\sqrt{2}\,m_t(\overline{m}_t)}{v s_\beta}\,, \qquad h_b = \frac{\sqrt{2}\,m_b(\overline{m}_t)}{v c_\beta}\,, \quad \text{(A.10)}$$

$$X_t = \frac{2|A_t|^2}{M_{\rm SUSY}^2}\Big(1-\frac{|A_t|^2}{12M_{\rm SUSY}^2}\Big),$$
$$X_b = \frac{2|A_b|^2}{M_{\rm SUSY}^2}\Big(1-\frac{|A_b|^2}{12M_{\rm SUSY}^2}\Big), \quad \text{(A.11)}$$
$$X_{tb} = \frac{|A_t|^2+|A_b|^2+2{\rm Re}(A_b^*A_t)}{2\,M_{\rm SUSY}^2}-\frac{|\mu|^2}{M_{\rm SUSY}^2}-\frac{|\,|\mu|^2-A_b^*A_t\,|^2}{6\,M_{\rm SUSY}^4}\,,$$

where $s_\beta=\sin\beta$, $c_\beta=\cos\beta$ and $\overline{m}_t$ is the t-quark pole mass which is related to the on–shell running mass m_t through

$$m_t(\overline{m}_t) = \frac{\overline{m}_t}{1+\frac{4}{3\pi}\,\alpha_s(\overline{m}_t)}\,. \quad \text{(A.12)}$$

The linear decomposition of the Higgs fields is carried out as

$$H_u = {\rm e}^{i\xi}\begin{pmatrix} H_u^+ \\ \frac{1}{\sqrt{2}}(v_u+H_u^0+iP_u^0)\end{pmatrix}, H_d = \begin{pmatrix} \frac{1}{\sqrt{2}}(v_d+H_d^0+iP_d^0) \\ H_d^-\end{pmatrix}, \quad \text{(A.13)}$$

where ξ is the relative phase between the two Higgs doublets which can be determined along with their respective VEVs by the minimization conditions on $\mathcal{L}_V$. In the presence of the above CP–violating parameters, we end up with one charged Higgs state and three neutral CP–mixed Higgs states in the Higgs sector, after rotating away the Goldstone

state. The mixing between the CP–even and CP–odd fields is given by

$$\mathcal{M}_N^2 = \begin{pmatrix} \mathcal{M}_S^2 & \mathcal{M}_{SP}^2 \\ \mathcal{M}_{PS}^2 & \mathcal{M}_P^2 \end{pmatrix}, \tag{A.14}$$

where $\mathcal{M}_P^2$ and $\mathcal{M}_S^2$ are the CP–preserving transitions and $\mathcal{M}_{SP}^2 = (\mathcal{M}_{PS}^2)^T$ contains the CP–violating mixing. The analytic form of the sub–matrices is given by [68]

$$\mathcal{M}_P^2 = m_a^2 = \frac{1}{s_\beta c_\beta}\left\{\mathcal{R}(m_{12}^2 e^{i\xi}) + v^2\left[2\mathcal{R}(\lambda_5 e^{2i\xi})s_\beta c_\beta + \frac{1}{2}\mathcal{R}(\lambda_6 e^{i\xi})c_\beta^2 + \frac{1}{2}\mathcal{R}(\lambda_7 e^{i\xi})s_\beta^2\right]\right\}, \tag{A.15}$$

$$\mathcal{M}_{SP}^2 = v^2 \begin{pmatrix} \mathcal{I}(\lambda_5 e^{2i\xi})s_\beta + \mathcal{I}(\lambda_6 e^{i\xi})c_\beta \\ \mathcal{I}(\lambda_5 e^{2i\xi})c_\beta + \mathcal{I}(\lambda_7 e^{i\xi})s_\beta \end{pmatrix}, \tag{A.16}$$

$$\begin{aligned} \mathcal{M}_S^2 = {} & m_a^2 \begin{pmatrix} s_\beta^2 & -s_\beta c_\beta \\ -s_\beta c_\beta & c_\beta^2 \end{pmatrix} \\ & - \begin{pmatrix} 2\lambda_1 c_\beta^2 + 2\mathcal{R}(\lambda_5 e^{2i\xi})s_\beta^2 + 2\mathcal{R}(\lambda_6 e^{i\xi})s_\beta c_\beta & \lambda_{34} s_\beta c_\beta + \mathcal{R}(\lambda_6 e^{i\xi})c_\beta^2 + \mathcal{R}(\lambda_7 e^{i\xi})s_\beta^2 \\ \lambda_{34} s_\beta c_\beta + \mathcal{R}(\lambda_6 e^{i\xi})c_\beta^2 + \mathcal{R}(\lambda_7 e^{i\xi})s_\beta^2 & 2\lambda_2 s_\beta^2 + 2\mathcal{R}(\lambda_5 e^{2i\xi})c_\beta^2 + 2\mathcal{R}(\lambda_7 e^{i\xi})s_\beta c_\beta \end{pmatrix}. \end{aligned} \tag{A.17}$$

Correspondingly, the charged Higgs boson mass is given by

$$M_{H^\pm}^2 = M_a^2 + \frac{1}{2}\lambda_4 v^2 - \mathcal{R}(\lambda_5 e^{2i\xi})v^2 . \tag{A.18}$$

The spontaneously CP–violating phase ξ appearing in the above equations is induced radiatively in the $\overline{\text{MS}}$ scheme [65, 66] and is renormalisation–scheme dependent. Thus one may adopt a renormalisation scheme different from $\overline{\text{MS}}$ in which ξ is set to zero order by order in perturbation theory. This can be achieved by requiring the bilinear Higgs-mixing mass $B\mu$ to be real at the tree level (by making use of the PQ U(1) symmetry), but to receive an imaginary counter–term $\mathcal{I}(B\mu)$, at higher orders which is determined by the vanishing of the CP–odd tadpole parameters T_{a_1} and T_{a_2} [65].

Appendix B

Higgs Interactions in a CP–Violating MSSM

The Higgs interactions of relevance to the di–photon decay mode include [90]:

- Interactions with W bosons: The Higgs interaction with $W^{\pm}$ boson pair is described by the Lagrangian

$$\mathcal{L}_{HW^+W^-} = g m_W \sum_i g_{H_i W^+ W^-} H_i W_\mu^+ W^{-\mu}, \tag{B.1}$$

  where $i = 1, 2, 3$ (Higgs mass eigenstates) and the coupling $g_{H_i W^+ W^-}$ is given in terms of the neutral Higgs-boson mixing matrix O as:

$$g_{H_i W^+ W^-} = c_\beta O_{\phi_1 i} + s_\beta O_{\phi_2 i}.$$

- Higgs–fermion–antifermion interactions: The effective Lagrangian governing the

interactions of the neutral Higgs bosons with quarks and charged leptons is

$$\mathcal{L}_{H_i\bar{f}f} = -\sum_{f=u,d,l} g_f \sum_{i=1}^{3} H_i\, \bar{f}\left(g^S_{H_i\bar{f}f} + i g^P_{H_i\bar{f}f}\gamma_5\right) f\,, \tag{B.2}$$

where $g_f = \frac{g_2 m_f}{2m_W}$ and, at the tree level, $(g^S, g^P) = (O_{\phi_1 i}/c_\beta, -O_{ai}\tan\beta)$ and $(g^S, g^P) = (O_{\phi_2 i}/s_\beta, -O_{ai}\cot\beta)$ for $f = (l, d)$ and $f = u$, respectively.

- Higgs–sfermion–sfermion interactions: These interactions can be written in terms of the sfermion mass eigenstates as

$$\mathcal{L}_{H\tilde{f}\tilde{f}} = v \sum_{f=u,d} g_{H_i\tilde{f}^*_j\tilde{f}_k}(H_i\, \tilde{f}^*_j\, \tilde{f}_k)\,, \tag{B.3}$$

where

$$v\, g_{H_i\tilde{f}^*_j\tilde{f}_k} = \left(\Gamma^{\alpha\tilde{f}^*\tilde{f}}\right)_{\beta\gamma} O_{\alpha i} U^{\tilde{f}*}_{\beta j} U^{\tilde{f}}_{\gamma k},$$

with $\alpha = (\phi_1, \phi_2, a) = (1, 2, 3)$, $\beta, \gamma = L, R$ and $j, k = 1, 2$.

The expressions for the couplings $\Gamma^{\alpha\tilde{f}^*\tilde{f}}$ to third–generation sfermions are given in the weak interaction basis $(\tilde{f}_L, \tilde{f}_R)$ by:

$$\Gamma^{a\tilde{b}^*\tilde{b}} = \frac{1}{\sqrt{2}}\begin{pmatrix} 0 & i\,h_b^*(s_\beta A_b^* + c_\beta\mu) \\ -i\,h_b(s_\beta A_b + c_\beta\mu^*) & 0 \end{pmatrix},$$

$$\Gamma^{\phi_1\tilde{b}^*\tilde{b}} = \begin{pmatrix} -|h_b|^2 v c_\beta + \frac{1}{4}\left(g_2^2 + \frac{1}{3}g_1^2\right) v c_\beta & -\frac{1}{\sqrt{2}}h_b^* A_b^* \\ -\frac{1}{\sqrt{2}}h_b A_b & -|h_b|^2 v c_\beta + \frac{1}{6}g'^2 v c_\beta \end{pmatrix},$$

$$\Gamma^{\phi_2\tilde{b}^*\tilde{b}} = \begin{pmatrix} -\frac{1}{4}\left(g_2^2 + \frac{1}{3}g_1^2\right) v s_\beta & \frac{1}{\sqrt{2}}h_b^*\mu \\ \frac{1}{\sqrt{2}}h_b\mu^* & -\frac{1}{6}g'^2 v s_\beta \end{pmatrix},$$

$$\Gamma^{a\tilde{t}^*\tilde{t}} = \frac{1}{\sqrt{2}}\begin{pmatrix} 0 & i\,h_t^*(c_\beta A_t^* + s_\beta\mu) \\ -i\,h_t(c_\beta A_t + s_\beta\mu^*) & 0 \end{pmatrix},$$

$$
\begin{aligned}
\Gamma^{\phi_1\tilde{t}^*\tilde{t}} &= \begin{pmatrix} -\frac{1}{4}\left(g_2^2-\frac{1}{3}g_1^2\right)vc_\beta & \frac{1}{\sqrt{2}}h_t^*\mu \\ \frac{1}{\sqrt{2}}h_t\mu^* & -\frac{1}{3}g'^2vc_\beta \end{pmatrix}, \\
\Gamma^{\phi_2\tilde{t}^*\tilde{t}} &= \begin{pmatrix} -|h_t|^2vs_\beta+\frac{1}{4}\left(g_2^2-\frac{1}{3}g_1^2\right)vs_\beta & -\frac{1}{\sqrt{2}}h_t^*A_t^* \\ -\frac{1}{\sqrt{2}}h_tA_t & -|h_t|^2vs_\beta+\frac{1}{3}g'^2vs_\beta \end{pmatrix}, \\
\Gamma^{a\tilde{\tau}^*\tilde{\tau}} &= \frac{1}{\sqrt{2}}\begin{pmatrix} 0 & i\,h_\tau^*(s_\beta A_\tau^*+c_\beta\mu) \\ -i\,h_\tau(s_\beta A_\tau+c_\beta\mu^*) & 0 \end{pmatrix}, \\
\Gamma^{\phi_1\tilde{\tau}^*\tilde{\tau}} &= \begin{pmatrix} -|h_\tau|^2vc_\beta+\frac{1}{4}\left(g_2^2-g_1^2\right)vc_\beta & -\frac{1}{\sqrt{2}}h_\tau^*A_\tau^* \\ -\frac{1}{\sqrt{2}}h_\tau A_\tau & -|h_\tau|^2vc_\beta+\frac{1}{2}g'^2vc_\beta \end{pmatrix}, \\
\Gamma^{\phi_2\tilde{\tau}^*\tilde{\tau}} &= \begin{pmatrix} -\frac{1}{4}\left(g_2^2-g_1^2\right)vs_\beta & \frac{1}{\sqrt{2}}h_\tau^*\mu \\ \frac{1}{\sqrt{2}}h_\tau\mu^* & -\frac{1}{2}g'^2vs_\beta \end{pmatrix}.
\end{aligned}
$$

- Interactions of neutral Higgs bosons and charginos: These are described by the following Lagrangian:

$$
\begin{aligned}
\mathcal{L}_{H\tilde{\chi}^+\tilde{\chi}^-} &= -g_f\sum_{i,j,k}H_i\overline{\tilde{\chi}_j^-}\left(g^S_{H_i\tilde{\chi}_j^+\tilde{\chi}_k^-}+i\gamma_5 g^P_{H_i\tilde{\chi}_j^+\tilde{\chi}_k^-}\right)\tilde{\chi}_k^-\,; \qquad \text{(B.4)} \\
g^S_{H_i\tilde{\chi}_j^+\tilde{\chi}_k^-} &= \frac{1}{2}\left\{[(C_R)_{i1}(C_L)^*_{k2}G_i^{\phi_1}+(C_R)_{j2}(C_L)^*_{k1}G_i^{\phi_2}]+[j\leftrightarrow k]^*\right\}, \\
g^P_{H_i\tilde{\chi}_j^+\tilde{\chi}_k^-} &= \frac{i}{2}\left\{[(C_R)_{j1}(C_L)^*_{k2}G_i^{\phi_1}+(C_R)_{j2}(C_L)^*_{k1}G_i^{\phi_2}]-[j\leftrightarrow k]^*\right\},
\end{aligned}
$$

where $g_f=\frac{g_2}{\sqrt{2}}$, $G_i^{\phi_1}=(O_{\phi_1 i}-is_\beta O_{ai})$, $G_i^{\phi_2}=(O_{\phi_2 i}-ic_\beta O_{ai})$, and $j,k=1,2$.

- Neutral Higgs boson interactions with charged Higgs pair: This effective trilinear Higgs self–interaction [68]–[70] is given by the Lagrangian:

$$
\mathcal{L}_{HH^+H^-}=v\sum_{i=1}^{3}g_{H_iH^+H^-}H_iH^+H^-; \qquad g_{H_iH^+H^-}=\sum_{\alpha=1}^{3}O_{\alpha i}g_{\alpha H^+H^-}, \qquad \text{(B.5)}
$$

where the effective couplings $g_{\alpha H^+H^-}$ read as:

$$
\begin{aligned}
g_{\phi_1 H^+H^-} &= 2s_\beta^2 c_\beta \lambda_1 + c_\beta^3 \lambda_3 - s_\beta^2 c_\beta \lambda_4 - 2s_\beta^2 c_\beta \mathcal{R}(\lambda_5) + s_\beta (s_\beta^2 - 2c_\beta^2)\, \mathcal{R}(\lambda_6) \\
&\quad + s_\beta c_\beta^2 \mathcal{R}(\lambda_7)\,, \\
g_{\phi_2 H^+H^-} &= 2s_\beta c_\beta^2 \lambda_2 + s_\beta^3 \lambda_3 - s_\beta c_\beta^2 \lambda_4 - 2s_\beta c_\beta^2 \mathcal{R}(\lambda_5) + s_\beta^2 c_\beta \mathcal{R}(\lambda_6) \\
&\quad + c_\beta (c_\beta^2 - 2s_\beta^2)\, \mathcal{R}(\lambda_7)\,, \\
g_{aH^+H^-} &= 2s_\beta c_\beta \mathcal{I}(\lambda_5) - s_\beta^2 \mathcal{I}(\lambda_6) - c_\beta^2 \mathcal{I}(\lambda_7)\,,
\end{aligned}
$$

a being the pseudoscalar Higgs interaction eigenstate.

Appendix C

The Higgs Sector of the NMSSM

The Higgs fields of the NMSSM consist of the usual two Higgs doublets together with the extra Higgs singlet,

$$H_u = \begin{pmatrix} H_u^+ \\ H_u^0 \end{pmatrix}, \quad H_d = \begin{pmatrix} H_d^0 \\ H_d^- \end{pmatrix}, \quad S. \tag{C.1}$$

As seen in the superpotential in eq. (4.3), the extra singlet is allowed to couple only to the Higgs doublets of the model, and consequently the couplings of the new fields to gauge bosons will only be manifest via their mixing with the other Higgs fields. The tree level Higgs potential is composed of three parts, $V = V_F + V_D + V_{\text{soft}}$ [114]:

$$\begin{aligned} V_F &= |\lambda S|^2 (H_d^\dagger H_d + H_u^\dagger H_u) + |\epsilon_{ij} \lambda H_d^i H_u^j + \kappa S^2|^2, \\ V_D &= \frac{g_2^2 + g_1^2}{8} (H_d^\dagger H_d - H_u^\dagger H_u)^2 + \frac{g_2^2}{2} (H_d^\dagger H_u)(H_u^\dagger H_d), \\ V_{\text{soft}} &= \overline{m}_1^2 H_d^\dagger H_d + \overline{m}_2^2 H_u^\dagger H_u + \overline{m}_3^2 |S|^2 - (\epsilon_{ij} \lambda A_\lambda S H_d^i H_u^j + \frac{1}{3} \kappa A_\kappa S^3 + h.c.). \end{aligned} \tag{C.2}$$

where A_λ and A_κ are (arbitrary) dimensionful parameters of order M_{SUSY}. We assume that all the new parameters in the model (compared to the MSSM), namely

λ, κ, A_λ and A_κ, are real, and so CP is conserved at tree–level. The 'MSSM limit' can be approached smoothly by letting λ and $\kappa \to 0$ on a linear trajectory (i.e. κ/λ constant), while keeping the effective μ parameter $\mu_{\text{eff}} = \lambda v_s/\sqrt{2}$ and the parameters A_λ and A_κ fixed. In this limit the Higgs singlet field decouples from the system completely, and the doublet Higgs sector of the MSSM in its canonical structure is regained.

The above potential is expanded around the VEVs of the three Higgs fields, v_u, v_d and v_s, after EWSB. These fields are now parametrised as follows:

$$H_u = e^{i\theta} \begin{pmatrix} H_u^+ \\ \frac{1}{\sqrt{2}}(v_u + S_2 + iP_2^0) \end{pmatrix}, \quad H_d = \begin{pmatrix} \frac{1}{\sqrt{2}}(v_d + S_1 + iP_1^0) \\ H_d^- \end{pmatrix}, \tag{C.3}$$

$$S = \frac{1}{\sqrt{2}} e^{i\varphi}(v_s + S_3 + iP_3^0).$$

Again, to ensure tree-level CP–conservation of the model, we can work in the limit where the three VEVs v_u, v_d and v_s are real and positive, and thus get rid of the phases θ and φ appearing with the fields H_u and S, respectively.

For this vacuum to be a local minimum, we obtain three relations, linking the three soft mass parameters to the three VEVs of the Higgs fields:

$$\begin{aligned}
\overline{m}_1^2 &= \frac{1}{8}\bar{g}^2(v_u^2 - v_d^2) - \frac{1}{2}\lambda^2 v_u^2 + \frac{1}{2}(\sqrt{2}A_\lambda + \kappa v_s)\lambda v_s \frac{v_u}{v_d} - \frac{1}{2}\lambda^2 v_s^2, \\
\overline{m}_2^2 &= \frac{1}{8}\bar{g}^2(v_d^2 - v_u^2) - \frac{1}{2}\lambda^2 v_d^2 + \frac{1}{2}(\sqrt{2}A_\lambda + \kappa v_s)\lambda v_s \frac{v_d}{v_u} - \frac{1}{2}\lambda^2 v_s^2, \\
\overline{m}_3^2 &= -\kappa^2 v_s^2 - \frac{1}{2}\lambda^2 v^2 + \kappa\lambda v_u v_d + \frac{1}{\sqrt{2}}\lambda A_\lambda \frac{v_u v_d}{v_s} - \frac{1}{\sqrt{2}}\kappa A_\kappa v_s.
\end{aligned} \tag{C.4}$$

The *local* stability of this vacuum is ensured by allowing only positive squared masses of the physical fields (i.e. the mass eigenstates), which leads to useful constraints on the parameters of the potential. It can be easily proved that the above vacuum is also a

global one. The requirement that the above vacuum be of lower energy than the other two possible CP–even vacua further constrains certain parameters of the model [128].

From the potential, the Higgs mass matrices and subsequently the mass eigenstates can be derived. After decoupling the zero–mass Goldstone modes, we are left with a potential of the form:

$$V_{\rm mass} = M^2_{H^\pm} H^+ H^- + \frac{1}{2}\,(P_1 \;\; P_2)\, M^2_- \begin{pmatrix} P_1 \\ P_2 \end{pmatrix} + \frac{1}{2}\,(S_1 \;\; S_2 \;\; S_3)\, M^2_+ \begin{pmatrix} S_1 \\ S_2 \\ S_3 \end{pmatrix}. \quad \text{(C.5)}$$

The charged Higgs mass eigenstates $H^\pm$ are given by

$$M^2_{H^\pm} = M^2_A + M^2_W - \frac{1}{2}(\lambda v)^2, \quad \text{(C.6)}$$

where

$$M^2_A = \frac{\lambda v_s}{\sin 2\beta}\left(\sqrt{2}A_\lambda + \kappa v_s\right). \quad \text{(C.7)}$$

Using the minimization conditions in eqs. (C.4), the entries of the tree-level CP–odd matrix M^2_- in eq. (C.5) can be written as

$$\begin{aligned} M^2_{-\,11} &= M^2_A, \\ M^2_{-\,12} &= \frac{1}{2}(M^2_A \sin 2\beta - 3\lambda\kappa v_s^2)\cot\beta_s, \\ M^2_{-\,22} &= \frac{1}{4}(M^2_A \sin 2\beta + 3\lambda\kappa v_s^2)\cot^2\beta_s \sin 2\beta - 3\kappa v_s A_\kappa/\sqrt{2}. \end{aligned} \quad \text{(C.8)}$$

where $\tan\beta_s \equiv v_s/v$.

And those for M_+^2 are given as

$$\begin{aligned}
M^2_{+\,11} &= M_A^2 + (M_Z^2 - \frac{1}{2}(\lambda v)^2)\sin^2 2\beta, \\
M^2_{+\,12} &= -\frac{1}{2}(M_Z^2 - \frac{1}{2}(\lambda v)^2)\sin 4\beta, \\
M^2_{+\,13} &= -\frac{1}{2}(M_A^2 \sin 2\beta + \lambda\kappa v_s^2)\cot\beta_s \cos 2\beta, \\
M^2_{+\,22} &= M_Z^2 \cos^2 2\beta + \frac{1}{2}(\lambda v)^2 \sin^2 2\beta, \\
M^2_{+\,23} &= \frac{1}{2}(2\lambda^2 v_s^2 - M_A^2 \sin^2 2\beta - \lambda\kappa v_s^2 \sin 2\beta)\cot\beta_s, \\
M^2_{+\,33} &= \frac{1}{4}M_A^2 \sin^2 2\beta \cot^2\beta_s + 2\kappa^2 v_s^2 + \kappa v_s A_\kappa/\sqrt{2} - \frac{1}{4}\lambda\kappa v^2 \sin 2\beta.
\end{aligned} \tag{C.9}$$

The CP–odd mass matrix given in eqs. (C.8) can be easily diagonalised to obtain CP–odd scalar mass terms:

$$M^2_{A_2} \approx M_A^2\,(1 + \frac{1}{4}\cot^2\beta_s \sin^2 2\beta), \tag{C.10}$$

$$M^2_{A_1} \approx -\frac{3}{\sqrt{2}}\kappa v_s A_\kappa, \tag{C.11}$$

while diagonalisation of the above CP–even mass matrix is much more cumbersome. However, an approximate solution [128] can be employed to obtain reasonably simple mass expressions for the physical CP–even Higgs bosons from it. For this purpose, both $1/\tan\beta$ and $1/M_A$ are taken as small parameters of magnitude $\approx \varepsilon$ (M_A gauged by the generic electroweak scale). Then, for not too large values of λ, κ and other scales, a hierarchical structure is observed in the CP–even mass matrix of the form:

$$\{M_{ij}^2\} = M_A^2 \begin{pmatrix} A & \varepsilon C^\dagger \\ \varepsilon C & \varepsilon^2 B \end{pmatrix}, \tag{C.12}$$

where B is a 2×2 matrix, C is a column vector and A is a scalar, all of order unity.

An auxiliary unitary transformation defined by the matrix,

$$V^\dagger = \begin{pmatrix} 1 - \frac{1}{2}\varepsilon^2\Gamma^\dagger\Gamma & -\varepsilon\Gamma^\dagger \\ \varepsilon\Gamma & \mathbf{1} - \frac{1}{2}\varepsilon^2\Gamma\Gamma^\dagger \end{pmatrix} + \mathcal{O}(\varepsilon^4), \tag{C.13}$$

with $\Gamma = C/A$, yields a block diagonal mass matrix of the form:

$$\begin{aligned} VM^2V^\dagger &= M_A^2 \begin{pmatrix} A + \varepsilon^2 C^\dagger C/A & 0 \\ 0 & \varepsilon^2(B - CC^\dagger/A) \end{pmatrix} + \mathcal{O}(\varepsilon^3) \\ &= \begin{pmatrix} M_{11}^2 + \frac{M_{13}^4}{M_{11}^2} & 0 & 0 \\ 0 & M_{22}^2 & M_{23}^2 - \frac{M_{13}^2 M_{12}^2}{M_{11}^2} \\ 0 & M_{23}^2 - \frac{M_{13}^2 M_{12}^2}{M_{11}^2} & M_{33}^2 - \frac{M_{13}^4}{M_{11}^2} \end{pmatrix} + \mathcal{O}(\varepsilon^3), \end{aligned} \tag{C.14}$$

where M_{ij}^2 are the entries of the CP–even mass matrix given in eqs. (C.9), and where terms in M_{12}^2/M_A^2 which is $\mathcal{O}(\varepsilon^3)$, have been neglected.

The rotation from the interaction states S_i to mass eigenstates H_i, $H = OS$, is carried out using matrix $O = R^\dagger V$, where R is given as

$$R = \begin{pmatrix} 1 & 0 & 0 \\ 0 & \cos\theta_H & -\sin\theta_H \\ 0 & \sin\theta_H & \cos\theta_H \end{pmatrix} \quad \text{with} \quad \tan\theta_H = \frac{M_{23}^2 - \frac{M_{13}^2 M_{12}^2}{M_{11}^2}}{M_{22}^2 - M_{H_1}^2}. \tag{C.15}$$

Which provides approximate CP–even Higgs boson mass expressions:

$$\begin{aligned} M_{H_3}^2 &= M_{11}^2 + \frac{M_{13}^4}{M_{11}^2} \\ &\approx M_A^2(1 + \frac{1}{4}\cot^2\beta_s \sin^2 2\beta) \end{aligned} \tag{C.16}$$

and

$$
\begin{aligned}
M^2_{H_{2/1}} &= \frac{1}{2}\left(M^2_{22}+M^2_{33}-\frac{M^4_{13}}{M^2_{11}}\right. \\
&\quad \left.\pm\sqrt{\left(M^2_{22}-M^2_{33}+\frac{M^4_{13}}{M^2_{11}}\right)^2+4\left(M^2_{23}-\frac{M^2_{13}M^2_{12}}{M^2_{11}}\right)^2}\right) \\
&\approx \frac{1}{2}\left\{M^2_Z+\frac{1}{2}\kappa v_s(4\kappa v_s+\sqrt{2}A_\kappa)\right. \\
&\quad \left.\pm\sqrt{\left[M^2_Z-\frac{1}{2}\kappa v_s(4\kappa v_s+\sqrt{2}A_\kappa)\right]^2+\cot^2\beta_s\left[2\lambda^2 v_s^2-M^2_A\sin^2 2\beta\right]^2}\right\}. \quad \text{(C.17)}
\end{aligned}
$$

The physical mass eigenstates A_i and H_i are labelled in ascending order of mass. It must be pointed out that the heavy CP–odd Higgs boson, A_2, is approximately degenerate with the heaviest CP–even Higgs boson, H_3, and the charged Higgs bosons.

Bibliography

[1] UA1 Collaboration, G. Arnison *et al.*, Phys. Lett. B **122** (1983) 103.

[2] UA1 Collaboration, G. Arnison *et al.*, Phys. Lett. B **126** (1983) 398.

[3] DØ Collaboration, S. Abachi *et al.*, Phys. Rev. Lett. **74** (1983) 2632 [arXiv:hep-ex/9503003].

[4] S. Glashow, Nucl. Phys. **22** (1961) 579; S. Weinberg, Phys. Rev. Lett. **19** (1967) 1264; A. Salam, *Elementary Particle Theory*, ed. N. Svartholm, Almqvist and Wiksells, Stockholm (1969), p. 367.

[5] C.N. Yang, R. Mills, Phys. Rev. **96** (1954) 191.

[6] M. Gell-Mann, Phys. Lett. **8** (1964) 214; G. Zweig, CERN-Report 8182/TH401 (1964); H. Fritzsch, M. Gell-Mann, H. Leutwyler, Phys. Lett. B **47** (1973) 365; D. Gross, F. Wilczek, Phys. Rev. Lett. **30** (1973) 1343;

[7] J. Goldstone, Nuovo Cim. **19** (1961) 154; J. Goldstone, A. Salam, S. Weinberg, Phys. Rev. **127** (1962) 965.

[8] P. W. Higgs, Phys. Lett. **12** (1964) 132; Phys. Rev. Lett. **13** (1964) 508; Phys. Rev. **145** (1966) 1156; F. Englert, R. Brout, Phys. Rev. Lett. **13** (1964) 321; G. S. Guralnik, C. R. Hagen, T. W. B. Kibble, Phys. Rev. Lett. **13** (1964) 585; T. W. Kibble, Phys. Rev. **155** (1967) 1554.

[9] A. Djouadi, arXiv:hep-ph/0503172.

[10] For a review, see J. F. Gunion, H. E. Haber, G. Kane, S. Dawson, *The Higgs Hunter's Guide*, Addison-Wesley, Reading, MA, 1990.

[11] S. Dawson, *The search for electroweak symmetry breaking*, World Scientific, Singapore (2004), p. 13.

[12] T. Hambye, K. Riesselmann, Phys. Rev. D **55** (1997) 7255 [arXiv:hep-ph/].

[13] M. Spira, Fortsch. Phys. **46** (1998) 203 [arXiv:hep-ph/9707337].

[14] Z. Kunszt, S. Moretti, W. J. Stirling, Z. Phys. C **74** (1997) 479 [arXiv:hep-ph/9611397].

[15] A. Djouadi, M. Spira, P. M. Zerwas, Phys. Lett. B **264** (1991) 440; A. Djouadi, D. Graudenz, M. Spira, P. M. Zerwas, Nucl. Phys. B **453** (1995) 17 [arXiv:hep-ph/9504378].

[16] T. Han, S. Willenbrock, Phys. Lett. B **273** (1991) 167.

[17] T. Han, G. Valencia, S. Willenbrock, Phys. Rev. Lett. **69** (1992) 3274 [arXiv:hep-ph/9206246].

[18] W. Beenakker, S. Dittmaier, M. Kramer, B. Plumper, M. Spira, P. M. Zerwas, Nucl. Phys. B **653** 151 [arXiv:hep-ph/0211352].

[19] S. Dawson, C. B. Jackson, L. H. Orr, L. Reina, D. Wackeroth, Nucl. Phys. Proc. Suppl. **133**, (2004) 111 [arXiv:hep-ph/0311105].

[20] V. Buscher, K. Jakobs, Int. J. Mod. Phys. Lett. A **20** (2005) 2523 [arXiv:hep-ph/0504099].

[21] ALEPH, DELPHI, L3, OPAL Collaborations, Phys. Lett. B **565** (2003) 61 [arXiv:hep-ex/0306033].

[22] CDF, DØ Collaborations, *Results of the Tevatron Higgs Sensitivity Study*, FERMILAB-PUB-03/320-E (2003).

[23] M. Carena *et al.*, arXiv:hep-ph/0010338; G. C. Blazey *et al.*, arXiv:hep-ex/0005012; V. Barger *et al.*, arXiv:hep-ph/0003154.

[24] D. Froidevaux, E. Richter-Was, Z. Phys. C **67** (1995) 213.

[25] Z. Kunszt, Nucl. Phys. B **247** (1984) 339; J. F. Gunion, Phys. Lett. B **253** (1991) 269; W. J. Marciano, F. E. Paige, Phys. Rev. Lett. **66** (1991) 2433.

[26] S. L. Glashow, D. V. Nanopoulos, A. Yildiz, Phys. Rev. D **18** (1978) 1724; Z. Kunszt, Z. Trocsanyi, W. J. Stirling, Phys. Lett. B **271** (1991) 247.

[27] L. Di Lella, Proceedings of Large Hadron Collider Workshop, Aachen, 1990, Report CERN 90-10.

[28] J. F. Gunion, G. L. Kane, J. Wudka, Nucl. Phys.B **299** (1988) 231.

[29] ATLAS Collaboration, *Technical Proposal*, CERN/LHCC/94-43, LHCC/P2, 15 December 1994.

[30] ATLAS Collaboration, *Detector and Physics Performance Technical Design Report*, LHCC 99-14/15 Volume II, 25 May 1999.

[31] W. Grimus, Fortschr. Phys. **36** (1988) 201; R. Decker, Fortschr. Phys. **37** (1989) 657; E. A. Paschos, U. Turke, Phys. Rep. **178** (1989) 145; B. Winstein, L. Wolfenstein, Rev. Mod. Phys. **65** (1993) 1113.

[32] P. G. Harris *et al.*, Phys. Rev. Lett. **82** (1999) 904.

[33] For a review, see S. Dar, arXiv:hep-ph/0008248.

[34] R. D. Peccei, H. R. Quinn, Phys. Rev. Lett. **38** (1977) 1440 and Phys. Rev. D **16** (1977) 1792.

[35] See e.g. M. Dine, *TASI lectures on the strong CP problem*, arXiv:hep-ph/0011376.

[36] WMAP: New three year results on the oldest light in the universe, 16 March 2006 [http://map.gsfc.nasa.gov/m_or/PressRelease_03_06.html].

[37] S. Tremaine, J. E. Gunn, Phys. Rev. Lett. **42** (1979) 407.

[38] For a review on dark matter, see G. Bertone, D. Hooper, J. Silk, Rev. Phys. Rept. **405** (2005) 279 [arXiv:hep-ph/0404175].

[39] J. E. Hill, Phys. Rev. Lett. **75** (1995) 2654 [arXiv:hep-ex/9504009]

[40] M. Fukugita, K. Ichikawa, M. Kawasaki, O. Lahav, Phys. Rev. D **74** (2006) 027302 [arXiv:hep-ph/0605362].

[41] A. Djouadi, arXiv:hep-ph/0503173.

[42] S. Weinberg, Phys. Lett. B **82** (1979) 387; M. Veltman, Acta. Phys. Polon. B **12** (1981) 437; C. H. L. Smith, G. G. Ross, Phys. Lett. B **105** (1981) 38.

[43] E. Witten, Nucl. Phys. B **185** (1981) 513; Nucl. Phys. B **231** (1984) 419; N. Sakai, Z. Phys. C **11** (1981) 153.

[44] For a review, see S. P. Martin, *Perspectives on Supersymmetry*, ed. G. L. Kane, World Scientific, Singapore, 1998 [arXiv:hep-ph/9709356].

[45] For reviews, see e.g.: H. E. Haber, G. L. Kane, Phys. Rep. **117** (1985) 75; P. Fayet, S. Ferrara, Phys. Rep. **32** (1977) 249; H. P. Nilles, Phys. Rep. **110** (1984) 1; R. Barbieri, Riv. Nuov. Cim. **11** (1988) 1.

[46] A. Alvarez-Gaume, E. Witten, Nucl. Phys. B **234** (1983) 269.

[47] E. Witten, Nucl. Phys. B **202** (1982) 253; I. Affleck, M. Dine, N. Seiberg, Nucl. Phys. B **241** (1981) 493; Nucl. Phys. B **256** (1986) 557.

[48] S. Dimopoulos, D. Sutter, Nucl. Phys. B **452** (1995) 496 [arXiv:hep-ph/9504415].

[49] A. Djouadi, S. Rosiers–Lees [conv.] *et al.*, Summary report of the MSSM Working Group for the "GDR–Supersymétrie", arXiv:hep-ph/9901246.

[50] A. H. Chamseddine, R. Arnowitt, P. Nath, Phys. Rev. Lett. **49** (1982) 970; R. Barbieri, S. Ferrara, C. A. Savoy, Phys. Lett. B **119** (1982) 343; L. Hall, J. Lykken, S. Weinberg, Phys. Rev. D **27** (1983) 2359.

[51] K. Inoue, A. Komatsu, S. Takeshita, Prog. Theor. Phys **68** (1982) 927; (E) *ibid.* **70** (1983) 330; I. Jack, D. Jones, S. Martin, M. Vaughn, Y. Yamada, Phys. Rev. D **50**.

[52] G. R. Farrar, P. Fayet, Phys. Lett. B **76** (1978) 575.

[53] H. Goldberg, Phys. Rev. Lett. **50** (1983) 1419; J. Ellis, J. Hagelin, D. V. Nanopoulos, K. Olive, M. Srednicki, Nucl. Phys. B **238** (1984) 453.

[54] L. O'Raifeartaigh, Nucl. Phys. B **96** (1975) 331.

[55] P. Fayet, J. Iliopoulos, Phys. Lett. B **51** (1974) 461.

[56] J. F. Gunion, H. E. Haber, Nucl. Phys. B **272** (1986) 1.

[57] ALEPH, DELPHI, L3, OPAL Collaborations, Eur. Phys. J. C **47** (2006) 547 [arXiv:hep-ex/0602042].

[58] H. E. Haber, R. Hempfling, Phys. Rev. Lett **66** (1991) 1815; Y. Okada, M. Yamaguchi, T. Yanagida, Prog. Theor. Phys. **85** (1991) 1; Phys. Lett. B **262**

(1991) 54; J. Ellis, G. Ridolfi, F. Zwirner, Phys. Lett. B **257** (1991) 83; Phys. Lett. B **262** (1991) 477.

[59] A. A. Barrientos Bendezú, B. A. Kniehl, Phys. Rev. D **59** (1999) 015009 [arXiv:hep-ph/9807480].

[60] J. Dai, J. F. Gunion, R. Vega, Phys. Lett. B **315** (1993) 355 [arXiv:hep-ph/9306319]; Phys. Lett. B **345** (1995) 29; J. R. Espinosa, J. F. Gunion, Phys. Rev. Lett. **82** (1999) 1084 [arXiv:hep-ph/9807275].

[61] J. Conway, K. Desch, J. F. Gunion, S. Mrenna, D. Zeppenfeld, arXiv:hep-ph/0203206.

[62] A. K. Datta, A. Djouadi, M. Guchait, F. Moortgat, Nucl. Phys. B **681** (2004) 31 [arXiv:hep-ph/0303095].

[63] F. Gianotti, M. PepeAltarelli, Nucl. Phys. Proc. Suppl. **89** (2000) 177 [arXiv:hep-ph/].

[64] M. Duhrssen, S. Heinemeyer, H. Logan, D. Rainwater, G. Weiglein, D. Zeppenfeld, Phys. Rev. D **70** (2004) 113009 [arXiv:hep-ph/0406323].

[65] A. Pilaftsis, Phys. Lett. B **435** (1998) 88 [arXiv:hep-ph/9805373].

[66] A. Pilaftsis, Phys. Rev. D **58** (1998) 096010 [arXiv:hep-ph/9803297].

[67] A. Pilaftsis, C. E. M. Wagner, Nucl. Phys. B **553** (1999) 3 [arXiv:hep-ph/9902371].

[68] S. Y. Choi, J. S. Lee, Phys. Rev. D **61** (2000) 015003 [arXiv:hep-ph/9907496].

[69] S. Y. Choi, J. S. Lee, Phys. Rev. D **61** (2000) 115002 [arXiv:hep-ph/9910557].

[70] S. Y. Choi, M. Drees, J. S. Lee, J. Song, Eur. Phys. J. C **25** (2002) 307 [arXiv:hep-ph/0204200].

[71] S. Y. Choi, K. Hagiwara, J. S. Lee, Phys. Rev. D **64** (2001) 032004 [arXiv:hep-ph/0103294].

[72] J. R. Ellis, J. S. Lee, A. Pilaftsis, Phys. Rev. D **70** (2004) 075010 [arXiv:hep-ph/0404167].

[73] M. Carena, J. R. Ellis, A. Pilaftsis, C. E. M. Wagner, Nucl. Phys. B **586** (2000) 92 [arXiv:hep-ph/0003180].

[74] M. Carena, J. R. Ellis, A. Pilaftsis, C. E. M. Wagner, Nucl. Phys. B **625** (2002) 345 [arXiv:hep-ph/0111245].

[75] S. Y. Choi, J. Kalinowski, G. Moorgat-Pick, P. M. Zerwas, Eur. Phys. J. C. **22** (2001) 563 [arXiv:hep-ph/0108117]; S. Y. Choi, A. Djouadi, M. Guchait, J. Kalinowski, H. S. Song, P. M. Zerwas, Eur. Phys. J. C **14** (2000) 535 [arXiv:hep-ph/0002033]; A. Bartl, S. Hesselbach, K. Hidaka, T. Kernreiter, W. Porod, Phys. Lett. B **573** (2003) 153 [arXiv:hep-ph/0307317]; A. Bartl, H. Fraas, O. Kittel, W. Majerotto, Phys. Rev. D **69** (2004) 035007 [arXiv:hep-ph/0308141].

[76] A. Dedes, S. Moretti, Phys. Rev. Lett. **84** (2000) 22 [arXiv:hep-ph/9908516]; Nucl. Phys. B **576** (2000) 29 [arXiv:hep-ph/9909418].

[77] S. Y. Choi. K. Hagiwara, J. S. Lee, Phys. Lett. B **529** (2002) 212 [arXiv:hep-ph/0110138].

[78] R. Godbole, D. J. Miller, S. Moretti, M. Muhlleitner, arXiv:hep-ph/0608079; arXiv:hep-ph/0602198; A. Skjold, P. Osland, Phys. Lett. B **329** (1994) 305 [arXiv:hep-ph/].

[79] S. Y. Choi, M. Drees, B. Gaissmaier, Phy. Rev. D **70** (2004) 014010 [arXiv:hep-ph/0403054].

[80] D. K. Ghosh, S. Moretti, Eur. Phys. J. C **42** (2005) 341 [arXiv:hep-ph/]; D. K. Ghosh, R. M. Godbole, D. P. Roy, Phys. Lett. B **628** (2005) 131 [arXiv:hep-ph/].

[81] N. Maekawa, Phys. Lett. B **282** (1992) 387.

[82] H. Georgi, A. Pais, Phys. Rev. D **10** (1974) 1246.

[83] A. Pomarol, Phys. Lett. B **287** (1992) 331 [arXiv:hep-ph/9205247]; N. Haba, Phys. Lett. B **398** (1997) 305 [arXiv:hep-ph/9609395].

[84] O. C. W. Kong, F. L. Lin, Phys. Lett. B **418** (1998) 217 [arXiv:hep-ph/9707433].

[85] M. Dugan, B. Grinstein, L. Hall, Nucl. Phys. B **255** (1985) 413.

[86] P. Nath, Phys. Rev. Lett. B **66** (1991) 2565; Y. Kuzikuri, N. Oshimo, Phys. Rev. D **45** (1992) 1806; *ibid.* **46** (1992) 3025.

[87] S. Dimopoulos, G. F. Giudice, Phys. Lett. B **357** (1995) 573 [arXiv:hep-ph/9507282]; A. Cohen, D. B. Kaplan, A. E. nelson, *ibid.* B **388** (1996) 588 [arXiv:hep-ph/9607394]; A. Pomarol, D. Tommasini, Nucl. Phys. B **488** (1996) 3 [arXiv:hep-ph/9507462].

[88] T. Ibrahim, P. Nath, Phys. Lett. B **418** (1998) 98 [arXiv:hep-ph/9707409]; Phys. Rev. D **58** (1998) 019901 [arXiv:hep-ph/9807501]; T. Falk, K. A. Olive, Phys. Lett. B **439** (1998) 71 [arXiv:hep-ph/9806236]; M. Brhlik, G. J. Good, G. L. Kane, *ibid.* D **59** (1999) 115004 [arXiv:hep-ph/9810457]; S. Pokorski, J. Rosiek, C. A. Savoy, Nucl. Phys. B **570** (2000) 81 [arXiv:hep-ph/9906206].

[89] For a review, see D. J. H. Chung, L. L. Everett, G. L. Kane, S. F. King, J. Lykken, L. T. Wang, arXiv:hep-ph/0312378.

[90] J. S. Lee *et al.*, Comput. Phys. Commun. **156** (2004) 283 [arXiv:hep-ph/0307377].

[91] J. Ellis, M. K. Gaillard, D. V. Nanopoulos, Nucl. Phys. B **106** (1976) 292.

[92] M. Gavela, G. Girardi, C. Malleville, P. Sorba, Nucl. Phys. B **193** (1981) 257

[93] J. R. Ellis, J. S. Lee, A. Pilaftsis, Mod. Phys. Lett. A **21** (2006) 1405 [arXiv:hep-ph/0605288].

[94] R. Hempfling, Phys. Rev. D **49** (1994) 6168; L. Hall, R. Rattazzi, U. Sarid, Phys. Rev D **50** (1994) 7048 [arXiv:hep-ph/9306309]; M. Carena, M. Olechowski, S. Pokorski, C. E. M. Wagner, Nucl. Phys. B **426** (1994) 269 [arXiv:hep-ph/9402253]; D. Pierce, J. Bagger, K. Matchev, R. Zhang, Nucl. Phys. B **491** (1997) 3 [arXiv:hep-ph/9606211] .

[95] J. A Coarasa, R. A. Jimenez, J. Sola, Phys. Lett. B **389** (1996) 312 [arXiv:hep-ph/9511402]; R. A. Jimenez, J. Sola, Phys. Lett. B **389** (1996) 53 [arXiv:hep-ph/9511292]; K. T. Matchev, D. M. Pierce, Phys. Lett. B **445** (1999) 331 [arXiv:hep-ph/9805275]; P. H. Chankowski, J. Ellis, M. Olechowski, S. Pokorski, Nucl. Phys. B **544** (1999) 39 [arXiv:hep-ph/9808275]; K. S. Babu, C. Kolda, Phys. Lett. B **451** (1999) 77 [arXiv:hep-ph/9811308].

[96] Particle Data Group, K. Hagiwara *et al.*, Phys. Rev. D **66** (2002) 010001; S. Eidelman *et al.*, Phys. Let. B **592** (2004) 1.

[97] J-F. Grivaz, talk given at the conference 'Physics at the LHC', Vienna, July 2004, arXiv:hep-ex/0411002.

[98] CMS Collaboration, *CMS Physics: Technical Design Report v2: Physics Performance*, CERN-LHCC-2006-021 (2006).

[99] J. E. Kim, H. P. Nilles, Phys. Lett. B **138** (1984) 150.

[100] N. K. Falck, Z. Phys. C **30** (1986) 247.

[101] See e.g. F. Zewinger, Int. J. Mod. Phys. A **3** (1988) 49, and references therein.

[102] See e.g. S. F. Giudice, A. Masiero, Phys. Lett. B **206** (1988) 480.

[103] I. Antoniadis, J. Ellis, J. S. Hagelin, D. V. Nanopoulos, Phys. Lett. B **194** (1987) 231; Report No. CERN-TH.4931/87 (unpublished); Report No. CERN-TH.5005/88 (unpublished); J. Ellis, J. S. Hagelin, S. Kelley, D. V. Nanopoulos, Phys. Lett B **209** (1988) 283.

[104] P. Fayet, Nucl. Phys. B **90** (1975) 104; Phys. Lett. B **64** (1976) 159; Phys. Lett. B **69** (1977) 489; Phys. Lett. B **84** (1979) 416; H. P. Nilles, M. Srednicki, D. Wyler, Phys. Lett. B **120** (1983) 346; J. M. Frere, D. R. Jones, S. Raby, Nucl. Phys. B **222** (1983) 11; J. P. Derendinger, C. A. Savoy, Nucl. Phys. B **237** (1984) 307; K. Inoue, A. Komatsu, S. Takeshita, Prog. Theor. Phys **68** (1982) 927; (E) *ibid.* **70** (1983) 330; M. Dine, W. Fischler, M. Srednicki, Phys. Lett. B **104** (1981) 199; A. I. Veselov, M. I. Vysotsky, K. A. Ter-Martirosian, Sov. Phys. JETP **63** (1986) 489 [Zh. Eksp. Teor. Fiz. **90** (1986) 838]; B. R. Greene, P. J. Miron, Phys. Lett. B **168** (1986) 26; J. R. Ellis, J. F. Gunion, H. E. Haber, L. Roszkowski, F. Zwirner, Phys. Rev. D **39** (1989) 844; M. Drees, Int. J. Mod. Phys. A **4** (1989) 3635; U. Ellwanger, M. Rausch de Traubenberg, C. A. Savoy, Phys. Lett. B **315** (1993) 331 [arXiv:hep-ph/9307322]; P. N. Pandita, Z. Phys. C **59** (1993) 575; S.

F. King, P. L. White, Phys. Rev. D **52** (1995) 4183 [arXiv:hep-ph/9505326]; D. A. Demir, JHEP **0511** (2005) 003 [arXiv:hep-ph/0408043].

[105] S. Weinberg, Phys. Rev. Lett. **40** (1978) 223; F. Wilczek, Phys. Rev. Lett. **40** (1978) 279.

[106] M. Cvetic, D. A. Demir, J. R. Espinosa, L. L. Everett, P. Langacker, Phys. Rev. D **56** (1997) 2861 [arXiv:hep-ph/9703317]; D. A. Demir, L. Everett, Phys. Rev. D **69** (2004) 015008 [arXiv:hep-ph/0306240]; T. Han, P. Langacker, B. McElrath, Phys. Rev. D **70** (2004) 115006 [arXiv:hep-ph/0405244]; D. A. Demir, L. Solmaz, S. Solmaz, Phys. Rev. D **73** (2006) 016001[arXiv:hep-ph/0512134]; S. F. King, S. Moretti, R. Nevzorov, Phys. Rev. D **73** (2006) 035009 [arXiv:hep-ph/0510419]; Phys. Lett. B **634** (2006) 278 [arXiv:hep-ph/0511256]; arXiv:hep-ph/0601269, and references therein.

[107] H. P. Nilles, M. Srednicki, D. Wyler, Phys. Lett. B **124** (1983) 337; A. B. Lahanas, Phys. Lett. B **124** (1983) 341; U. Ellwanger, Phys. Lett. B **133** (1983) 187; J. Bagger, E. Poppitz, Phys. Rev. Lett. **71** (1993) 2380 [arXiv:hep-ph/9307317]; J. Bagger, E. Poppitz, L. Randall, Nucl. Phys. B **426** (1994) 3 [arXiv:hep-ph/9405345]; V. Jain, Phys. Lett. B **351** (1995) 481 [arXiv:hep-ph/9407382]; C. F. Kolda, S. Pokorski, N. Polonsky, Phys. Rev. Lett. **80** (1998) 5263 [arXiv:hep-ph/9803310].

[108] S. A. Abel, S. Sarkar, P. L. White, Nucl. Phys. B **454** (1995) 663 [arXiv:hep-ph/9506359]; S. A. Abel, Nucl. Phys. B **480** (1996) 55 [arXiv:hep-ph/9609323].

[109] C. Panagiotakopoulos, K. Tamvakis, Phys. Lett. B **446** (1999) 224 [arXiv:hep-ph/9809475].

[110] C. Panagiotakopoulos, K. Tamvakis, Phys. Lett. B **469** (1999) 145 [arXiv:hep-ph/9908351]; C. Panagiotakopoulos, A. Pilaftsis, Phys. Rev. D **63** (2001) 055003 [arXiv:hep-ph/0008268]; A. Dedes, C. Hugonie, S. Moretti, K. Tamvakis, Phys. Rev. D **63** (2001) 055009 [arXiv:hep-ph/0009125].

[111] A. Menon, D. E. Morrissey, C. E. M. Wagner, Phys. Rev. D **70** (2004) 035005 [arXiv:hep-ph/0404184]; V. Barger, P. Langacker, H.-S. Lee, Phys. Lett. B **630** (2005) 85 [arXiv:hep-ph/0508027]; J. F. Gunion, D. Hooper, B. McElrath, Phys. rev. D **73** (2006) 015011 [arXiv:hep-ph/0509024]; G. Belanger, F. Boudjema, C. Hugonie, A. Pukhov, A. Semenov, JCAP **0509** (2005) 001 [arXiv:hep-ph/0505142].

[112] M. Bastero-Gil, C. Hugonie, S. F. King, D. P. Roy, S. Vempati, Phys. Lett. B **489** (2000) 359 [arXiv:hep-ph/0006198]; S. W. Ham, S. K. Oh, C. M. Kim, E. J. Yoo, D. Son, Phys. Rev. D **70** (2004) 075001 [arXiv:hep-ph/0406062]; K. Funakubo, S. Tao, F. Toyoda, Prog. Theor. Phys. **114** (2005) 369 [arXiv:hep-ph/0501052].

[113] M. Carena, M. Quiros, M. Seco, C. E. M. Wagner, Nucl. Phys. B **650** (2003) 24 [arXiv:hep-ph/0208043]; T. Konstandin, T. Prokopec, M. G. Schmidt, M. Seco, Nucl. Phys. B **738** (2006) 1 [arXiv:hep-ph/0505103].

[114] K. Funakabo, S. Tao, Prog. Theor. Phys. **113** (2005) 821 [arXiv:hep-ph/0409294].

[115] M. Masip, R. Muñoz-Tapia, A. Pomarol, Phys. Rev. D **57** (1998) 5340 [arXiv:hep-ph/9801437].

[116] U. Ellwanger, C. Hugonie, Eur. Phys. J. C **25** (2002) 297 [arXiv:hep-ph/9909260].

[117] U. Ellwanger, J. F. Gunion, C. Hugonie, arXiv:hep-ph/0111179; D. J. Miller, S. Moretti, arXiv:hep-ph/0403137.

[118] U. Ellwanger, J.F. Gunion, C. Hugonie, S. Moretti, arXiv:hep-ph/0305109; arXiv:hep-ph/0401228.

[119] S. Baffioni, talk presented at GdR Supersymétrie 2004, 5-7 July 2004, Clermont-Ferrand, France.

[120] D. Zerwas, S. Baffioni, private communication.

[121] U. Ellwanger, J. F. Gunion, C. Hugonie, JHEP **0507** (2005) 041 [arXiv:hep-ph/0503203].

[122] S. Moretti, K. Odagiri, P. Richardson, M. H. Seymour, B. R. Webber, JHEP **0204** (2002) 028 [arXiv:hep-ph/0204123]; G. Corcella *et al.*, JHEP **0101** (2001) 010 [arXiv:hep-ph/0011363].

[123] T. Sjostrand, L. Lonnblad, S. Mrenna, arXiv:hep-ph/0108264.

[124] U. Ellwanger, J. F. Gunion, C. Hugonie, JHEP **0502** (2005) 066 [arXiv:hep-ph/0406215].

[125] C. Hugonie, private communication.

[126] U. Ellwanger, C. Hugonie, Comput. Phys. Commun. **175** (2006) 290 [arXiv:hep-ph/0508022].

[127] G. Belanger, F. Boudjema, S. Moretti, in preparation.

[128] D. J. Miller, R. Nevzorov, P. M. Zerwas, Nucl. Phys. B **681** (2004) 3 [arXiv:hep-ph:0304049].